

APPLICATION OF ULTRASONIC BURNING RATE MEASUREMENT METHOD ON
CLOSED BOMBS

A THESIS SUBMITTED TO
THE GRADUATE SCHOOL OF NATURAL AND APPLIED SCIENCES
OF
MIDDLE EAST TECHNICAL UNIVERSITY

BY

BERKAN MUMCU

IN PARTIAL FULFILLMENT OF THE REQUIREMENTS
FOR
THE DEGREE OF MASTER OF SCIENCE
IN
AEROSPACE ENGINEERING

SEPTEMBER 2013

Approval of the thesis:

**APPLICATION OF ULTRASONIC BURNING RATE MEASUREMENT METHOD ON
CLOSED BOMBS**

submitted by **BERKAN MUMCU** in partial fulfillment of the requirements for the degree of
**Master of Science in Aerospace Engineering Department, Middle East Technical
University** by,

Prof. Dr. Canan Özgen
Dean, Graduate School of **Natural and Applied Sciences** _____

Prof. Dr. Ozan Tekinalp
Head of Department, **Aerospace Engineering** _____

Assoc. Prof. Dr. D. Funda Kurtuluş
Supervisor, **Aerospace Engineering Dept., METU** _____

Ö. Uğur Arkun, M.S.
Co-Supervisor, **Roketsan Missiles Industries Inc.** _____

Examining Committee Members:

Prof. Dr. M. Cevdet Çelenligil
Aerospace Engineering Dept., METU _____

Assoc. Prof. Dr. D. Funda Kurtuluş
Aerospace Engineering Dept., METU _____

Prof. Dr. Yusuf Özyörük
Aerospace Engineering Dept., METU _____

Assoc. Prof. Dr. Oğuz Uzol
Aerospace Engineering Dept., METU _____

Ö. Uğur Arkun, M.S.
Roketsan Missiles Industries Inc. _____

Date: 11.09.2013

I hereby declare that all information in this document has been obtained and presented in accordance with academic rules and ethical conduct. I also declare that, as required by these rules and conduct, I have fully cited and referenced all material and results that are not original to this work.

Name, Last name : Berkan MUMCU

Signature :

ABSTRACT

APPLICATION OF ULTRASONIC BURNING RATE MEASUREMENT METHOD ON CLOSED BOMBS

MUMCU, Berkan

M. S., Department of Aerospace Engineering

Supervisor: Assoc. Prof. Dr. D. Funda KURTULUŞ

Co-supervisor: Ömer Uğur ARKUN

September 2013, 99 pages

In this thesis study, detailed information about solid rocket motors and ultrasonic burning rate measurement method is given. An experimental setup is prepared for applying the ultrasonic burning rate measurement method. Before performing the burning tests, some pre-tests are performed for affirming the ultrasonic sensor and obtaining some experimental coefficients. Two different types of propellants, which do not include aluminum, are produced for the burning tests. The first type of the propellants has two different batches while the second type has one batch. Coupling materials, which are compatible with these propellants, are prepared. Uncertainty analysis is performed to get burning rate uncertainties of ultrasonic burning rate measurement method and test motor firing method. After that, burning rate measurement experiments are made by using ultrasonic burning rate measurement method. The results of these experiments are compared with each other and test motor firings. Finally, the applicability of the ultrasonic burning rate measurement method is discussed.

Key-words: Ultrasonic Burning Rate Measurement Method, Solid Rocket Motors, Solid Propellants, Burning Rate Measurement Methods, Closed Bombs

ÖZ

ULTRASONİK YANMA HIZI ÖLÇÜM YÖNTEMİNİN KAPALI BOMBALARA UYGULANMASI

MUMCU, Berkan

Yüksek Lisans, Havacılık ve Uzay Mühendisliği Bölümü

Tez Yöneticisi: Doç. Dr. D. Funda KURTULUŞ

Yardımcı Tez Yöneticisi: Ömer Uğur ARKUN

Eylül 2013, 99 sayfa

Bu tez çalışmasında, katı yakıtlı roket motorları ve ultrasonik yanma hızı ölçüm yöntemi hakkında detaylı bilgi verilmiştir. Ultrasonik yanma hızı ölçüm yöntemini uygulayabilmek için bir test düzeneği hazırlanmıştır. Yanma testi yapılmadan önce, ultrasonik sensörü doğrulamak ve bazı deneysel katsayıları elde etmek için bazı ön testler yapılmıştır. Yanma testleri için alüminyum içermeyen iki çeşit yakıt üretilmiştir. Yakıt çeşitlerinden biri iki farklı kafile içerirken, diğer yakıt çeşidi tek kafile içermektedir. Bu yakıtlarla uyumlu arayüz malzemeleri üretilmiştir. Ultrasonik yanma hızı ölçüm yöntemi ve test motoru ateşleme yönteminin yanma hızı belirsizliklerini bulmak için belirsizlik analizi yapılmıştır. Bundan sonra, yanma hızı ölçüm deneyleri ultrasonik yanma hızı ölçüm yöntemi kullanılarak yapılmıştır. Deneylerin sonuçları hem kendi aralarında hem de test motoru ateşlemeleriyle kıyaslanmıştır. Son olarak, ultrasonik yanma hızı ölçüm yöntemin uygulanabilirliği tartışılmıştır.

Anahtar Kelimeler: Ultrasonik Yanma Hızı Ölçüm Yöntemi, Katı Yakıtlı Roket Motorları, Katı Yakıtlar, Yanma Hızı Ölçüm Yöntemleri, Kapalı Bombalar

To Özge, my family and my grandfather

ACKNOWLEDGEMENT

I would like to express my deepest thanks and gratitude to Assoc. Prof. Dr. D. Funda KURTULUŞ for her supervision, understanding, goodwill and great guidance.

I would like to thank to Uğur ARKUN, for his crucial suggestions, sharing his experience and his great support, and ROKETSAN for supporting this study.

I would like thank to my colleagues Özen ATAK, Onur Ozan KALKAN, Funda KÖMBE and İsa TUFAN for their great support and advises during performing the tests and the preparation of this thesis. I also would like to thank to my colleagues Yusuf ATA, Osman YÜCEL, Aykut DAĞKIRAN, Çağlayan DUYGU, Sevda AÇIK, Çağrı TAŞAR, and in particular Hasan ÖLMEZ for their invaluable suggestions and supports.

I specially would like to thank my precious love Özge YAMANKILIÇ. She always encouraged me when I felt desperate about this study. She is the wonderful woman behind this success. I am very grateful for her great love, constant encouragement and endless support during this difficult period of my life.

I would like to thank my wonderful family; Nazmi MUMCU, Fatma MUMCU and Selim MUMCU who supported and encouraged me at every moment of my whole life.

Lastly, this thesis is dedicated to my darling, my family and my grandfather, who make the completion of this work possible.

Rest in peace grandfather...

TABLE OF CONTENTS

ABSTRACT.....	V
ÖZ.....	VI
ACKNOWLEDGEMENT.....	VIII
TABLE OF CONTENTS.....	IX
LIST OF TABLES.....	XII
LIST OF FIGURES.....	XIII
LIST OF SYMBOLS.....	XV
CHAPTERS	
1 INTRODUCTION.....	1
1.1 LITERATURE SURVEY.....	1
1.2 SCOPE OF THE THESIS.....	6
1.3 CONTENTS OF THE THESIS REPORT.....	7
2 SOLID ROCKET MOTORS AND SOLID PROPELLANTS.....	9
2.1 INTRODUCTION.....	9
2.2 SOLID ROCKET MOTORS.....	9
2.2.1 Main Parts of the Solid Rocket Motor.....	10
2.2.2 Solid Rocket Motor Performance Parameters.....	14
2.3 SOLID PROPELLANTS.....	17
2.3.1 Introduction.....	17
2.3.2 Classification of Solid Propellants.....	17
2.3.3 Solid Propellant Ingredients.....	19
3 BURNING RATE MEASUREMENT METHODS.....	21
3.1 INTRODUCTION.....	21
3.2 STRAND BURNER METHOD.....	21
3.3 TEST MOTOR FIRINGS.....	22

3.4	X-RAY METHOD	23
3.5	PLASMA CAPACITANCE GAGES	24
3.6	ULTRASONIC BURNING RATE MEASUREMENT METHOD.....	25
4	ULTRASONIC BURNING RATE MEASUREMENT METHOD	27
4.1	INTRODUCTION.....	27
4.2	MEASURED QUANTITIES	28
4.2.1	Signal Travel Time.....	28
4.2.2	Chamber Pressure.....	30
4.2.3	Chamber Temperature.....	30
4.3	BURNING RATE CALCULATION METHOD	30
4.4	MECHANICAL WAVE VELOCITY	31
4.5	EFFECT OF PRESSURE ON MECHANICAL WAVE VELOCITY	32
4.6	ACOUSTIC IMPEDANCE	32
5	EXPERIMENTAL SETUP AND PROCEDURE.....	35
5.1	INTRODUCTION.....	35
5.2	CLOSED BOMB EXPERIMENTAL SETUP CONFIGURATION.....	35
5.2.1	Closed Bomb.....	36
5.2.2	Ultrasonic Transducer	37
5.2.3	Coupling Material	38
5.2.4	Propellant	39
5.2.5	Inhibitor.....	40
5.2.6	Pressure Sensor	40
5.2.7	Data Acquisition System.....	41
5.2.8	Nitrogen Tanks.....	41
5.2.9	Igniter	42
5.3	CLOSED BOMB TEST EXPERIMENTAL PROCEDURE	43
5.4	WATER COLUMN EXPERIMENTAL SETUP AND ITS PROCEDURE.....	46
6	UNCERTAINTY ANALYSIS.....	49
6.1	INTRODUCTION.....	49

6.2	UNCERTAINTY ANALYSIS OF ULTRASONIC BURNING RATE MEASUREMENT METHOD	49
6.3	UNCERTAINTY ANALYSIS OF TEST MOTOR FIRING METHOD	52
7	RESULTS	55
7.1	DESCRIPTION OF THE TEST CASES	55
7.2	WATER COLUMN EXPERIMENTAL SETUP RESULTS	55
7.3	REFERENCE MECHANICAL WAVE VELOCITY	57
7.4	ACOUSTIC IMPEDANCE	57
7.5	PRESSURE VARIATION COEFFICIENTS	59
7.6	BURNING RATE	60
7.6.1	The First Test	61
7.6.2	The Second Test	64
7.6.3	The Third Test	67
7.6.4	The Fourth Test	70
7.6.5	The Fifth Test	72
7.6.6	The Sixth Test	75
7.6.7	The Seventh Test	78
7.6.8	The Eighth Test	80
7.6.9	Comparison of the Ultrasonic Tests for Propellant 2	83
8	CONCLUSION AND FUTURE WORK	85
8.1	CONCLUSION	85
8.2	FUTURE WORK	86
	REFERENCES	89
	APPENDIX A	93

LIST OF TABLES

TABLES

Table 4.1 Summary of Countries and Agencies Applied Ultrasonic Measurement Method [1] .	28
Table 6.1 Uncertainties of Ultrasonic Burning Rate Measurement Method.....	52
Table 6.2 Uncertainties of Ultrasonic Burning Rate Measurement Method.....	53
Table 7.1 Test Case Descriptions.....	55
Table 7.2 Web Thickness of the Water.....	56
Table 7.3 Reference Mechanical Wave Velocities	57
Table 7.4 Acoustic impedance and conducted energy for all tests	58
Table 7.5 Pressure and signal travel time	59
Table 7.6 Pressure Variation Coefficients	60
Table 8.1 Differences of the Tests	86

LIST OF FIGURES

FIGURES

Figure 1.1 VPI/NASA Ultrasonic Burn Rate Apparatus [3].....	2
Figure 1.2 Simple interaction configuration of transducer, coupling material and propellant	3
Figure 1.3 ONERA Test Setup [5].....	3
Figure 1.4 HMX propellant’s burning rates [5]	4
Figure 1.5 Burn rates obtained by ultrasonic burn rate measurement method and optical method [6].....	4
Figure 1.6 Burning rate and total uncertainty in burning rate [9]	5
Figure 1.7 Experimental setup of UIUC [10]	6
Figure 2.1 Main parts of a solid rocket motor [12]	10
Figure 2.2 Traditional metallic motor case [14].....	11
Figure 2.3 Composite motor case and loads on it [15]	11
Figure 2.4 General view of case insulation [16]	12
Figure 2.5 Installation of the pyrotechnique igniter [11]	12
Figure 2.6 Simple diagram of a nozzle [13].....	13
Figure 2.7 Propellant grain configurations [11].....	14
Figure 2.8 Thermodynamic energy vs flame temperature for homogeneous propellants [27]	18
Figure 3.1 Crawford bomb mechanism with strand burner [32].....	22
Figure 3.2 Test motor firing [11]	23
Figure 3.3 Real time radioscopy configuration [9]	24
Figure 3.4 Plasma capacitance gage application configuration [34].....	24
Figure 4.1 Acoustic wave and schematic view of signals [39].....	29
Figure 4.2 Signal travel time.....	29
Figure 4.3 The main coupling material and the other samples cutted with lathe at different thicknesses (Test 1).....	32
Figure 5.1 Experimental setup configuration [41]	36
Figure 5.2 Closed bomb	37
Figure 5.3 Ultrasonic transducer.....	38
Figure 5.4 Coupling material; for propellants with aluminum (right), for propellants without aluminum (left)	38
Figure 5.5 Coupling materials for each test (after cutting) and schematic view of their mounted area.....	39
Figure 5.6 Propellant samples for Test 5-6-7-8 (Propellant 2 Batch 1)	40
Figure 5.7 Inhibitor and propellant	40
Figure 5.8 Pressure sensor	41
Figure 5.9 Data acquisition system	41
Figure 5.10 Nitrogen tanks	42

Figure 5.11 Igniter	42
Figure 5.12 Propellant and coupling material after sticking operations and schematic view of sticking control position.....	44
Figure 5.13 Schematic view of upper lid before assembling on closed bomb.....	45
Figure 5.14 Final configuration of the closed bomb	45
Figure 5.15 Adjustment screen	46
Figure 5.16 Water column experiment setup	47
Figure 6.1 Burning rate of ultrasonic method with variations	52
Figure 6.2 Burning time for test motors [11]	53
Figure 6.3 Burning rate of test motor with variations	54
Figure 7.1 Signal travel time versus time (first water column test)	56
Figure 7.2 Change of mechanical wave velocity with pressure.....	59
Figure 7.3 Gates of the signal	60
Figure 7.4 Sent and reflected signals for Test 1 at the initial time.....	61
Figure 7.5 Signal travel time (a), pressure (b) and signal peak (c) for Test 1.....	63
Figure 7.6 Normalized burning rate versus normalized combustion pressure for Test 1	64
Figure 7.7 Reflected signals for Test 2 at the initial time	65
Figure 7.8 Signal travel time (a), pressure (b) and signal peak (c) for Test 2.....	66
Figure 7.9 Normalized burning rate versus normalized combustion pressure for Test 2	67
Figure 7.10 Reflected signals for Test 3 at the initial time	68
Figure 7.11 Signal travel time (a), pressure (b) and signal peak (c) for Test 3.....	69
Figure 7.12 Normalized burning rate versus normalized combustion pressure for Test 3	70
Figure 7.13 Reflected signals for Test 4 at the initial time	71
Figure 7.14 Signal travel time (a) and signal peak (b) for Test 4	72
Figure 7.15 Reflected signals for Test 5 at the initial time	72
Figure 7.16 Signal travel time (a), pressure (b) and signal peak (c) for Test 5.....	74
Figure 7.17 Normalized burning rate versus normalized combustion pressure for Test 5	75
Figure 7.18 Reflected signals for Test 6 at the initial time	76
Figure 7.19 Signal travel time (a), pressure (b) and signal peak (c) for Test 6.....	77
Figure 7.20 Normalized burning rate versus normalized combustion pressure for Test 6	78
Figure 7.21 Reflected signals for Test 7 at the initial time	78
Figure 7.22 Signal travel time (a), pressure (b) and signal peak (c) for Test 7.....	79
Figure 7.23 Normalized burning rate versus normalized combustion pressure for Test 7	80
Figure 7.24 Reflected signals for Test 8 at the initial time	80
Figure 7.25 Signal travel time (a), pressure (b) and signal peak (c) for Test 8.....	82
Figure 7.26 Normalized burning rate versus normalized combustion pressure for Test 8	82
Figure 7.27 Comparison of propellant 2 tests	83

LIST OF SYMBOLS

a	burning rate coefficient
A_b	burning surface area
A_e	nozzle exit area
A_t	nozzle throat area
C	mechanical wave velocity
C_c	mechanical wave velocity in the coupling material
C_f	thrust coefficient
C_p	mechanical wave velocity in the propellant
C^*	characteristic exhaust velocity
F	thrust force
g_0	gravitational acceleration at sea level
I	transmitted radiation
I_0	source radiation at 1 meter
I_s	specific impulse
I_t	total impulse
i	conduction coefficient
K	burning surface area to nozzle throat area ratio
k_p	solid propellant wave velocity pressure variation coefficient
ℓ	material path length
l_p	coupling material wave velocity pressure variation coefficient
\dot{m}	mass flow rate
m_p	propellant mass
n	burning rate pressure exponent
N_x	total number of stations on x-axis
N_z	total number of stations on z-axis
P	pressure
P_{amb}	ambient pressure
P_{ref}	reference pressure
P_c	chamber pressure

P_e	gas exhaust pressure
R_b	propellant burning rate, instant propellant burning rate
R_s	distance from the source to the collection point
T	temperature
t	time
t_b	burning time
T_s	burning surface temperature
V_e	gas exhaust velocity
W	thickness
W_b	thickness of burned propellant
W_c	thickness of coupling material
W_p	thickness of propellant
Y	reflection coefficient
Z	acoustic impedance
γ	specific heat ratio
ε	nozzle expansion ratio
π_K	temperature sensitivity of pressure, % / K
ρ	density
σ_p	temperature sensitivity of burning rate, % /K
$\hat{\partial}$	partial derivative operator
μ	material attenuation coefficient
τ	time of flight
α	thermal diffusivity

Subscripts:

<i>del</i>	delivered
<i>ini</i>	initial
<i>ref</i>	reference
<i>th</i>	theoretical
<i>ref</i>	reference

CHAPTER 1

INTRODUCTION

In solid rocket motors, thrust is produced by combustion of the propellant at high pressure values. Knowing the properties of the solid propellant, especially the burn rate of the propellant is needed for solid propellant development, detailed characterization of developed propellant and production process of the propellant. Burn rate of the propellant must be measured by experimental methods, because there is no theory about guessing the burn rate of the propellant. In literature five experimental burn rate measurement methods step forward. These methods are:

1. Strand Burners
2. Test Motor Firings
3. Flash X-Ray Method
4. Plasma Capacitance Gages
5. Ultrasonic Burn Rate Measurement Method

These methods will be introduced in detail in following chapters, but the ultrasonic burn rate measurement is the most advantageous of them, because high accurate, local, instantaneous, economical measurement is done by this method. Besides, only one test is enough to get pressure versus burn rate data for a large pressure interval [1].

1.1 Literature Survey

Literature review is based on the subject of ultrasonic burn rate measurement method. Ultrasonic burn rate measurement method has been the subject of search since the 1960's; however it is still a trend topic with its specific difficulties. With the help of developing computing technology and the sensors these difficulties are tried to defeat.

The study of Hale [2] in 1967 and the study of Wright [3] were two of the first studies at using ultrasonic technique for measuring the burn rate of solid propellant. These researchers studied for NASA Langley Research Center and Virginia Polytechnic Institute's joint experiment on ultrasonic burning rate measurement of a solid propellant. The experiment was made with an end burning open combustion chamber, which can be seen in Figure 1.1. The propellant was about 2000 grams and had about 75 mm. thickness. The display of waveforms and data collection rate in this study was limited because of the lack of usable computational power at

that time; although, this study really became the basis of the future studies of the ultrasonic burn rate measurement method.

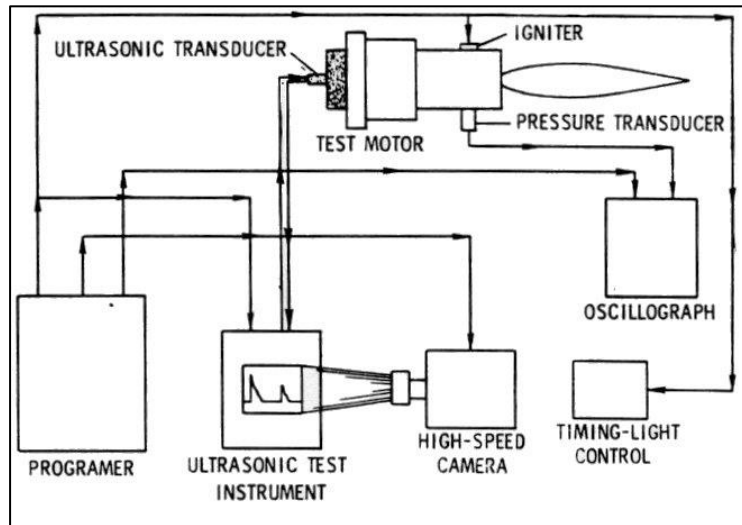


Figure 1.1 VPI/NASA Ultrasonic Burn Rate Apparatus [3]

ONERA Company has studied on ultrasonic measurement of energetic materials since 1979 [4]. Cauty and others [5] applied ultrasonic technique for measuring the burn rate and the temperature sensitivity of the solid propellant. According to this study, successful attempts were made at ONERA on measuring the burn rate of the solid propellants for room temperature, but at other some initial temperature conditions some problems were detected due to wave propagation condition change because of the temperature. In their study, an ultrasonic burn rate measurement tool was tried to develop, which can work between -40°C to 60°C temperature range.

One of the key parameter of their study was producing ultrasonic transducers which can operate at low and high temperatures. Another key parameter of their study was using a coupling material to protect the transducer from the hot combustion gases. Simple interaction configuration of transducer, coupling material and propellant is given in Figure 1.2.

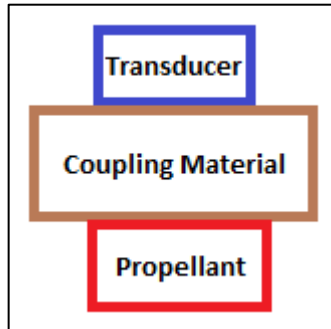


Figure 1.2 Simple interaction configuration of transducer, coupling material and propellant

The experimental setup, which is shown in Figure 1.3, contains a closed bomb. This closed bomb can operate up to 45 MPa.

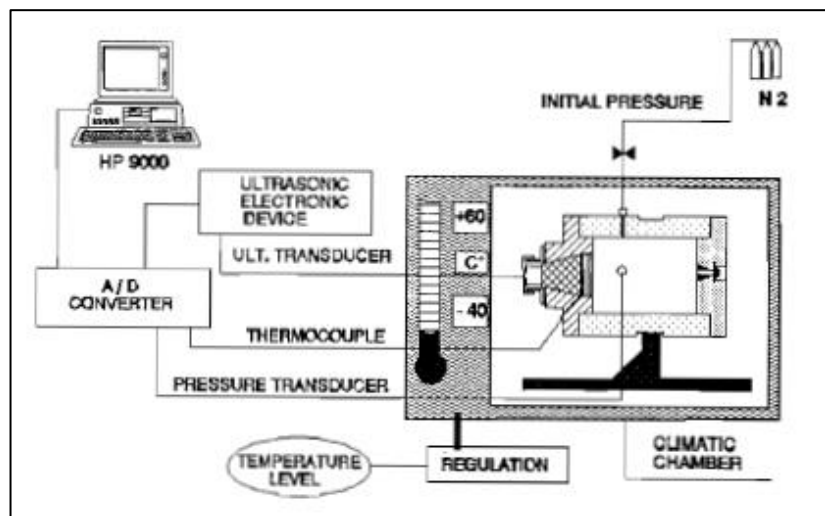


Figure 1.3 ONERA Test Setup [5]

In this experimental setup, three types of propellant's burning rate were measured at different initial temperature conditions. Mechanical wave velocity of coupling material and solid propellant were measured before the tests. Besides, wave velocity pressure variation coefficients of coupling material and propellant were calculated.

The obtained results for all propellants at different initial temperatures were good and reasonable, which makes that study successful and another milestone of ultrasonic burning rate measurement method. The results of the tests made with HMX propellant is shown in Figure 1.4:

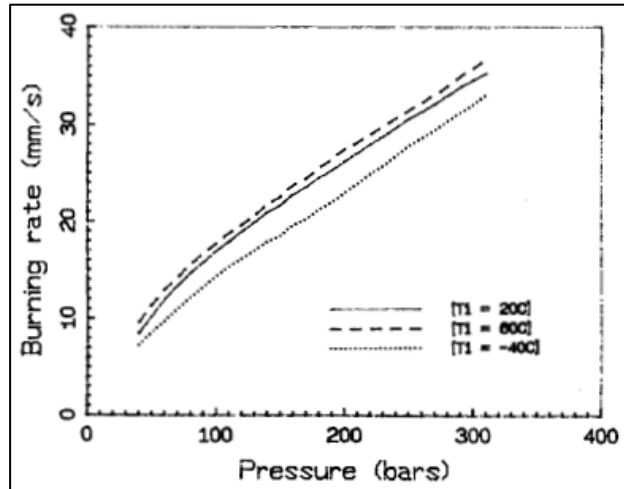


Figure 1.4 HMX propellant's burning rates [5]

Delft University and TNO has made researches about ultrasonic measurement. Louwers and others [6] have made studies with Hydraziniumnitroformate (HNF) and Polymethyl methacrylate (PMMA) coupling material. The aim of their study is creating an experimental setup for the basis of ramjet studies. The experimental setup consists of an open combustion bomb and ultrasonic burn rate measurement device.

Besides ultrasonic burn rate measurement method, optical measurement method is applied in the same experiment to compare results of both methods. The results of both methods are given in Figure 1.5:

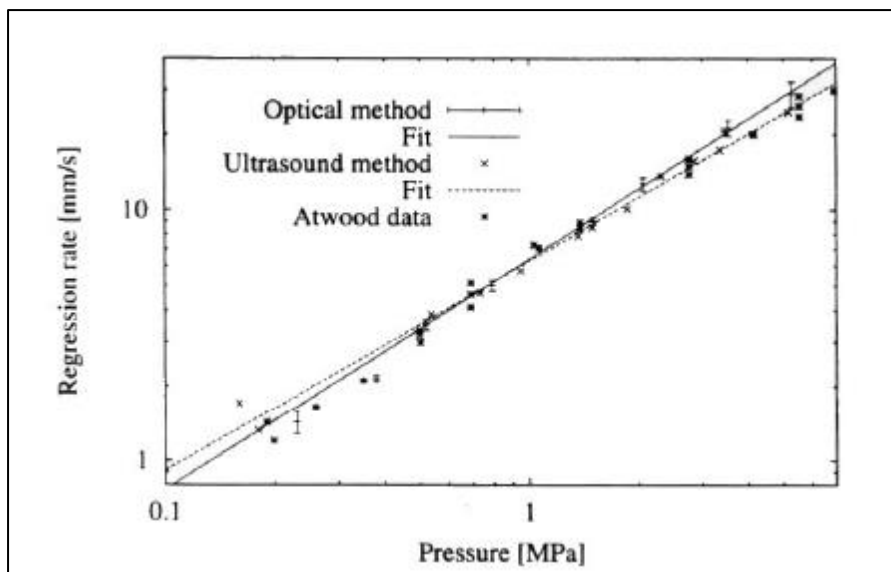


Figure 1.5 Burn rates obtained by ultrasonic burn rate measurement method and optical method [6]

University of Alabama in Huntsville (UAH) has gained ultrasonic measurement capability by using ONERA based technology. Di Salvo and others [7] has studied on steady state ballistics of solid propellants by using ultrasonic technique. Therefore, Di Salvo and others [7] has suffered effort on transient ballistics of solid propellants. Besides, Rochford [8] has made research on temperature sensitivity of solid propellants by the help of the ultrasonic measurement method. Another study is Dauch and others' study [9] about the uncertainty analysis of the ultrasonic burn rate measurement method. About 3% uncertainty of the measurement method is detected in their study. The results of the study are shown in Figure 1.6:

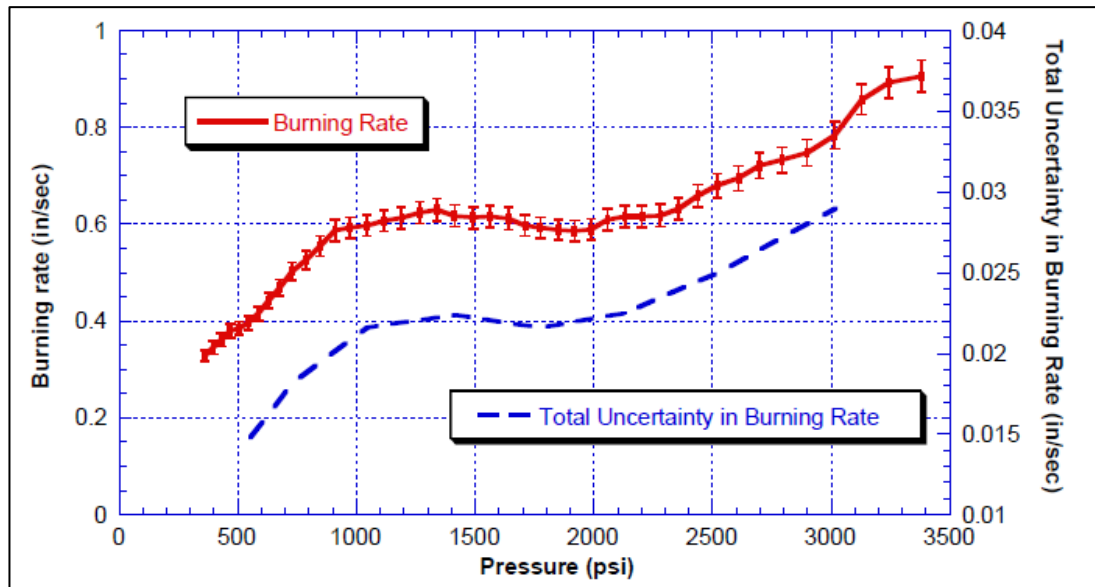


Figure 1.6 Burning rate and total uncertainty in burning rate [9]

The University of Illinois at Champaign-Urbana (UIUC) is another university which uses ultrasonic technique for their researches. Krier and others [10] use an experimental setup containing two combustion bombs. The first bomb has a rotary valve which adjusts the pressure during the combustion. The second bomb has two nozzles, because one of the nozzles is closable to control pressure transition during combustion.

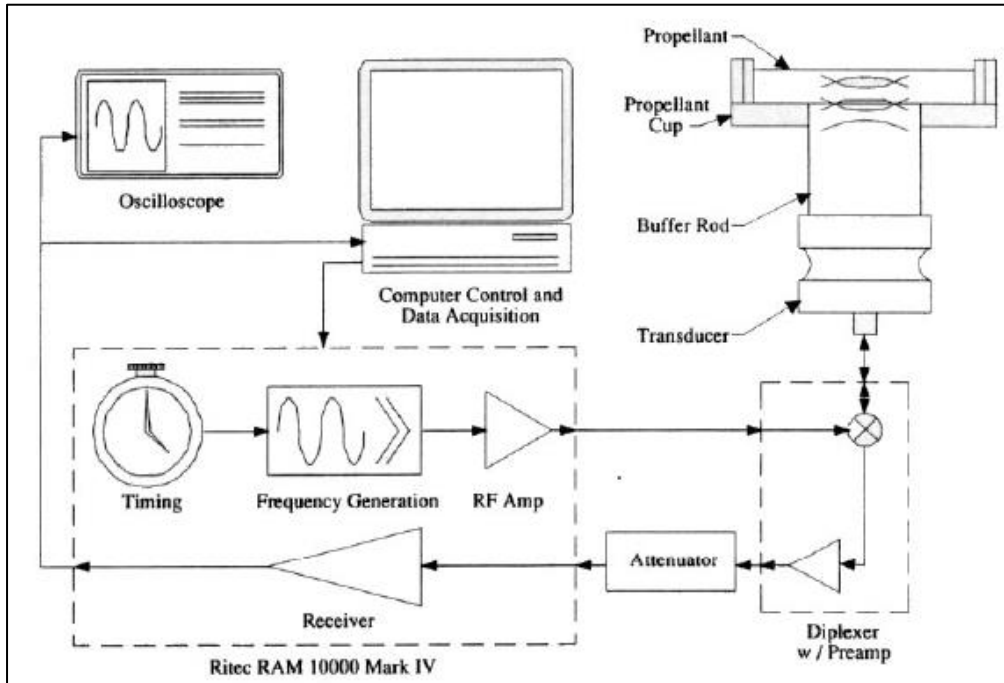


Figure 1.7 Experimental setup of UIUC [10]

Tests are practiced with propellants which have averagely 25 grams weight and 12 mm thickness. Besides the steady-state burning rate measurement, the aim of the study is measuring pressure versus transient burning rate of the solid propellant.

1.2 Scope of the Thesis

The aim of this study is applying ultrasonic burn rate measurement method to closed bombs. Solid propellants, which do not include aluminum, are used in the application of this method.

Before the test, solid propellants, coupling materials and inhibitors are produced and prepared for every test. Different sized samples are used for measuring reference mechanical wave velocity of these materials.

Some studies and measurements are performed before the test for making correct burning rate measurement. One of them is signal travel time measurement with water column experiment setup. In this experiment, water represents the burning propellant; so, the ultrasonic sensor affirmation can be done by this test.

Another study, which is performed before the burning test, is determining the reference mechanical wave velocity of the coupling material and the propellant. Reference mechanical wave velocity determination is performed by using different size samples. Reference mechanical wave velocity is used when calculating the burning rate of the propellant.

Determining wave velocity pressure variation coefficients of coupling material and propellant is also important for calculating the burning rate of the propellant. These values affect the burning rate calculation of the propellant when ultrasonic burning rate method is used, because of this reason wave velocity pressure variation coefficients of coupling material and propellant are found for each burning test.

An uncertainty analysis is performed for determining burning rate uncertainties of the ultrasonic burning rate measurement method and the test motor firing method.

Finally, ultrasonic burning rate measurement method is applied for solid propellants in closed bomb. Signal travel time and pressure are measured at the burning test. By the help of the burning rate calculation formula, instantaneous burning rate versus pressure data are obtained. These data are compared with test motor firing results.

1.3 Contents of the Thesis Report

In Chapter 2, information about the solid rocket motors, solid propellants and burning rate measurement methods is given. Firstly, solid rocket motors are introduced part by part. Secondly, information about solid propellant types and their properties are given. Lastly, burning rate measurement methods are explained and compared in detail.

In Chapter 3, burning rate measurement methods are tried to be explained. Five main methods are told in detail.

In Chapter 4, ultrasonic burning rate measurement method, which is the main interest of this study, is described.

Chapter 5 contains the schematic view and description of the experimental setup. Every part of the experimental setup is introduced and showed in this chapter. Also experimental procedure is told. Furthermore, information about the water column test and its procedure is given.

In Chapter 6, uncertainty analysis of burning rate is performed for ultrasonic burning rate measurement method and test motor firing method.

In Chapter 7, the results of the performed pre-tests and pre-calculations are given. The burning rate results of the propellants are also given and described in detail after the burning tests in closed bomb.

CHAPTER 2

SOLID ROCKET MOTORS AND SOLID PROPELLANTS

2.1 Introduction

Rocket is a system which produces thrust by ejecting the combustion products of the energetic material burning inside it. This energetic material is called propellant.

There are some basic application fields of the rockets. First of all, rockets are used as propulsion systems in missiles. Then, rockets are used for main propulsion system and for other propulsion systems like spin control, attitude control, stage separation and gyro unloading in space crafts. Another application field of the rockets is space launch vehicles [11].

The rockets can be classified into three types according to their thrust producing types. The first type is chemical rocket propulsion which gets energy by combusting chemical propellants at high pressures. Liquid propellant engines, solid rocket motors, hybrid propellant rocket propulsion, gaseous propellant rocket engines are examples of chemical rocket propulsion. The second type is nuclear rocket engines systems motors which can be thought as advanced liquid propellant engines. Nuclear rocket engines systems need more development to be used, so they are still not used in a flying system. Fusion, isotope decay engine and nuclear fission reactor rocket are common types of nuclear rocket engines systems. The third type is electric rocket propulsion which uses electric power for producing thrust. Since the power sources of this system are not very efficient and light, this propulsion type is not very preferable. Electrothermal rocket propulsion, the electrostatic engine and the electromagnetic engine are main types of electric rocket propulsion [11].

By looking thrust producing types it can be said that chemical rocket propulsion is the most preferred type of propulsion and solid rocket motors are the most common used type of chemical rocket propulsion. Solid rocket motors will be told in detail in the following parts.

2.2 Solid Rocket Motors

Solid rocket motors are less complicated type of chemical rocket propulsion, because they do not have moveable parts and their working principle is simpler. Due to its working principle, the solid propellant is ignited and burnt in the combustion chamber with high pressure until the solid propellant finishes. The combustion gases pass through the nozzle for producing thrust. Since the solid propellant burns unstoppably, adjusting the throttle of a solid rocket motor instantaneously is impossible. Although the solid rocket motors can produce high thrust for a

space launch vehicle's booster, they can produce low thrust for a small spacecraft mini thruster. Because of their large application area, simplicity and lower cost, the solid propellant rockets are used widespread. Main parts of a solid rocket motor can be seen in Figure 2.1:

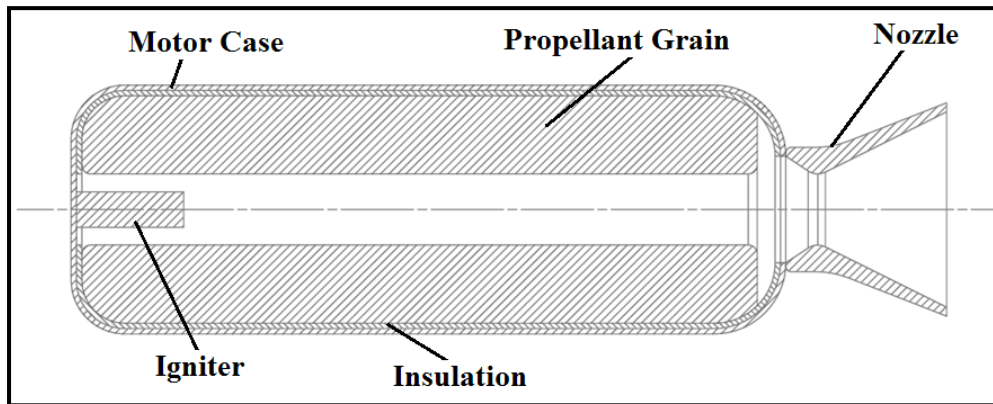


Figure 2.1 Main parts of a solid rocket motor [12]

2.2.1 Main Parts of the Solid Rocket Motor

The solid rocket motors basically have five main parts which are motor case, insulation, igniter, nozzle and the propellant grain. These parts are introduced in detail in the following sections.

2.2.1.1 Motor Case

Motor case is the outer part of the solid rocket motor. Basically, motor case is designed to withstand the combustion pressure and temperature of the motor with a safety of factor. Besides withstanding the combustion pressure, the case must meet the requirements of the rocket motor. It must be as light as possible to provide advantage for rocket's mission profile and it must be an interface for other parts of the solid rocket motor like nozzle or igniter. The case of the solid rocket motor can be made from either metal or composite material [13]. Metal cases have some advantages which make them preferable. Metal cases are durable for the loads of the rocket. Therefore, metal cases are easy to product. Metal cases can also be used at the high combustion temperatures, so less insulation is used which provides an advantage for loading more propellant.

Generally, three materials are used when producing the metal cases. Steel is one of the metallic materials, which is used for metallic case production. HP steel, HY steel, low alloy steel and maraging steel are the most widely used steel types. Titanium is another material which is used in the metallic case production. Despite titanium is not very resistive to buckling, its strength to density ratio is desirable for increasing the performance of the rocket. Aluminum is the third metallic material which is used in case production. Aluminum is not very applicable for big motors, but it can be used in small motor applications or for some motor cases where the corrosion can be a problem [14]. Traditional metallic motor case can be seen in Figure 2.2;

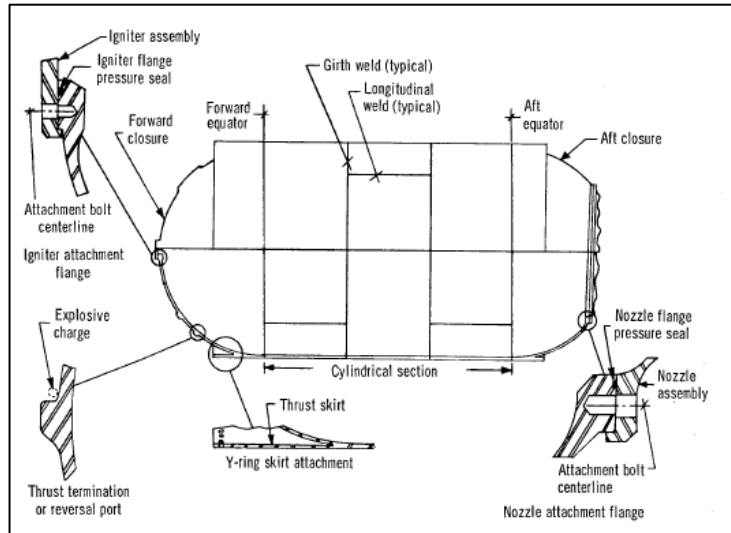


Figure 2.2 Traditional metallic motor case [14]

Composite motor cases are another state of art in designing solid rocket motors. Composite cases are advantageous for their lighter weight, because weight is a critical concern in designing solid rocket motors. Despite its weight is an advantage, non-yielding behavior, non-homogeneity and anisotropy of the composite materials are disadvantages of using them. Therefore, composite materials are more sensitive to temperature and environment effects than metal cases. Fiber, resin and lamina are the mostly used composite materials when producing composite cases [15].

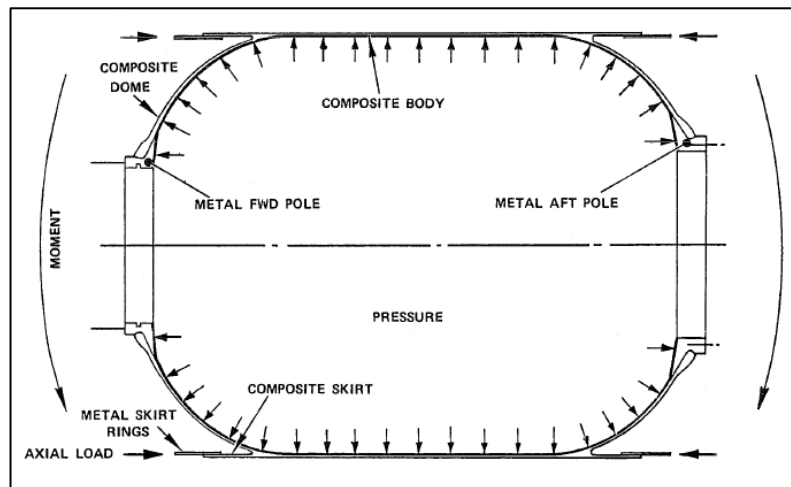


Figure 2.3 Composite motor case and loads on it [15]

2.2.1.2 Insulation

During the combustion process of the propellant high temperature combustion gases occur. Because of these gases, thermal insulation of the case is needed. Therefore, insulation has other missions, too. Insulation attaches propellant and case to each other, inhibits specific burning surfaces of propellant, transfers the strain of the motor case to the propellant and stretches the composite motor cases. Thermal environment determination, material selection, thermal and structural analysis are important design factors of insulation. Generally, insulation consists of rubber or EPDM with strengthening materials like kevlar, carbon or silica [16].

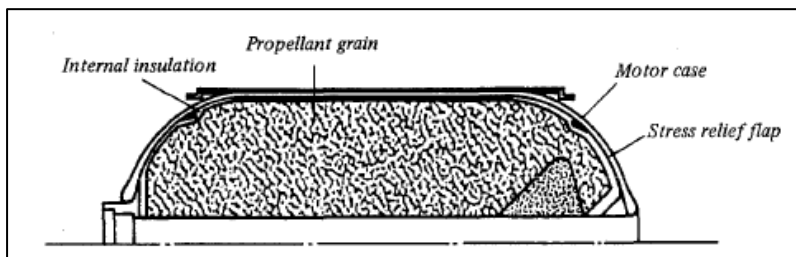


Figure 2.4 General view of case insulation [16]

2.2.1.3 Igniter

Main purpose of the igniter is starting the combustion in the chamber by igniting the surface of the propellant. There are two common types of igniters. The first type is pyrogen igniters. Pyrogen igniters are small rocket motors which ignites bigger rocket motors. Despite traditional solid rocket motor's propellant formulation and design technique are used by pyrogen igniters, their purpose is not producing thrust. The second type is pyrotechnique igniters. Explosive solid materials or small solid propellant pellets are used as heat sources in pyrotechnique igniters [17]

Pyrotechnique igniters are commonly applied in solid rocket motor applications. Depending on the design criteria, pyrotechnique igniter's installation on the case can be different.

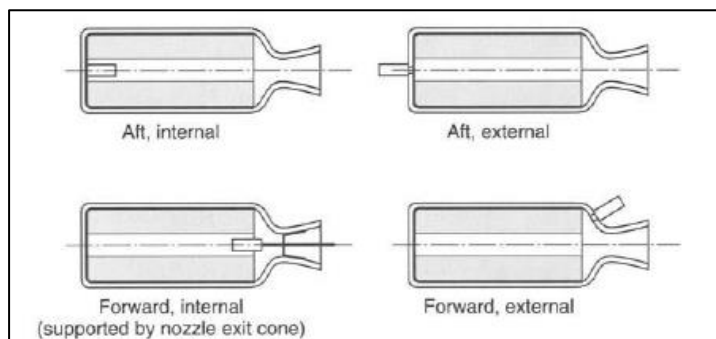


Figure 2.5 Installation of the pyrotechnique igniter [11]

2.2.1.4 Nozzle

Hot combustion gases are expanded and accelerated in the nozzle for producing thrust. Because of this reason, nozzle must be durable for hot environment conditions and erosion. So, the materials used in nozzle production must be carefully chosen. Generally, usual composite materials, ablative materials and thermostable insulators are used for nozzle production [13].

There are a lot of parameters for designing the nozzle. The most important ones are [18]:

- Burning time of the motor
- Internal combustion pressure of the motor
- Propellant type
- Throat diameter of the nozzle
- Expansion ratio of the nozzle
- Available place for mounting the nozzle
- Case integration of the nozzle
- Cost and reliability of the nozzle

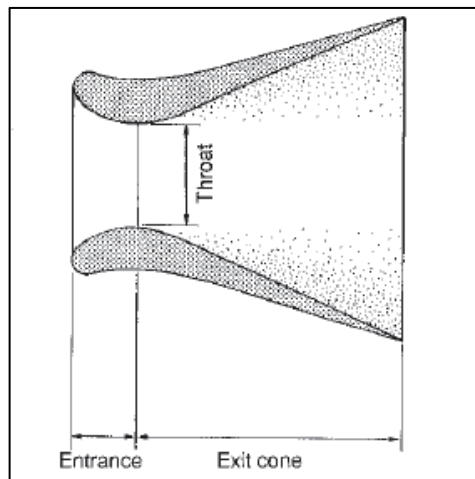


Figure 2.6 Simple diagram of a nozzle [13]

2.2.1.5 Propellant Grain

The energetic part of the solid rocket motors is settled in the propellant grain. Two main configurations of the propellant grains step forward which are free standing and case bonded grains.

Free standing grains are produced independently from the case and they are placed in the case after their production. Some support elements are required for free standing grains. Case bonded grains are produced inside the motor case by using the case as a mold. Because of this reason, case bonded grains are united to the case or the insulation material. For both types of grains, some port geometries are applied to meet the performance requirements [11].

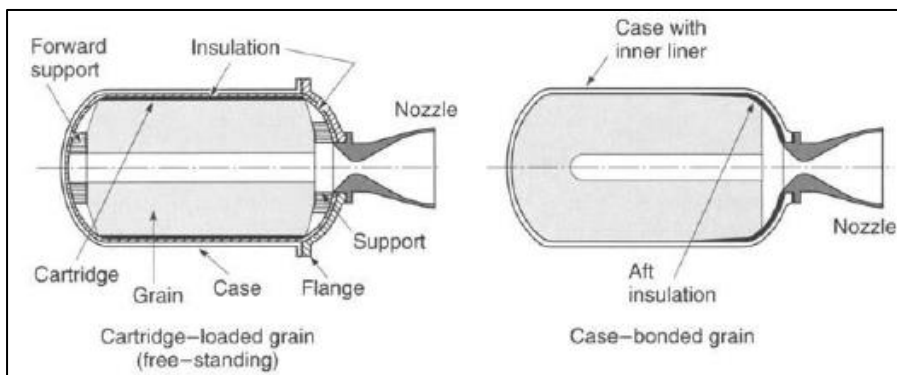


Figure 2.7 Propellant grain configurations [11]

2.2.2 Solid Rocket Motor Performance Parameters

Solid rocket motors' main goal is producing thrust by ejecting the combustion gases from the motor. During this operation, some physical, chemical and thermodynamic phenomena occur. These phenomena, which affect the propulsive force of the motor, can be defined with some ballistic parameters. These parameters are introduced in detail in the following sections.

2.2.2.1 Thrust

Thrust is the propulsive force produced by ejecting the combustion products to the out of the motor with high velocity. For a solid rocket motor, produced thrust can be divided into two types; thrust due to momentum change and thrust due to pressure difference.

Thrust due to momentum change is created by ejected mass. It is formulized as follows;

$$F = \dot{m} \cdot V_e \tag{2.1}$$

where \dot{m} is the mass flow rate and V_e is the gas exhaust velocity.

Thrust due to pressure difference occurs because of the difference of ambient pressure and the gas exhaust pressure at the nozzle exit. It is formulized as follows;

$$F = (P_e - P_{amb})A_e \quad (2.2)$$

where P_e is the gas exhaust pressure, P_{amb} is the ambient pressure and the A_e is the nozzle exit area.

Total thrust of the rocket motor is the sum of thrust due to momentum change and pressure difference.

$$F = \dot{m} \cdot V_e + (P_e - P_{amb})A_e \quad (2.3)$$

2.2.2.2 Total and Specific Impulse

Total impulse is a motor performance parameter which is proportional to the energy of the all propellant inside the motor. It is defined as integration of the force over the burning time of the motor [11].

$$I_t = \int F \cdot dt \quad (2.4)$$

where I_t is the total impulse, F is thrust and dt is the time derivative.

Specific impulse shows the total impulse of the propellant per unit weight. It is an important design parameter, the higher specific impulse the better motor performance [11].

$$I_s = \frac{I_t}{m_p \cdot g_o} = \frac{C_f \cdot C^*}{g_o} \quad (2.5)$$

where I_s is the specific impulse, m_p is total propellant mass, g_o is the gravitational acceleration, C_f is the thrust coefficient and C^* is the characteristic exhaust velocity.

2.2.2.3 Characteristic Exhaust Velocity

Characteristic exhaust velocity (C^*) is a commonly used parameter to describe motor's performance and compare the performance of different motors. It is related to combustion efficiency. It can be defined in terms of nozzle throat area (A_t), combustion chamber pressure (P_c) and mass flow rate (\dot{m}) as in Eq. (2.6):

$$C^* = \frac{A_t \cdot P_c}{\dot{m}} \quad (2.6)$$

2.2.2.4 Thrust Coefficient

Thrust coefficient is a factor that shows the nozzle performance and the effect of combustion pressure on the nozzle. Thrust coefficient is defined in two ways; delivered thrust coefficient and theoretical thrust coefficient. Delivered thrust coefficient is determined by experimental results; however theoretical thrust coefficient is calculated by theoretical values. Delivered thrust coefficient is given in Eq. (2.7) and theoretical thrust coefficient is given in Eq. (2.8):

$$C_{f,del} = \frac{F_{del}}{A_t \cdot P_c} \quad (2.7)$$

where $C_{f,del}$ is the delivered thrust coefficient and F_{del} is delivered thrust.

$$C_{f,th} = \sqrt{\frac{2 \cdot \gamma^2}{\gamma - 1} \left(\frac{2}{\gamma + 1} \right)^{\frac{\gamma + 1}{\gamma - 1}}} \left[1 - \left(\frac{P_e}{P_c} \right)^{\frac{\gamma - 1}{\gamma}} \right] + \frac{P_e - P_{amb}}{P_c} \cdot \varepsilon \quad (2.8)$$

where $C_{f,th}$ is the theoretical thrust coefficient, γ is ratio of specific heats and ε is nozzle expansion ratio.

2.2.2.5 Nozzle Expansion Ratio

Nozzle expansion ratio (ε) is the ratio of nozzle exit area to nozzle throat area. Nozzle expansion ratio is a critical design parameter for the nozzle, because it is one of the parameters that determine the characteristics of gas flow from the nozzle.

$$\varepsilon = \frac{A_e}{A_t} \quad (2.9)$$

2.2.2.6 Burning Rate

Burning rate is another important design parameter for solid rocket motors, since it directly affects the internal pressure and thrust of the motor. Because of this reason, burning rate of the propellant is detected, measured and analyzed during design process. Burning rate can be empirically defined as a function of pressure which is called Vielle's or Saint Robert's burning law [11]:

$$R_b = a \cdot P_c^n \quad (2.10)$$

where R_b is burning rate, a and n are empirical constants.

The main aim of this thesis study is introducing and applying ultrasonic burn rate measurement method, so burning rate and burning rate measurement methods will be discussed in detail in Chapter 4.

2.3 Solid Propellants

2.3.1 Introduction

Solid propellants are used in rocket and gun production fields. Solid propellants are very energetic materials. Energy level of a solid propellant can be defined with energy density which is created energy of a propellant per unit volume. In order to get high energy density, the material density of the propellant should be high. In solid rocket motor applications propellant is burned under control to get target thrust. Chemical ingredients of a propellant can be different due to mission specification of the motor. Different chemical composition of solid propellants causes different type of propellants with different performance and combustion characteristics [19].

2.3.2 Classification of Solid Propellants

Solid propellants can be divided into two groups according to their main ingredients, interconnection type and physical structure which are homogeneous and heterogeneous propellants.

2.3.2.1 Homogeneous Propellants

Homogeneous propellants have chemically linked ingredients and their physical structure is homogeneous. There are three types of homogeneous propellants.

The first type is single-base propellants. The basic component of single-base propellants is Nitrocellulose (NC). Ethyl alcohol or diethyl ether is used for gelatinizing the NC. K_2SO_4 or KNO_3 can be added in little amounts as flame suppressor. NC is chemically stabilized for some cases with little quantity of diphenylamine. Flame temperature of single-base propellants is about $1590K^\circ$.

The second type is double-base propellants. The basic component of double-base propellants is Nitrocellulose (NC), like single-base propellants. Energetic nitrate esters are used for gelatinizing the NC. Some kind of chemicals like dibutylphthalate (DBP), diethylphthalate (DEP) and triacetin (TA) are used as plasticizers and stabilizers. Besides these chemicals, amines are added to double-base propellants as anti-aging materials. Flame temperature of double-base propellants can be about $2570-2690K^\circ$ depending on the ingredients. According to

requirements, burning rate catalyst, burning rate catalyst modifier, combustion instability suppressant, opacifier and flame suppressant can also be added to double-base propellants.

The last type is triple-base propellants. Triple-base propellants are similar to double-base propellants which are produced by adding crystalline nitroguanidine (NQ) to double-base propellants. Flame temperature of triple-base propellants is about 3050K°. Thermodynamic energy versus flame temperature relationship of homogeneous propellants is given in Figure 2.8 [27]:

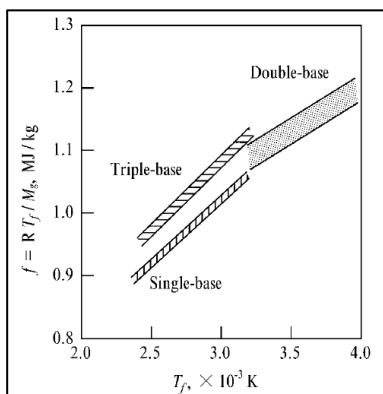


Figure 2.8 Thermodynamic energy vs flame temperature for homogeneous propellants [27]

2.3.2.2 Heterogeneous Propellants

Heterogeneous propellants have physically mixed ingredients and their physical structure is heterogeneous. Heterogeneous propellants are occurred by binding crystalline oxidizer particles in polymeric fuel matrix. AP and AN are the most commonly applied oxidizers, while HTPB, CTPB and PBAN are the most commonly used binders. Furthermore, aluminum particles can be added for increasing the energy of the propellant. According to requirements, curing agent burning rate catalyst, burning rate catalyst modifier, combustion instability suppressant, high energy additive, bonding agent and plasticizer can also be added to heterogeneous propellants.

Heterogeneous propellants can be categorized into two groups according to their oxidizer types. The first type is AP-composite propellants. Generally ammonium based chemicals like AP or AN, are used as oxidizer for this type of propellants. The most popular composite propellant is AP-HTPB propellant due to its high energy potential and good mechanical properties. Azido polymers also can be used with AP or AN to form composite propellant. Sometimes aluminum particles are added to increase the specific impulse. Current study focuses on AP-HTPB type of heterogeneous propellant.

Other type is nitramine composite propellants. This type of propellants includes crystalline nitramines like HMX and RDX as oxidizer. This type of propellants resembles AP-composite

propellants, because they are binded with polymeric binders. Advantage of nitramine composite propellants is reducing infrared emissions.

2.3.3 Solid Propellant Ingredients

A solid propellant can include a lot of chemical materials due to its desired composition. Solid propellants can be classified in two types according to their chemical composition and physical structure; homogeneous and heterogeneous propellants. These propellants mainly include fuels, oxidizers, binders, burning rate catalysts, plasticizers, curing agents and other additives.

2.3.3.1 Fuels

Fuel is one of two basic ingredients of a solid propellant which produce high energy during combustion. Generally, small metal particles (5-200 μm) are used as fuel in solid propellants. Metal fuel increases the density, combustion heat, combustion temperature and specific impulse of the propellant because of its high heat of reaction and density. Most widely used metal fuel is aluminum with mass fractions 12 to 22 percent [20]. Besides aluminum, boron is used as metal fuel. Boron is a high energy fuel with lighter weight than aluminum, but it cannot be burned very efficiently in combustion chamber. However, it can be combusted considerably efficient if it has very small particle size. Beryllium is another metal fuel applied in solid propellant applications. It can easily be burnt, but because of its toxicity beryllium is not preferred [11]. In the current study there is no fuel in the propellants. However, some experiments should be performed with propellants which include small aluminum particles as fuel for the future study.

2.3.3.2 Oxidizers

Oxidizer is another basic ingredient of solid propellant which produces high energy during combustion. Ammonium perchlorate (AP) is the most commonly used oxidizer in solid propellant applications [21]. The reasons of this fact are; its good properties like being compatible with other propellant ingredients, having good performance and quality and also being easily available [11]. Ammonium nitrate (AN) is another type of oxidizer. AN has low performance when compared with AP, but it can be preferred because of its low cost, smokeless exhaust [22]. Besides these two materials, potassium perchlorate (KP), potassium nitrate (KN) and ammonium dinitramine (ADN) are used as oxidizer. In the current study, AP is used as oxidizer in the propellants.

2.3.3.3 Binders

Binders are another type of material used in solid propellants. Binders' main goal is sticking the other ingredients of the propellant together. Because of this reason, binders are important for structural properties of the solid propellant. Therefore, binders can act as fuels because they oxidize during the combustion of the solid propellant. Since it has desirable mechanical properties and can be used with more solid quantity, Hydroxyl terminated polybutadiene

(HTPB) is the most widely used type of binder [23]. Other common types of binders are Carboxyl terminated polybutadiene (CTPB) and Nitrocellulose (NC). Glycidylazide polymers (GAP) are also sometimes used as binder because of their high energy potential, despite of their toxic decomposition products [24]. In the current study, HTPB is used as binder in the propellants.

2.3.3.4 Burning rate catalysts

Burning rate catalysts are important components of solid propellants because they are able to change the burning rate of the propellants and used for homogeneous propellants. There are many types of burning rate catalysts. Most common burning rate catalysts are compound burning rate catalysts, nanometal burning rate catalysts, nanometal oxide burning rate catalysts, ferrocene burning rate catalysts [25]. These catalysts increase the burning rate of the propellant. On the other hand, there are some catalysts such as lithium fluoride which decrease the burning rate of the propellant [11]. In current study, no burning rate catalysts are used.

2.3.3.5 Plasticizers

Plasticizers are needed for increasing processability of the solid homogeneous propellants. They also develop the mechanical features of the cured propellant. Plasticizers are liquid materials which have low molecular weight and low viscosity. Plasticizers also act as fuel in propellant composition. General types of plasticizers are esters and hydrocarbons [26]. In current study, there is no plasticizer.

2.3.3.6 Curing Agents

Curing agents are only used in composite solid propellants. They are useful for solidifying the binder of the propellant. Little quantity of curing agents can affect the reproducibility, aging and physical property of the propellant. HMDI (hexamethylenediisocyanide) , TDI (toluene-2,4-diisocyanide), IPDI (isophoronediiisocyanide), DDI (dimeryldiisocyanate) are widespread types of the curing agents [19]. In the current study, IPDI is used as curing agent for the Propellant 1 and DDI is as curing agent for Propellant 2.

2.3.3.7 Other Additives

According to the requirements of the propellant, there can be some other additives in the propellant. Little quantity of these additives are used in propellants. Some examples of the additives are opacifiers, bonding agents, desensitizing agents and organic agents [11].

CHAPTER 3

BURNING RATE MEASUREMENT METHODS

3.1 Introduction

An important aspect in the design of internal ballistics of solid rocket motor is the determination of propellant burning rate. Propellant burning rate can be determined by experimental methods. After literature survey, it is observed that five main burning rate measurement methods step forward. These are strand burner method, test motor firings, x-ray method, plasma capacitance gages and ultrasonic burning rate measurement method.

3.2 Strand Burner Method

Strand burners are mechanisms which measure the burning rate of the propellant linearly at controlled temperature and pressure. Small amount of propellant samples, which are called strands, are used for strand burner experiments. A strand resembles to stick whose burning surfaces are coated with inhibitor except one surface. The reason of this situation is providing cigarette type linear burning. Strand burners are connected to large volume tank which is called Crawford bomb. Crawford bomb is filled with inert gas which simulates the combustion pressure [28].

In the strand burner mechanism, propellant is burned from one surface of it and the burning time of the propellant is measured. Burning time can be measured by getting electrical signals from embedded wires [29], by using ultrasonic waves [30] or by optical technique [31]. Since the length of the propellant is known, the average burning rate of the propellant can be obtained by dividing the propellant length to burning time. A lot of strand burner tests are required to constitute a wide range of pressure versus burning rate information about the propellant which is very time consuming. The burning rate value is average burning rate for average pressure, so instantaneous measurement cannot be made by this method.



Figure 3.1 Crawford bomb mechanism with strand burner [32]

3.3 Test Motor Firings

Test motor firings are a good way of obtaining information about the motor performance. Therefore, test motor firings are good opportunity for getting information about propellant, especially burning rate of the propellant. Test motors can be reduced size or actual size depending on the condition. If reduced cost, practicability and many tests in limited time are needed, reduced size small test motors are used. Reduced size test motor firings are preferred for their good correlation with actual size motor burning rates. Reduced size test motor firings should be done when final propellant formulation is close for getting more accurate burning rate results and the temperature sensitivity of the chamber pressure. Different configurations of reduced size test motors can be applied due to the requirements. Ultimate burning rate measurement is made by firing actual size test motors. These test motors are generally statically fired for making burning rate measurement [33].

As in strand burner tests, average burning rate of propellant is calculated by dividing the propellant thickness to burning time.

$$R_b = \frac{W_b}{t} \quad (3.1)$$

Besides, a lot of test motor firings are required to constitute a wide range of pressure versus burn rate information about the propellant which is very time consuming. The burning rate value is average burning rate for average pressure, so instantaneous measurement cannot be made by this method.



Figure 3.2 Test motor firing [11]

3.4 X-Ray Method

Transmitted radiation (I) of X-ray is dependent to source radiation at 1 meter (I_o), distance from the source to the collection point (R_s), material attenuation coefficient (μ) and material path length (ℓ), as it can be seen in Equation (3.1).

$$I = \left(\frac{I_o}{R_s^2} \right) \cdot \exp \left[\sum_{i=1}^n \mu_i \ell_i \right] \quad (3.2)$$

There are two approaches for obtaining the burning surface location by using x-ray method.

In the first approach, whole change of transmitted radiation is linked to propellant thickness. X-ray is directed perpendicularly to the burning surface of the propellant in this approach. Less radiation attenuation is got when the propellant burns. By this way, a calibration curve can be obtained by making experiments with much propellant samples whose thicknesses are known.

In the second approach, x-ray is directed parallel to burning surface of the propellant. This approach resembles to medical x-ray visualization method. Radiation source, test material, energy converter and recording materials are used for this approach. By this way, propellant thickness change with time can be observed which allows burning rate calculation [33].

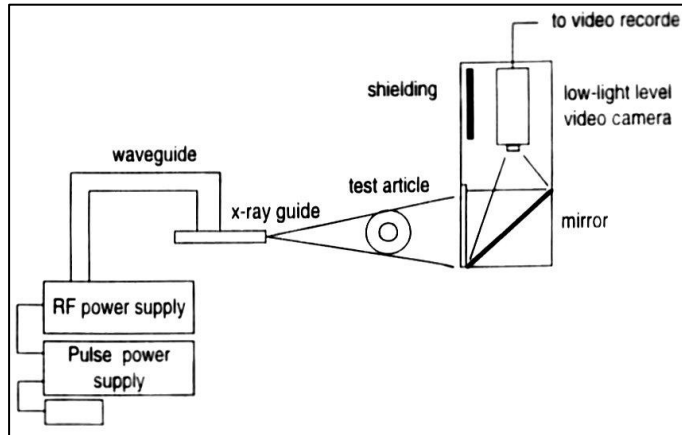


Figure 3.3 Real time radiography configuration [9]

X-ray method is an expensive method. In test area special protection from x-ray is needed. This method does not provide any numerical data, so that sensitive measurements cannot be performed.

3.5 Plasma Capacitance Gages

This method is based on change of electrical capacity with time. Material thickness between two electrodes is directly associated with the change of electrical capacity with time. In this burning rate measurement method, one of the electrodes is put on the case of the motor and the other one is the plasma of the hot combustion gases. Electrical capacity increases during the burning process. Propellant burning rate can be obtained by calibrating the polarization frequency of the electrodes.

This method can be applied to test motors and has low cost. On the other hand, the method needs more development to understand its physics and it can only be applied to non-aluminized propellants [1]. An example configuration of plasma capacitance gage application is given in Figure 3.4:

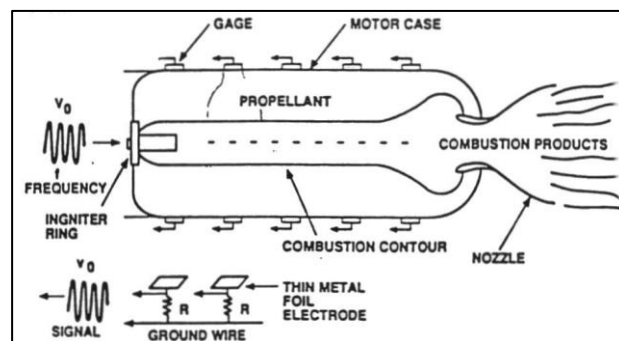


Figure 3.4 Plasma capacitance gage application configuration [34]

3.6 Ultrasonic Burning Rate Measurement Method

Ultrasonic burning rate measurement method is the main interest of this thesis study and it is the preferred and applied method. The reasons of these can be stated as;

- The system is not very expensive compared to previous systems explained in this chapter
- Instantaneous pressure versus burning rate data can be obtained in opposition to strand-burner and test motor firing
- Wide range of pressure versus burning rate data can be get for each test in opposition to strand-burner, test motor firing and x-ray method
- The system has high maturity advantage on x-ray method and plasma capacitance gage

Detailed information about this method is given in Chapter 4.

CHAPTER 4

ULTRASONIC BURNING RATE MEASUREMENT METHOD

4.1 Introduction

Ultrasound is the sound energy which is in the wave form and has high frequency over 20 kHz. This high frequency is over the human hearing range. Ultrasound wave has low wavelength so that it can easily reflect from any object's surface [35]. This property of the ultrasound wave makes the ultrasonic burning rate measurement method a non-intrusive measurement method.

The burning rate or the degradation rate of the energetic materials used in solid propulsion systems can be determined by applying experimental methods based on ultrasound wave propagation [36]. The primary usage aim of the ultrasonic burning rate measurement method is determining the burning rate of the propellant as a function of the pressure. Besides burning rate determination; propellant characterization is also possible by applying the ultrasonic burning rate measurement method [1].

The basis of ultrasonic burn rate measurement method resembles to standard emission/reception non-destructive techniques. Acoustic wave is emitted from a transducer which travels through the propellant. This acoustic wave reflects from the propellant's burning surface and returns to transducer. Acoustic wave reflects from the propellant's surface because of the acoustic impedance difference of the propellant and the combustion products. Displacement of the burning surface echo is detected by a special electronic device from start of the burning till the end of the burning. The transducer does not directly contact with the propellant. There is a hardening resin coupling material which is inserted between the propellant and the transducer. The coupling material protects the transducer from the severe chamber conditions and provides zero thickness measurement of the propellant. The acoustic impedance of the propellant and the coupling material must be adapted to each other to reduce the amplitude of the echo coming from the interface between the propellant and the coupling material [37].

Ultrasonic measurement method is applied for some objectives by some countries and agencies. The summary of these countries and agencies is given in Table 4.1:

Table 4.1 Summary of Countries and Agencies Applied Ultrasonic Measurement Method [1]

<i>Contry</i>	<i>Agency</i>	<i>Publishment Dates</i>	<i>Applications</i>
France	ONERA/ SNPE	1979 to present	<ul style="list-style-type: none"> - Uncured propellant burning rate - Propellant burning rate - Temperature sensitivity - Propellant response function - Erosive burning - Motor ballistics - Motor insulator erosion
Netherlands	TNO/ Delft University	1985 to present	<ul style="list-style-type: none"> - Laboratory hybrid rocket regression rate - Laboratory ramjet regression rates - Oxidizer burning rates
United States	AEDC	1990's	<ul style="list-style-type: none"> - Motor ballistics - Motor insulator erosion
	PSU	1980's to present	<ul style="list-style-type: none"> - Propellant burning rate - Laboratory hybrid regression rates - Propellant acoustic admittance
	UAH	1995 to present	<ul style="list-style-type: none"> - Propellant steady/ transient burning rate - Propellant temperature sensitivity - Propellant response function
	UIUC	1995 to present	<ul style="list-style-type: none"> - Propellant steady/ transient burning rate - Propellant response function
	VPI	1967	<ul style="list-style-type: none"> - Propellant burning rates
India	Vikaram	1990's	<ul style="list-style-type: none"> - Small motors burning rate
Sweden	SvenskaFlygmotor AB	1964	<ul style="list-style-type: none"> - Small hybrid motor regression rate

4.2 Measured Quantities

In constant volume chambers, ultrasonic burning rate measurement method is applied for determining pressure dependent burning rate. An experimental setup is needed to measure burning rate of the propellant with ultrasonic burn rate measurement method. In this experimental setup, signal travel time (τ) and chamber pressure (P_c) are measured for calculating the burning rate of the propellant.

4.2.1 Signal Travel Time

Experimental setup includes a constant volume chamber which is usually called 'closed bomb'. The details of the experimental setup and the experimental procedure are explained in Chapter 5. There is propellant inside the closed bomb which is attached to coupling material. The coupling

material is also attached to ultrasonic transducer which is outside of the closed bomb. The ultrasonic transducer emits acoustic wave through the coupling material and the propellant and receives two reflected signals. The first one is interface echo which occurs at the interface between the coupling material and the propellant. The second one is the surface echo coming from the burning surface of the propellant [38]. How the acoustic wave passes through and reflects from the materials is shown in Figure 4.1. The pulse (signal) sent from the transducer is a square pulse(signal); so that detection of the sent and received signal is easier. The schematic view of the sent and received signals is also given in Figure 4.2:

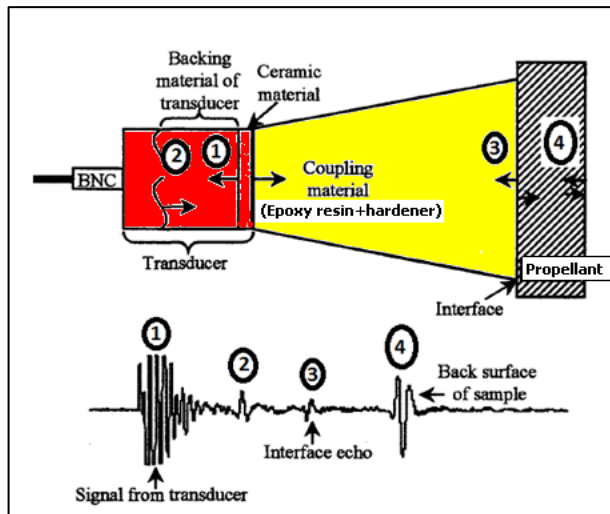


Figure 4.1 Acoustic wave and schematic view of signals [39]

Signal travel time is the time which is elapsed between sent and received signal. It is possible to calculate the remaining length of the burning propellant by measuring the difference between the signal travel time of the interface echo and the surface echo. In ultrasonic burning rate measurement method, measuring the signal travel time correctly is an important aspect.

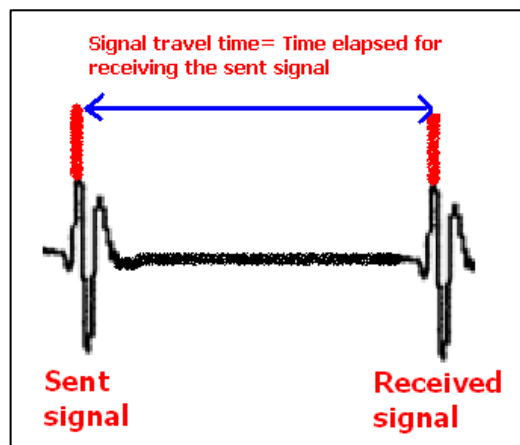


Figure 4.2 Signal travel time

4.2.2 Chamber Pressure

Ultrasonic burning rate measurement method provides instantaneous burning rate measurement with respect to pressure data simultaneously. Besides the signal travel time data, chamber pressure data are also collected. Since the burning rate is calculated as a function of chamber pressure instantly, the pressure must be measured during the test. Pressure sensors are used to measure the pressure of combustion chamber. Pressure sensor and ultrasonic transducer work simultaneously; so that, for every measured pressure value the burning rate data can be obtained.

4.2.3 Chamber Temperature

Mechanical wave velocity of the materials can change by the effect of temperature. Because of this reason, it can be thought that the combustion chamber temperature should be measured. However, in their study Traineau and Kuentzmann [42] showed that the effect of the temperature profile on mechanical wave velocity is very small. Furthermore, in their another study Traineau and Kuentzmann [40] state that the effect of the temperature profile can be neglected [40]. In the current study effect of temperature on mechanical wave velocity is neglected, too.

4.3 Burning Rate Calculation Method

In the combustion process of solid materials generally there exists a condensed phase and a gaseous products phase. The interface between these two phases is called the burning surface. The dispersion rate of the burning surface, or in other words, regression rate of the condensed phase is called burning rate. Due to its important effect on the performance, the cost of propulsive instruments and also for understanding the combustion process, knowing the burning rate of the propellant is very important and critical. Since there is no theory about predicting the burn rate of the propellants, burning rate is measured by experimental methods.

Burning rate of the propellant can be determined by dividing the time of burning to web thickness of the propellant. This method is applied for test motor static firings and strand burners. This type of burn rate is the average burning rate of the propellant for the average combustion pressure. It is assumed that the burning rate is only pressure dependent for solid rocket motors until 30 MPa chamber pressure. When this assumption is used, Vieille's law, which is given in Eq. (4.1) is applicable.

$$R_b = a.P_c^n \tag{4.1}$$

where R_b is the burn rate of the propellant, P_c is the chamber pressure, a and n are the empirical constants based on experimental measurements [33].

Burning rate of the propellant is defined only as a function of chamber pressure according to Vieille's law. In ultrasonic burn rate measurement method, burn rate of the propellant is

dependent to chamber pressure, mechanical wave velocity and time derivative of the chamber pressure because the measurement made by ultrasonic transducer is instantaneous.

Instantaneous burn rate (R_b) and the thickness of the burned propellant (W_b) can be calculated as function of reference mechanical wave velocity in the propellant ($C_{p,ref}$), chamber pressure (P_c), time of flight (τ), solid propellant wave velocity pressure variation coefficient (k_p), initial thickness of the propellant ($W_{p,ini}$), thickness of coupling material (W_c), reference mechanical wave velocity in the coupling material ($C_{c,ref}$), burning surface temperature (T_s), reference temperature (T_{ref}), thermal diffusivity (α) and coupling material wave velocity pressure variation coefficient (l_p) as in Eq. (4.2) and Eq. (4.3) [5]:

$$W_b(t) = \frac{C_{p,ref}}{2 \cdot (1 - k_p \cdot (P - P_{ref}))} \left\{ \frac{2W_{p,ini}}{C_{p,ref}} - \Delta\tau(t) + \frac{2W_c l_p \cdot (P - P_{ref})}{C_{c,ref}} \right\} \quad (4.2)$$

$$R_b(t) = \frac{C_{p,ref}}{2 \cdot (1 - k_p \cdot (P_c - P_{ref}))} \left\{ \frac{d\Delta\tau(t)}{dt} - \left[k_p \cdot \frac{\left(\frac{2W_{p,ini}}{C_{p,ref}} - \Delta\tau(t) + \frac{2W_c l_p \cdot (P_c - P_{ref})}{C_{c,ref}} \right)}{1 - k_p \cdot (P_c - P_{ref})} + \frac{2W_c l_p}{C_{c,ref}} \right] \cdot \frac{dP_c}{dt} \right\} \quad (4.3)$$

Steady-state burning assumption is made for getting the burning rate equation. Effect of temperature on mechanical wave velocity is also neglected in the same equation. The derivation of Eq. (4.3) is given in Appendix A.

4.4 Mechanical Wave Velocity

Mechanical wave velocity differs depending on the material in which the wave disperses. To make a correct burning rate measurement, mechanical wave velocity of the propellant and the coupling material should be determined correctly. Reference mechanical wave velocity (C_{ref}) is calculated as in Eq. (4.4) for any material:

$$C_{ref} = \frac{2 \cdot (W_2 - W_1)}{(\tau_2 - \tau_1)} \quad (4.4)$$

where **1** and **2** subscripts represent the different samples of the same material which have different lengths. Different size samples of the propellant and the coupling material are produced for applying Eq. (4.4). The main sample is cutted by lathe for getting cylindrical shaped samples with different sizes. The main sample and the other samples cutted with lathe are shown in Figure 4.3:



Figure 4.3 The main coupling material and the other samples cutted with lathe at different thicknesses (Test 1)

4.5 Effect of Pressure on Mechanical Wave Velocity

The mechanical wave velocity changes with respect to stress and the temperature distribution on the material. Mechanical wave velocity of the propellant is given in Eq. (4.5) as a function of temperature and the pressure:

$$\frac{C_{p,ref}}{C} = [1 - k_p \cdot (P - P_{ref})] [1 + k_t \cdot (T - T_{ref})] \quad (4.5)$$

As told before the effect of the temperature can be neglected [40]. In this study the effect of the temperature is also neglected. Eq. (4.5) is simplified as a function of the pressure in this condition:

$$\frac{C_{p,ref}}{C} = [1 - k_p \cdot (P - P_{ref})] \quad (4.6)$$

Although Eq. (4.5) and Eq. (4.6) are given for the propellant, they can be used for the coupling material, too. Any material's wave velocity pressure variation coefficient (k_p) is obtained by measuring the mechanical wave velocity for different pressure values. After this procedure, by using the data set ($C_{p,ref} / C_p$) vs. ($P - P_{ref}$) graph is drawn. The slope of this graph gives the pressure variation coefficient of the material.

4.6 Acoustic Impedance

Acoustic waves travel inside the materials because of the sound pressure. Acoustic waves disperse inside the solid materials, because atoms or molecules of the solids are elastically bonded. Acoustic impedance of materials is important for ultrasonic burning rate measurement method, since acoustic waves must pass through the materials with minimum energy loss. Conduction of acoustic waves between two materials, which have different acoustic impedances, causes acoustic energy loss. If the acoustic impedance difference between two materials is big, conduction of the sound wave becomes hard.

Acoustic impedance (Z) is multiplication of material density (ρ) and mechanical wave velocity (C) [43]. In this reference paper, impedances are given in $[\text{kg}/\text{m}^2.\text{s}]$ and they are not complex values. They are real values.

$$Z = \rho.C \quad (4.7)$$

Wave intensity of reflected wave from the interface of coupling material and propellant between coupling material is defined with reflection coefficient (Y). Reflection coefficient shows the ratio of reflected acoustic energy to total acoustic energy. Remaining acoustic energy is conducted from the coupling material to the propellant and defined with conduction coefficient (i).

$$Y = \left(\frac{Z_p - Z_c}{Z_p + Z_c} \right)^2 \quad (4.8)$$

$$i = 1 - Y \quad (4.9)$$

where subscript p stands for propellant and c for coupling material.

CHAPTER 5

EXPERIMENTAL SETUP AND PROCEDURE

5.1 Introduction

An experimental setup is prepared for performing ultrasonic burn rate measurement method experiments. This experimental setup includes mechanical and electrical parts. The basic parts of the experimental setup are listed below;

- Closed bomb
- Ultrasonic transducer
- Coupling material
- Propellant
- Inhibitor
- Pressure sensor
- Data acquisition system
- Nitrogen tanks
- Igniter

5.2 Closed Bomb Experimental Setup Configuration

Configuration of the experimental setup, which is prepared for burning tests, is given in Figure 5.1:

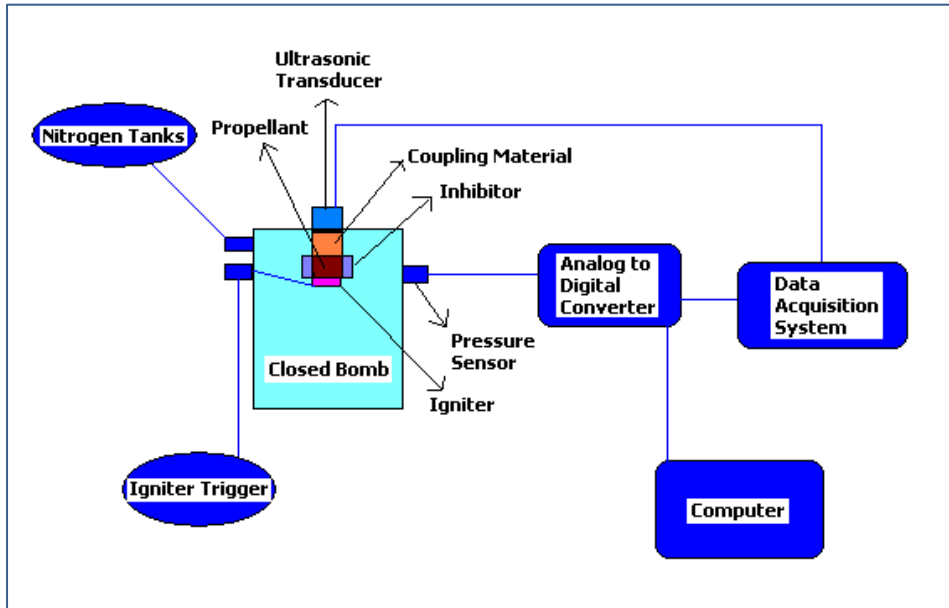


Figure 5.1 Experimental setup configuration [41]

5.2.1 Closed Bomb

Closed bomb is a metallic reservoir which can stand high pressures. Little amount of propellant is burned in closed bomb. The closed bomb, which is used in this experimental setup (Figure 5.2), is made of steel. It has 7 liters volume and can be adjusted to more little volumes. It has 750 mm length and 260 mm diameter. Maximum expected operation pressure (MEOP) of the experiments is 5000 Psi. However, the closed bomb of this experimental setup is designed to withstand up to 10000 Psi.

Due to safety concerns, structural and thermal analysis of closed bomb has been made. Hydrostatic pressure test has been performed to see closed bomb's anti-leakage and pressure resistance characteristics. There is a rupture disc on the closed bomb due to safety concerns, too. It opens and discharges the gas inside the closed bomb when the combustion pressure exceeds 5000 Psi.

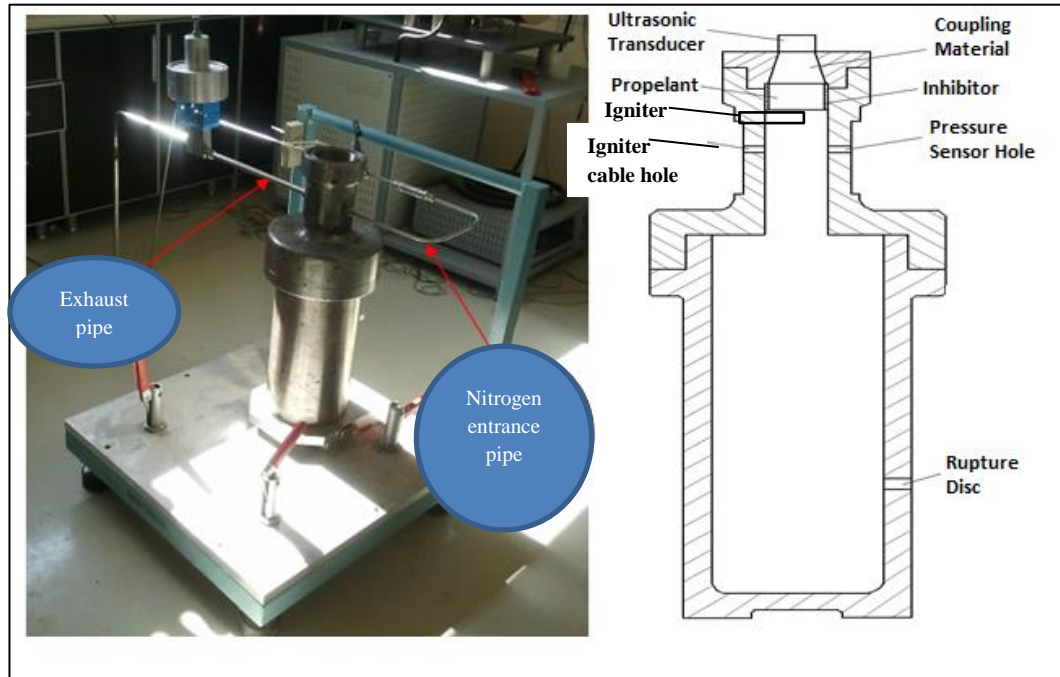


Figure 5.2 Closed bomb

5.2.2 Ultrasonic Transducer

Ultrasonic transducer is very important part of experimental setup. Ultrasonic signals are sent and received by ultrasonic transducer. By the help of the ultrasonic transducer, signal travel time is measured. In this experimental setup; 1 inch diameter Sofratest WC-100-1-X type ultrasonic transducer which has 1 MHz frequency is used. The ultrasonic transducer is connected to the data acquisition system with a BNC connector.

Ultrasonic transducer's another mission is pre-detection of propellant's and coupling material's physical properties. In this condition, referred physical properties are mechanical wave velocity and cavity in the materials. Same batch propellants or same batch coupling materials are thought to have similar mechanical wave velocities. After producing same batch propellants, mechanical wave velocities of them are measured. If their mechanical wave velocities are similar to each other, it can be decided that there is no problem about their production process. Furthermore, any cavity inside the propellant can cause difficulty for acoustic wave dispersion. If the return of sent signal can be detected properly, it is obvious that there is no cavity inside the propellant. The same procedures are valid for coupling material.

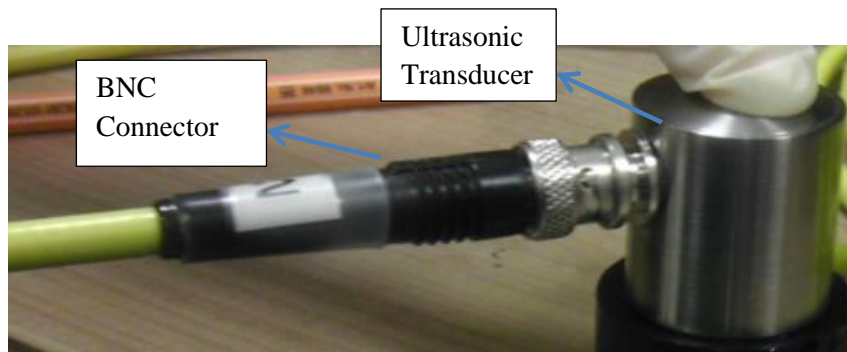


Figure 5.3 Ultrasonic transducer

5.2.3 Coupling Material

Coupling material is the material which is made of epoxy resin and hardener. Besides epoxy resin and hardener, SiO_2 is added for the aluminum including propellants' coupling material. The main function of the coupling material is protecting the ultrasonic transducer from the effects of hot combustion gases. It also creates a signal between the ultrasonic transducer's signal and propellant's reflected signal. Coupling materials are acoustically coupled with propellants and they have strong resistance to hot combustion gases. Preparation process of coupling material is explained in Section 5.3. In Figure 5.4 coupling materials with and without aluminum are showed before cutting process.



Figure 5.4 Coupling material; for propellants with aluminum (right), for propellants without aluminum (left)

Coupling materials can't be used with the shape seen in Figure 5.4, because in closed bomb they are used with smaller sizes. They are cut with lathe to give them their special shape. The coupling materials used in tests and the part where the coupling material is mounted are shown in Figure 5.5:

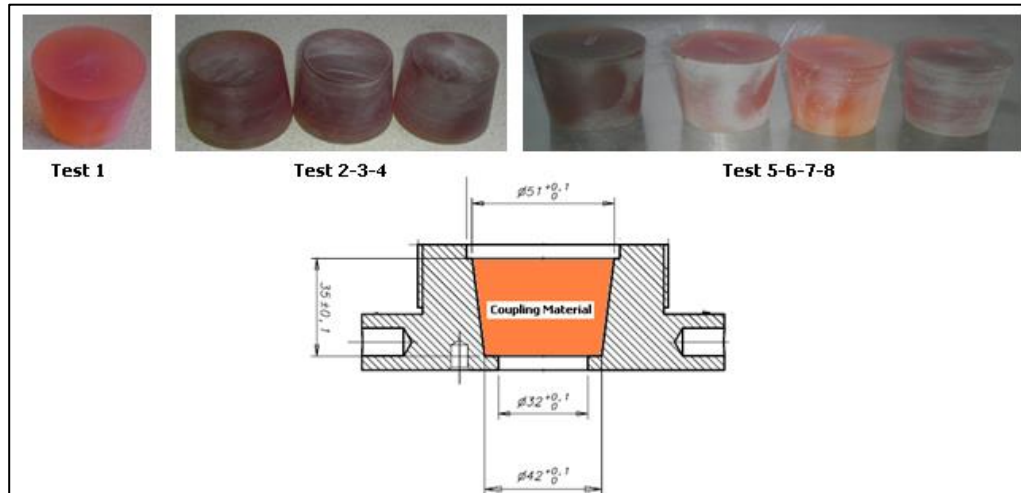


Figure 5.5 Coupling materials for each test (after cutting) and schematic view of their mounted area

Same type coupling material's three different batches are prepared for eight coupling materials. The first batch is used for Test 1, the second batch is used for Test 2-3-4 and the third batch is used for Test 5-6-7-8. All batches are produced with same chemical compounds. Only difference between them is production date. In other words, they are same materials produced at different time. The coupling materials used in the tests is coupling materials for the propellants without aluminum.

It should be emphasized that although coupling material for the propellants with aluminum is prepared, it can't be used in the test because there are big cavities inside this type of coupling material. During its mixing process the mixture gets hotter because of the SiO_2 in it. When it gets hotter it starts to swell and this causes cavities in the coupling material. To solve this problem, applying another material for SiO_2 and cooling the mixture during the mixing process should be made.

5.2.4 Propellant

Main interest of the current study is the burning rate of the solid propellants. Propellant is burnt inside the closed bomb. In the burning tests two different types of propellants are used. Both of the propellants are heterogeneous AP-composite propellants without aluminum. Their oxidizer is ammonium perchlorate (AP) and their binder is hydroxyl terminated polybutadiene (HTPB). For the first propellant, two different batches of propellants are prepared. Just like the coupling material; all batches are produced with same chemical compounds, only difference between them is production date. Test 1 is performed with the first propellant's first batch and Test 2-3-4 are performed with first propellant's second batch. For the second propellant, only one batch of propellant is prepared and Test 5-6-7-8 are performed with this propellant. Preparation process of coupling material is explained in Section 5.3.



Figure 5.6 Propellant samples for Test 5-6-7-8 (Propellant 2 Batch 1)

5.2.5 Inhibitor

A special inhibitor is prepared for these experiments. Inhibitor is made by mixing resin and hardener with a mass ratio 12.5 to 1. The main goal of the inhibitor is preventing the burning of lateral surfaces of the propellant. This is important because only bottom side of the propellant should burn for getting right signal travel time. Preparation process of inhibitor is explained in Section 5.3.

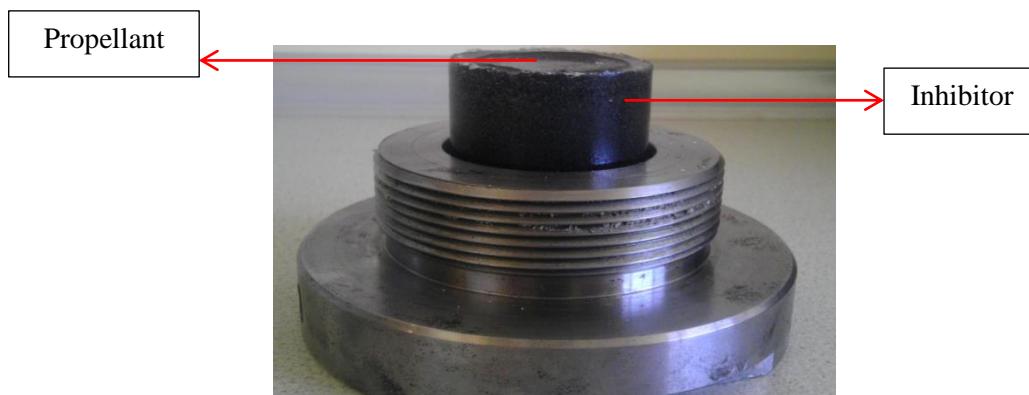


Figure 5.7 Inhibitor and propellant

5.2.6 Pressure Sensor

Pressure sensor is needed to measure the combustion chamber pressure. In this experimental setup, High-Pressure Sensor is used. This high pressure sensor can be used for ballistic pressure measurements ranging from 100 bars to 6000 bars. This type of sensor has lower mechanical and thermal stress and largely reduced surface pressure in the sealing part. The sensor has $\pm 1\%$ linearity. The measured results are screened in volts so; there is no need to voltage amplifier. Voltage values are converted to pressure data with the help of a conversion coefficient which is calculated before.

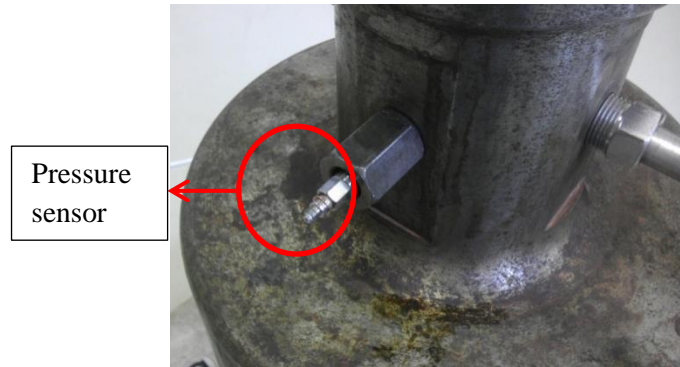


Figure 5.8 Pressure sensor

5.2.7 Data Acquisition System

High speed ultrasonic pulser receiver and acquisition system is used in the current study. This experimental setup's data acquisition system allows maximum 5 ultrasonic data collection cards. SFT4001 HPCI is the ultrasonic card used in the data acquisition system. Every card allows using 2 ultrasonic channels. For each channel, the signals are digitized and can be very rapidly transferred into PC memory via the PCI bus and DMA channel. Furthermore, every channel measures signal amplitude and signal time with two programmable gates. However, the system is suitable for sampling rates up to 10000 Hz, the ultrasonic cards used in system are limited to 5000 Hz measurement frequency. ACL 8112PG A/D card is used for pressure data collection. This type of card allows using 2 channels. It is a 12 bits card.



Figure 5.9 Data acquisition system

5.2.8 Nitrogen Tanks

Nitrogen gas is used to pressurize the closed bomb before the test. In order to get desired pressure value before the burning test, the closed bomb is filled with nitrogen gas. Besides, for leaktightness test little amount of nitrogen is filled just before the burning test. Nitrogen is

provided from nitrogen tanks which allow adjusting the filling pressure. Nitrogen gas is exhausted with combustion gases by exhaust pipes. In current experiments parallel connected 15 nitrogen tanks are used. They are filled up to 230 bar pressure. Maximum pressure output from the tanks is 200 bar and generally the closed bomb filled with 70 bar for the initial pressure.



Figure 5.10 Nitrogen tanks

5.2.9 Igniter

The igniter used in the experimental setup is a special igniter, which is located into velostat bag and has pyrotechnique charge. Velostat is a material which is used for packaging materials and it is impregnated with carbon black to make it electrically conductive. This igniter is glued to inhibitor's surface with a special adhesive. The igniter is ignited with a trigger, by giving 100 mA current to start burning of the propellant.

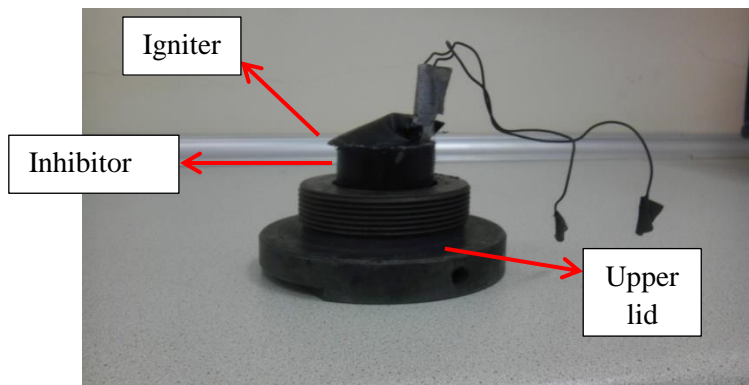


Figure 5.11 Igniter

5.3 Closed Bomb Test Experimental Procedure

In this section experimental procedure for closed bomb ultrasonic burning rate measurement test is explained step by step;

- **Propellant preparation:** Composite propellant is prepared by mixing, pouring into cylindrical molds and curing in an oven. The molds are cylindrical and have 40 mm diameter. The lengths of molds are different from each other and have 19-20-21-22-23-24-25 mm lengths. After curing, propellants are removed from the molds. Final condition of the propellant is shown in Figure 5.6. Two different types of propellants are produced by this method and used in the tests. Their difference comes from the quantity of the chemical compounds used. Same type of propellant can be produced at different times which are different batches of the same propellant. In the current study, Propellant 1 has two different batches; however, Propellant 2 has single batch.
- **Coupling material preparation:** Coupling material consists of epoxy resin and hardener. In the current study, Araldite DBF epoxy resin and HY 951 hardener are the ingredients of the coupling material. There is 11 to 1 mass ratio between epoxy resin and the hardener. After preparing the ingredients, they should be mixed in a pot for 5 minutes. Then, the mixture poured into a mold. For removing the air in the mixture, it is vacuumed at 12 mmHg pressure for 15 minutes. The vacuumed mixture should be cured in a curing oven at 27°C for 24 hours. After curing operation, coupling material is taken out of the mold (Figure 5.4). For using the coupling material in the tests, it should be cut into a truncated cone shape by using a lathe. The final product of coupling material and its shape is given in Figure 5.5.
- **Thickness measurement of propellant and coupling material:** The thickness of the propellant and the coupling material is measured with caliper and the measurements are recorded.
- **Reference mechanical wave velocity measurement and cavity control:** After thickness measurement, cavity control is made to propellant and coupling material with an ultrasonic transducer. If the return of sent signal can be detected properly, there is no cavity. Besides, the propellant and coupling material's reference mechanical wave velocity is measured with ultrasonic transducer to provide input for burning rate calculation.
- **Bonding operations:** There are two bonding operations. The first operation is bonding of the coupling material to upper lid of closed bomb. EA 934 adhesive is used for

bonding coupling material to upper lid of closed bomb. After that, the second operation, which is bonding the propellant to the coupling material, is applied. Araldite Rapid adhesive is used in this operation.

- **Bond Line control:** Ultrasonic transducer (U.T.) is used to control bond line quality. Acoustic wave is sent to coupling material which is on the upper lid of closed bomb. While the wave passes through to coupling material, some of it reflects back from the coupling material-propellant interface and the remaining part passes through the propellant and reflects back from propellant's surface. If the reflected two signals from the coupling material-propellant interface and propellant surface can be seen clearly, this means that bonding operations are successful. The schematic view of sticking control position is given in Figure 5.12.

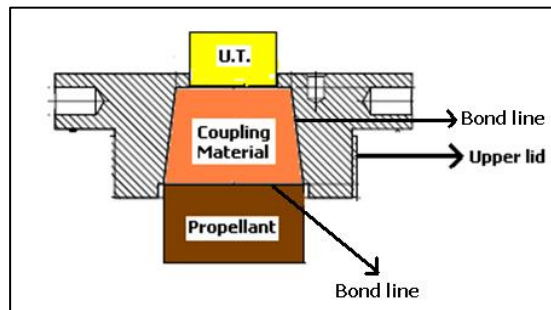


Figure 5.12 Propellant and coupling material after sticking operations and schematic view of sticking control position

- **Inhibitor preparation:** Inhibitor is made of resin and hardener. In the current study, Araldite CY208 resin and HY 956 hardener are used with 12.5 to 1 mass ratio. They are mixed in a pot for 5 minutes. After the mixing operation, the inhibitor is poured into a mold which contains the propellant. Propellant's burning surface is covered with a sticky tape to prevent it from inhibitor. Only lateral surface of the propellant is filled with inhibitor. After pouring operation, the inhibitor is cured for minimum 24 hours in a curing oven at 27°. Final configuration of propellant and inhibitor can be seen in Figure 5.7.
- **Igniter placement:** Igniter of the system is put on the burning surface of the propellant and bonded to inhibitor. Araldite Rapid adhesive is used for bonding igniter to inhibitor. In Figure 5.11 igniter and inhibitor can be seen clearly.
- **Closed bomb assembling:** After placing the igniter, the upper lid of the closed bomb is ready for assembly. In Figure 5.13 schematic view of, upper lid and the materials mounted in it, is shown.

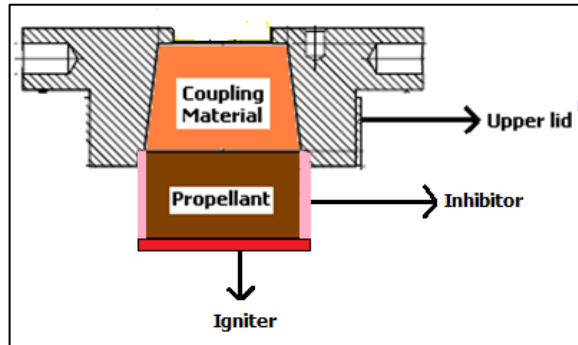


Figure 5.13 Schematic view of upper lid before assembling on closed bomb

- Upper lid is mounted on the closed bomb. After that, pressure sensor is assembled. Next operation is getting the cables of the igniter out of the closed bomb through a glass to metal sealed adaptor and closing the igniter cable hole. The last operation is mounting the ultrasonic transducer on the upper lid. The final configuration of the closed bomb after the assembly operations is given in Figure 5.14:

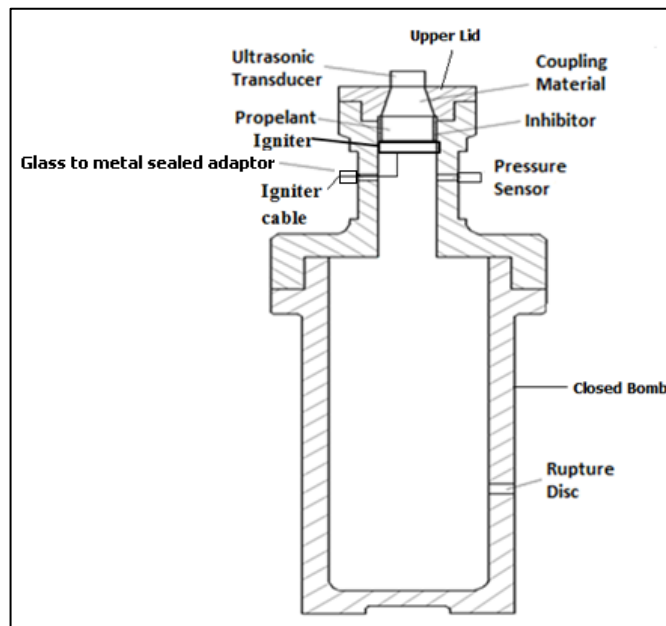


Figure 5.14 Final configuration of the closed bomb

- **Anti-leakage test:** After the assembly of the closed bomb an anti-leakage test is performed. It is pressurized with nitrogen gas up to 100 Psi and connection points are checked with foam. If there is any leakage, reassembly of the leakage point is performed until no leakage assured.

- **Initial pressure adjustment:** After leakage test of the closed bomb, it is pressurized with nitrogen gas to initial test pressure.
- **Getting ready for the ignition:** After pressurizing the closed bomb to its initial pressure, last adjustments should be made before the ignition. On software control screen, gate position adjustment and gain quantity determination are performed before the ignition. Adjustment on the screen of computer before the test is given in Figure 5.15:



Figure 5.15 Adjustment screen

- **Ignition:** Finally, 100 mA ignition signal is applied for 2 seconds and the propellant burns.
- **Data collection:** During the burning of the propellant, signal travel time (τ) and combustion pressure (P_c) versus time data are collected.
- **Burning rate calculation:** Burning rate of the propellant is calculated by using the collected data and the coefficients which are determined before the test

5.4 Water Column Experimental Setup and Its Procedure

Water column experimental setup is a plexiglas, 100 mm length cylindrical apparatus. Before the burning tests, some tests are performed with water column experiment setup for affirming the ultrasonic transducer and data acquisition system. In other words, water column experimental setup is just for affirmation the ultrasonic transducer and the data acquisition

system before the main burning tests. Working principle of water column experiment setup can be summarized as follows;

- The piston's moving system is conducted to a gas supplier (generally nitrogen gas tube).
- When the valve is opened, nitrogen gas enters into the piston's moving system, the piston and the cylinder part inside the column move to left.
- The transparent pipe's open side is put in a water bucket.
- Since the cylinder part moves to left, water is sucked by transparent pipe inside column.
- By the help of the ultrasonic transducer, acoustic waves are emitted into the column.
- Then valve is closed, nitrogen gas discharges from the pistons moving system, the piston and the cylinder part inside the column move right.
- Since the cylinder part moves to right, water is discharged by transparent pipe inside column.
- The discharge of all of the water represents burning of a cylindrical propellant from one side.
- During the discharge of the water, signal travel time of the signals emitted into water is collected by data acquisition system.

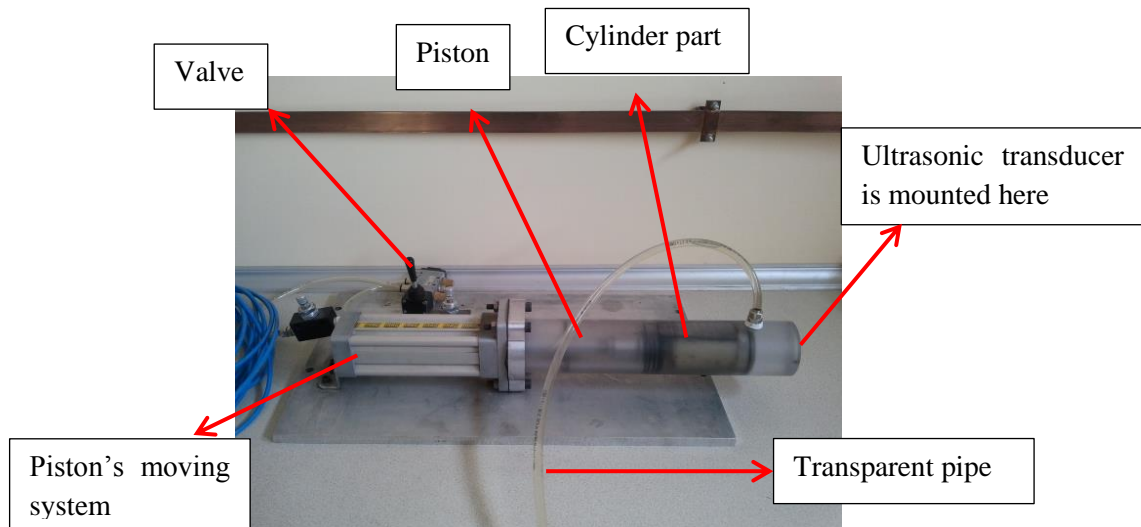


Figure 5.16 Water column experiment setup

Affirmation of the ultrasonic transducer and the data collection system is made by calculating the thickness of the water inside the column and comparing it with the measured thickness of the water inside the water column. Results of this test are given in Section 7.2.

CHAPTER 6

UNCERTAINTY ANALYSIS

6.1 Introduction

In this study burning rate of the propellants are measured with ultrasonic burning rate measurement method. The results of the tests are compared with burning rate results of the test motor firings. In order to have meaningful results, an uncertainty analyses are performed for ultrasonic burning rate measurement and test motor firing methods. The uncertainty analysis study, which is made in University of Alabama, is taken as a model in the current study [44]. In that study it is told that the total uncertainty is formed of bias limit and precision limit. Bias limit is the systematic or constant part of the total uncertainty while precision limit is the random part of the total uncertainty. Total uncertainty is given in Eq. (6.1) [44]:

$$U = \sqrt{B^2 + P^2} \quad (6.1)$$

where U is the total uncertainty, B is bias limit and P is precision limit.

After determining the uncertainty of the parameters which affect the burning rate of the propellant, Monte Carlo simulation [44] is applied to determine distribution of the burning rate. By taking into account the defined uncertainties, random values of the parameters are produced. Random burning rates are calculated by using random parameters, in 3σ standard deviation. For every pressure point 10000 iterations are performed and 10000 random burning rates are generated.

6.2 Uncertainty Analysis of Ultrasonic Burning Rate Measurement Method

In the burning rate calculation equation Eq. (4.3) it can be seen that there are 8 parameters affecting the burning rate of the propellant. These parameters are, chamber pressure (P_c), signal travel time (τ), initial thickness of the propellant ($W_{p,ini}$), thickness of coupling material (W_c), reference mechanical wave velocity in the propellant ($C_{p,ref}$), reference mechanical wave velocity in the coupling material ($C_{c,ref}$), solid propellant wave velocity pressure variation coefficient (k_p) and coupling material wave velocity pressure variation coefficient (l_p).

Some of these parameters obtained by direct measurement (P_c , τ , $W_{p,ini}$, W_c) and some of them are obtained by calculation ($C_{p,ref}$, $C_{c,ref}$, k_p , l_p). Firstly, uncertainty of parameters which are obtained by direct measurement is calculated and then uncertainty of parameters which are obtained by calculation is determined.

For pressure measurements High-Pressure sensor is used. There are two bias limits determining the uncertainty of the combustion pressure (P_c). The first one is error of the pressure sensor itself. This sensor's accuracy is found about 0.014% at full scale. Full scale of the sensor is 8702 Psi (600 bars). This means 1.22 Psi error. Another error comes from calibration of sensor. Dead weight tester is used for the calibration of sensors. Dead weight tester has 0.05% reading error. Dead weight tests are made with an average of 2500 Psi pressure; so, the error is 1.25 Psi. The precision limit comes from the digitization of the data acquisition system and random pressure measurements. Digitization error of the data acquisition system is 4.25 Psi. It is determined by analogy from another uncertainty analysis study, in which similar data acquisition system is used [45]. Furthermore, random pressure measurements give 7.25 Psi error. Total uncertainty of the pressure can be calculated as:

$$U = \sqrt{1.22^2 + 1.25^2 + 4.25^2 + 7.25^2} = 8.6 \text{ Psi}$$

Another parameter, which is directly measured, is signal travel time (τ). Total uncertainty of signal travel time is determined by taking into account the digitization error of the data acquisition error and random measurement error. Digitization error of the data acquisition system is 0.02 μ s. Just like in pressure case; it is determined by analogy from another uncertainty analysis study, in which similar data acquisition system is used [45]. The error coming from the random measurements is 0.135 μ s. Total uncertainty of the signal travel time is:

$$U = \sqrt{0.02^2 + 0.135^2} = 0.14 \mu\text{s}$$

Initial thickness of the propellant ($W_{p,ini}$) is another directly measured parameter. There are two error sources of initial thickness of the propellant which are non-perpendicularity of the propellant surface and random thickness measurement error. Non-perpendicularity of the propellant surface must be less than 1 degree. 1 degree non-perpendicularity means 0.70 mm difference in length for the 40 mm propellant diameter. Besides, random thickness measurements are made with caliper and 0.35 mm error is found. Total uncertainty of the initial thickness of the propellant can be found as:

$$U = \sqrt{0.70^2 + 0.35^2} = 0.78 \text{ mm}$$

The last directly measured parameter is thickness of the coupling material (W_c). There are two error sources of initial thickness of the coupling material which are non-perpendicularity of the propellant surface and random thickness measurement error. Non-perpendicularity of the coupling material surface must be less than 1 degree. 1 degree non-perpendicularity means 0.89 mm difference in length for the 51 mm coupling material diameter. Besides, random thickness measurements are made with caliper and 0.083 mm error is found. Total uncertainty of the initial thickness of the propellant can be found as:

$$U = \sqrt{0.89^2 + 0.083^2} = 0.894 \text{ mm}$$

The uncertainty of the calculated parameters is determined by the Eq. (6.2) [44]:

$$U_x^2 = \sum_{k=1}^N \left(\frac{\partial x}{\partial a_k} \right)^2 P_{a_k}^2 + \sum_{k=1}^N \left(\frac{\partial x}{\partial a_k} \right)^2 B_{a_k}^2 + \sum_{k=1}^N \left(\frac{\partial x}{\partial b_k} \right)^2 P_{b_k}^2 + \sum_{k=1}^N \left(\frac{\partial x}{\partial b_k} \right)^2 B_{b_k}^2 + 2 \sum_{k=1}^{N-1} \sum_{i=k+1}^N \left(\frac{\partial x}{\partial a_k} \right) \left(\frac{\partial x}{\partial a_i} \right) B_{a_i a_k} + 2 \sum_{k=1}^{N-1} \sum_{i=k+1}^N \left(\frac{\partial x}{\partial a_k} \right) \left(\frac{\partial x}{\partial a_i} \right) B_{b_i b_k} \quad (6.2)$$

In this equation; x is the calculated parameter, a and b are two directly measured parameters to which x is dependent, U is total uncertainty, P is precision limit and B is bias limit.

Reference mechanical wave velocity in the propellant ($C_{p,ref}$) is a calculated parameter. By looking Eq. (4.4), it can easily be said that reference mechanical wave velocity in the propellant is dependent to initial thickness of the propellant ($W_{p,ini}$) and signal travel time (τ). By using Eq. (6.2) total uncertainty of the reference mechanical wave velocity in the propellant is found 25.53 m/s.

Uncertainty of the reference mechanical wave velocity in the coupling material ($C_{c,ref}$) is calculated very similar to reference mechanical wave velocity in the propellant. Again by looking Eq. (4.4), it can be understood that reference mechanical wave velocity in the coupling material is dependent to thickness of the coupling material (W_c) and signal travel time (τ). By using Eq. (6.2) total uncertainty of the reference mechanical wave velocity in the coupling material is found 27.62 m/s.

Solid propellant wave velocity pressure variation coefficient (k_p) is a function of chamber pressure (P_c) and signal travel time (τ). Total uncertainty of solid propellant wave velocity pressure variation coefficient is found by applying Eq. (6.2). The value of the total uncertainty of solid propellant wave velocity pressure variation coefficient is calculated as $1.61 \times 10^{-6} \text{ Mpa}^{-1}$.

The last calculated parameter is coupling material wave velocity pressure variation coefficient (l_p). Like solid propellant wave velocity pressure variation coefficient, coupling material wave velocity pressure variation coefficient is a function of chamber pressure (P_c) and signal travel time (τ). By using Eq. (6.2) the total uncertainty of coupling material wave velocity pressure variation coefficient is found as $5.91 \times 10^{-6} \text{ Mpa}^{-1}$.

Table 6.1 Uncertainties of Ultrasonic Burning Rate Measurement Method

	P_c [Psi]	τ [μ s]	$W_{p,ini}$ [mm]	W_c [mm]	$C_{p,ref}$ [m/s]	$C_{c,ref}$ [m/s]	k_p [1/MPa]	I_p [1/MPa]
Uncertainty	± 8.6	± 0.14	± 0.78	± 0.894	± 25.53	± 27.62	$\pm 1.61 \times 10^{-6}$	$\pm 5.91 \times 10^{-6}$

After determining the uncertainties, direct Monte-Carlo simulation is applied to obtain burning rate variation. The results show that relative uncertainty of the burning rates changes from 2.68% to 2.76%. Normalized pressure versus normalized burning rate with variations, which is obtained from the simulation, is shown in Figure 6.1. Normalization is done by dividing the pressure values to the maximum pressure obtained through all tests and dividing the burning rate values to the maximum burning rate obtained through all tests.

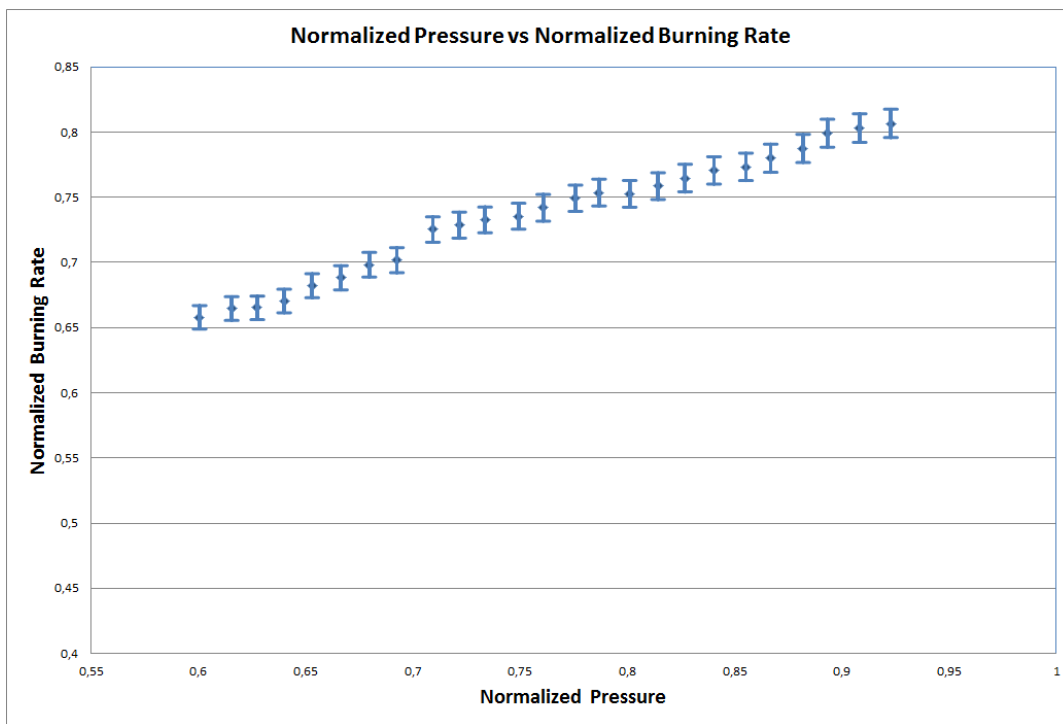


Figure 6.1 Burning rate of ultrasonic method with variations

6.3 Uncertainty Analysis of Test Motor Firing Method

As told in Section 3.3 before, average burning rate is obtained for average chamber pressure in the test motors. In the burning rate calculation equation of the test motors (Eq. 3.1), it can be seen that there are 2 parameters affecting the burning rate of the propellant. These parameters are, burnt web thickness of propellant (W_b) and burning time (t_b). These two parameters are obtained by direct measurement.

Propellant web thickness of the test motor (W_b) is obtained by measurements made with caliper. The uncertainty of the propellant web thickness is determined by the measurement error of the caliper itself and random error coming from random measurements. The caliper has 0.01 mm measurement accuracy. As a result of random measurements of the web thickness, 0.13 mm error is obtained. Total uncertainty of the web thickness of the propellant is found as:

$$U = \sqrt{0.13^2 + 0.01^2} = 0.13 \text{ mm}$$

Burning time (t_b) is another parameter which affects the burning rate uncertainty of the test motor. In the test motors, burning time is defined as the time from the 10% maximum of the pressure (or thrust) to web burnout. Web burnout is determined by taking the aft tangent-bisector point on the pressure-time (or thrust-time) curve [11]. These definitions are given in Figure 6.2:

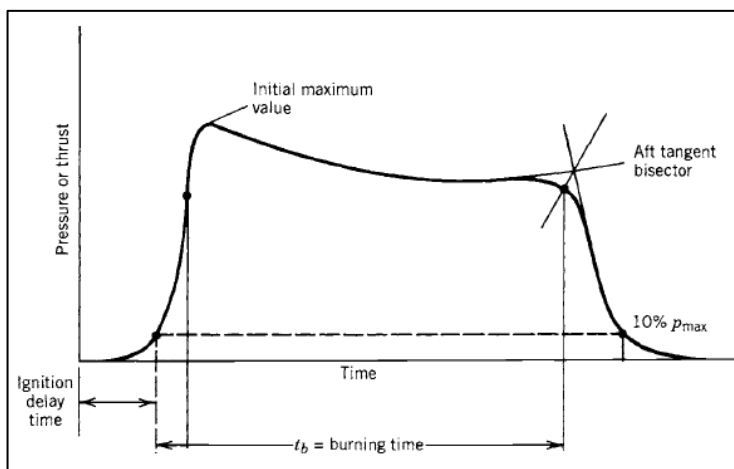


Figure 6.2 Burning time for test motors [11]

Random burning time is determined from the pressure-time curve and 0.06 seconds error is found for the test motor firing. Also the data collection system has 0.00025 seconds error itself. Total uncertainty of the initial thickness of the propellant can be found as;

$$U = \sqrt{0.06^2 + 0.00025^2} = 0.06 \text{ s}$$

The uncertainties of test motor are given in Table 6.2:

Table 6.2 Uncertainties of Ultrasonic Burning Rate Measurement Method

	W_b [mm]	t_b [s]
Uncertainty	± 0.13	± 0.06

As in the ultrasonic burning rate measurement method, direct Monte-Carlo simulation is applied for test motor to obtain burning rate variation after determining the uncertainties. The results show that relative uncertainty of the burning rates changes from 5.76% to 6.13%. Normalized pressure versus normalized burning rate with variations, which is obtained from the simulation, is shown in Figure 6.3. Normalization is done by dividing the pressure values to the maximum pressure obtained through all tests and dividing the burning rate values to the maximum burning rate obtained through all tests.

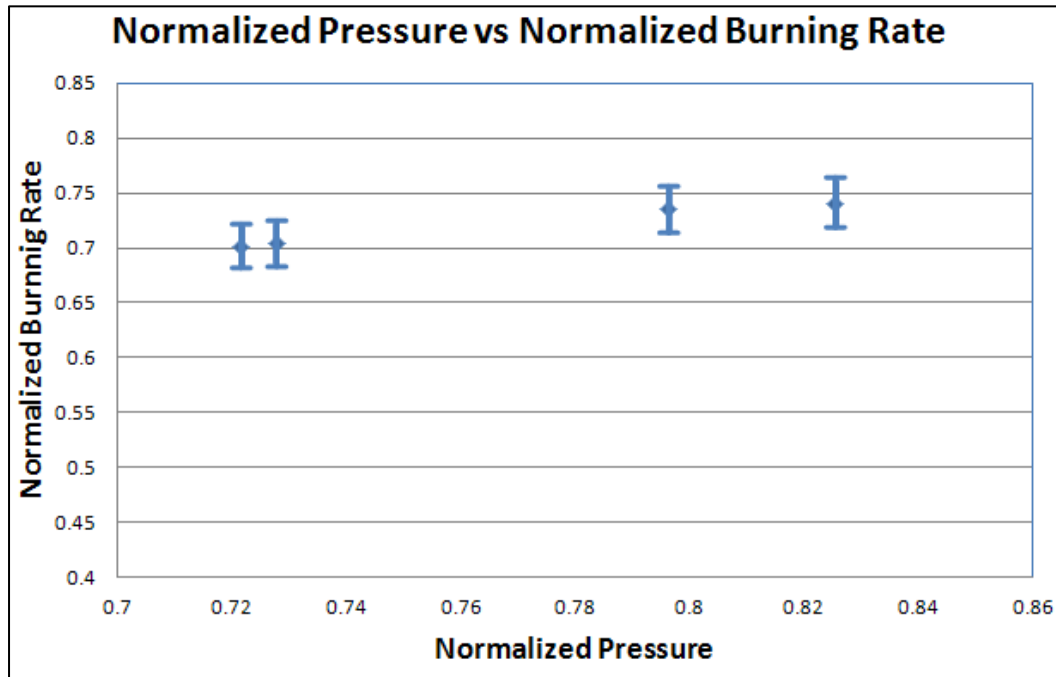


Figure 6.3 Burning rate of test motor with variations

Test motor firing has maximum 6.13% uncertainty since ultrasonic burning rate measurement method has maximum 2.76% uncertainty. These results show that ultrasonic burning rate measurement method has lower uncertainty than the test motor firings. It can be said that ultrasonic burning rate measurement method is more accurate than the test motor firing. Furthermore, the burning rates obtained from the ultrasonic burning rate measurement method and test motor firings compared in Chapter 7. According to uncertainty analysis, up to 8.89% difference (total of the uncertainties) between these methods is acceptable.

CHAPTER 7

RESULTS

7.1 Description of the Test Cases

In this study, 8 different burning rate measurement tests are performed. In tests two different propellant formulations, Propellant 1 and Propellant 2, are used which do not include aluminum. Two different batches are produced for the Propellant 1 although single batch is used for Propellant 2. Besides, three different batches of the same coupling material are prepared for the tests. Types and batches of the propellants and coupling materials are shown in Table 7.1

Table 7.1 Test Case Descriptions

Test No	Propellant No/ Batch No of that Propellant	Coupling Material No/ Batch No of that Coupling Material
1	Propellant 1 / Batch 1	Coupling Material 1 / Batch 1
2	Propellant 1 / Batch 2	Coupling Material 1 / Batch 2
3	Propellant 1 / Batch 2	Coupling Material 1 / Batch 2
4	Propellant 1 / Batch 2	Coupling Material 1 / Batch 2
5	Propellant 2 / Batch 1	Coupling Material 1 / Batch 3
6	Propellant 2 / Batch 1	Coupling Material 1 / Batch 3
7	Propellant 2 / Batch 1	Coupling Material 1 / Batch 3
8	Propellant 2 / Batch 1	Coupling Material 1 / Batch 3

7.2 Water Column Experimental Setup Results

Signal travel time versus time graph is shown in Figure 7.1 for the first water column experiment.

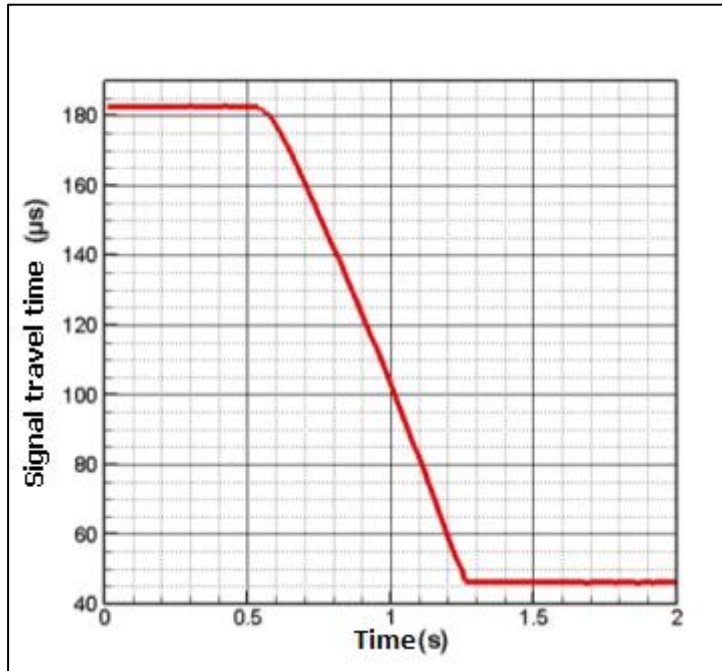


Figure 7.1 Signal travel time versus time (first water column test)

As it can be seen in the graph, data collection time is greater than the test time, because all of the test data is wanted to be collected. Actually, test starts at 0.59 second which is the start time of decrease in the graph and test finishes at 1.26 second which is the finish time of decrease in the graph. 5 tests are performed with water column experimental setup. By using Eq. (4.4), web thickness of the water is calculated and compared with measured thickness.

Table 7.2 Web Thickness of the Water

Test Number	Time of Flight [μ s]	Mechanical Wave Velocity in Water [m/s]	Measured Web Thickness of Water [mm]	Calculated Web Thickness of Water [mm]	Difference [%]
1	136.092	1484	100	100.98	0.98
2	136.051	1484	100	100.95	0.95
3	136.063	1484	100	100.96	0.96
4	136.115	1484	100	101.00	1
5	136.103	1484	100	100.99	0.99

There is average 0.98% difference between the calculated and measured web thickness of the water. It is thought that this difference is acceptable and ultrasonic transducer and data acquisition system can be used.

7.3 Reference Mechanical Wave Velocity

For the all test cases, the reference mechanical wave velocity of propellant and coupling material are calculated by using Eq. (4.4). The reason of calculating reference mechanical wave velocity is providing input for burning rate calculations. As it can obviously be seen in Eq. (4.3), reference mechanical wave velocity affects the burning rate of the propellants.

Table 7.3 Reference Mechanical Wave Velocities

Test No	Reference Mechanical Wave Velocity of Coupling Material [m/s]	Reference Mechanical Wave Velocity of Propellant [m/s]
Test 1	2620	1890
Test 2	2624	1893
Test 3	2621	1895
Test 4	2616	1896
Test 5	2618	1891
Test 6	2623	1890
Test 7	2617	1885
Test 8	2621	1893

7.4 Acoustic Impedance

Acoustic impedance of propellant and coupling material is calculated by using Equation (4.7). Besides acoustic impedance, reflected and conducted energy are determined for all test cases by the help of Eq. (4.8) and Eq. (4.9). Acoustic impedance and the amount of energy conducted from coupling material to the propellant are tabulated. These results show that the acoustic impedance of the propellant and the coupling material is compatible.

Table 7.4 Acoustic impedance and conducted energy for all tests

Test 1		
	Coupling Material	Propellant
ρ [kg/m ³]	1102	1704
C [m/s]	2620	1890
Z [kg/m ² /s]	2887240	3220560
Conducted energy [%]	99.702	
Test 2		
	Coupling Material	Propellant
ρ [kg/m ³]	1108	1718
C [m/s]	2624	1893
Z [kg/m ² /s]	2907392	3252174
Conducted energy [%]	99.687	
Test 3		
	Coupling Material	Propellant
ρ [kg/m ³]	1108	1718
C [m/s]	2621	1895
Z [kg/m ² /s]	2904068	3255610
Conducted energy [%]	99.674	
Test 4		
	Coupling Material	Propellant
ρ [kg/m ³]	1108	1718
C [m/s]	2616	1896
Z [kg/m ² /s]	2898528	3257328
Conducted energy [%]	99.660	
Test 5		
	Coupling Material	Propellant
ρ [kg/m ³]	1105	1695
C [m/s]	2618	1891
Z [kg/m ² /s]	2892890	3205245
Conducted energy [%]	99.738	
Test 6		
	Coupling Material	Propellant
ρ [kg/m ³]	1105	1695
C [m/s]	2623	1890
Z [kg/m ² /s]	2898415	3203550
Conducted energy [%]	99.750	
Test 7		
	Coupling Material	Propellant
ρ [kg/m ³]	1105	1695
C [m/s]	2617	1885
Z [kg/m ² /s]	2891785	3195075
Conducted energy [%]	99.752	
Test 8		
	Coupling Material	Propellant
ρ [kg/m ³]	1105	1695
C [m/s]	2621	1893
Z [kg/m ² /s]	2896205	3208635
Conducted energy [%]	99.738	

7.5 Pressure Variation Coefficients

For the test cases, pressure variation coefficients are obtained from the mechanical wave velocity change of materials depending on pressure increase. To perform this operation, closed bomb is pressurized with inert gas (nitrogen gas) to increase the pressure step by step. Then, the coupling material and propellant's signal travel time is measured. After measuring the signal time travel, mechanical wave velocities are calculated. The measurements are tabulated in Table 7.5.

Table 7.5 Pressure and signal travel time

Pressure [MPa]	Signal Travel Time of Coupling Material [μ s]	Signal Travel Time of Propellant [μ s]
0.1	27.817	53.383
3.4	27.700	53.517
4.3	27.683	53.467
5.5	27.650	53.400
7.0	27.650	53.333
8.9	27.633	53.183
10.1	27.617	53.133
11.2	27.583	53.067
12.3	27.583	52.983

The $(C_{p,ref}/C_p)$ and $(C_{c,ref}/C_c)$ vs. $(P-P_{ref})$ graph is given in Figure 7.2 and the slope of this graph gives the pressure variation coefficient of the materials.

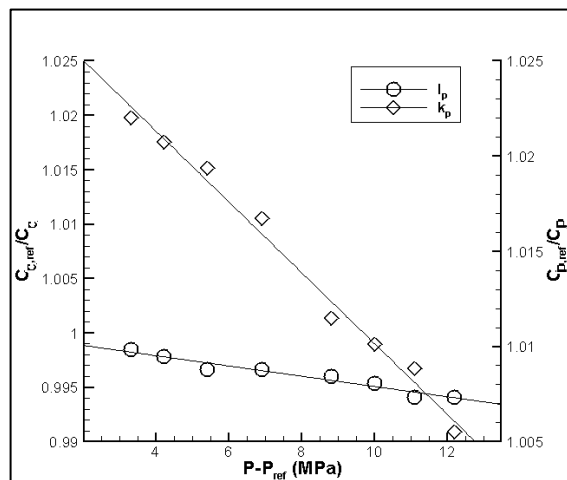


Figure 7.2 Change of mechanical wave velocity with pressure

Table 7.6 Pressure Variation Coefficients

	Coupling Material	Propellant
Pressure Variation Coefficient [MPa ⁻¹]	0.00047	0.0018

7.6 Burning Rate

Some adjustments should be made before the burning test, like determining the gate of the signal and amplitude of the signal. These are important factors which affect the data collection process. If the amplitude of the signal is not defined correctly, signal loss or unexpected increase of signal peak can occur. Arranging the gate positions are also critical. Gates follow the reflected signal from the propellant's surface. If the gates' positions are not determined correctly, again signal loss or unexpected increase of signal peak can occur. The gates can be seen oscilloscope view of the sent and received signals are also given in Figure 7.3.

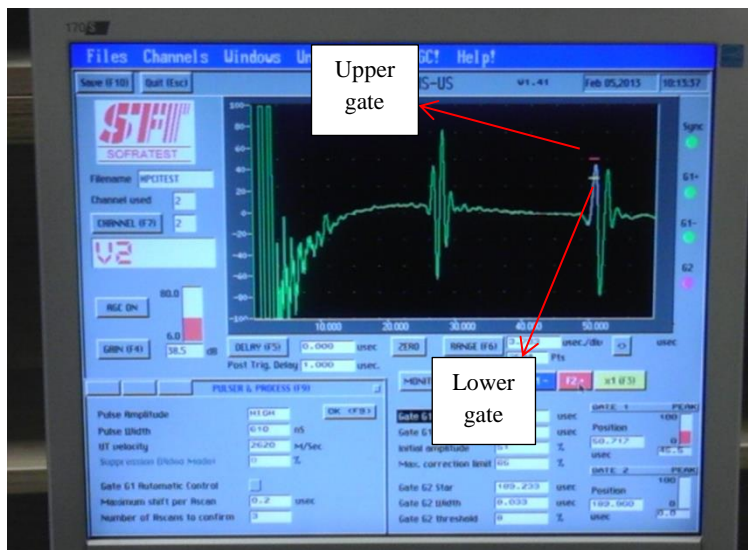


Figure 7.3 Gates of the signal

Before showing the results of the burning tests, the physics of the test should be emphasized briefly. The propellant is ignited inside the closed bomb. After ignition of the propellant, propellant starts to burn from one side like a cigarette. During the burning process acoustic waves are sent and received by transducer through the coupling material and the propellant. The sent wave reflects back from the propellant's burning surface since there is large impedance difference between the solid propellant and the hot gas phase burning chamber. The signal travel time of the signals are collected during the test. The signal travel time decreases during the test because the propellant burns and propellant's thickness decreases during the test. The combustion pressure data is also collected during the test. The pressure increases during the test

because the burning takes place in a closed bomb and there is no gas exit during the test. After collecting the pressure and signal travel time data, the burning rate of the propellant is calculated for every sampled pressure data point.

The burning rate results are normalized for all tests. Normalization is done by dividing the pressure values to the maximum pressure obtained through all tests and dividing the burning rate values to the maximum burning rate obtained through all tests.

7.6.1 The First Test

The first test is performed with a composite propellant which does not include any aluminum particles. Types and batches of the propellant and the coupling material used in this test are described in Table 7.1. The propellant has 24.25 mm initial thickness and the coupling material has 35.03 mm initial thickness. Signal configuration of the test at the initial time is given in Figure 7.4:

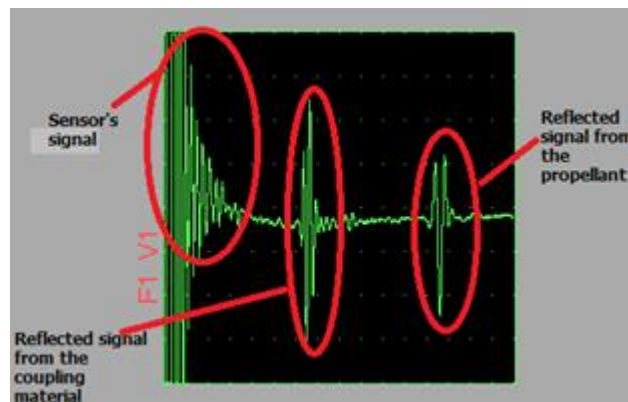
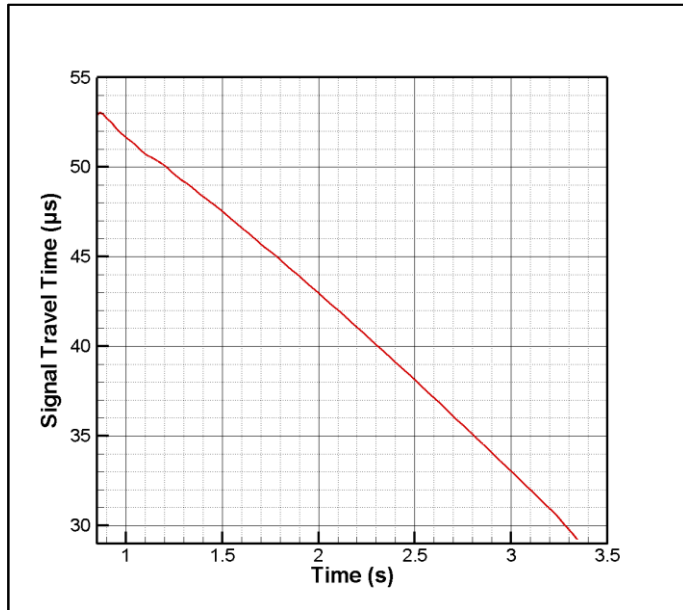
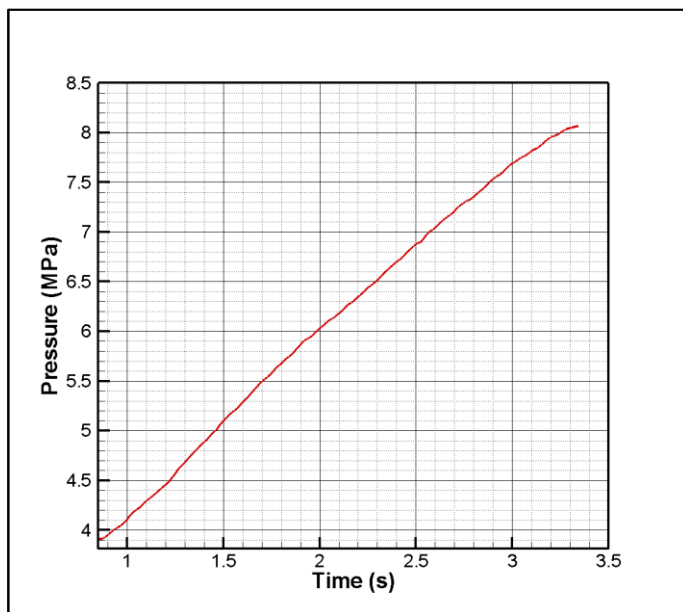


Figure 7.4 Sent and reflected signals for Test 1 at the initial time

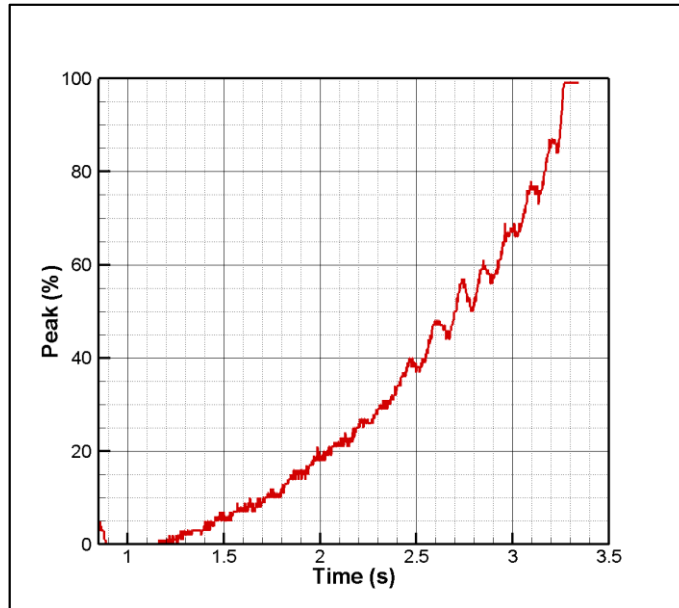
Signal travel time, pressure and signal peak obtained from the data acquisition system are shown in Figure 7.5.



a) Signal travel time



b) Pressure



c) Signal peak

Figure 7.5 Signal travel time (a), pressure (b) and signal peak (c) for Test 1

As it can be seen from Figure 7.5, signal travel time's decrease and pressure's increase finish at 3.334 second and this situation shows that the test finishes at 3.344 second. The signal's peak reaches to maximum at 3.344 second, as expected. Consistency of these results is a sign of test's success.

After getting the raw data from the software of experimental setup, the burning rate is calculated by using Eq. (4.3). Also 4 test motor firings are made with the same propellant and the burning rate is calculated by using Eq. (3.1). The results are plotted in Figure 7.6.

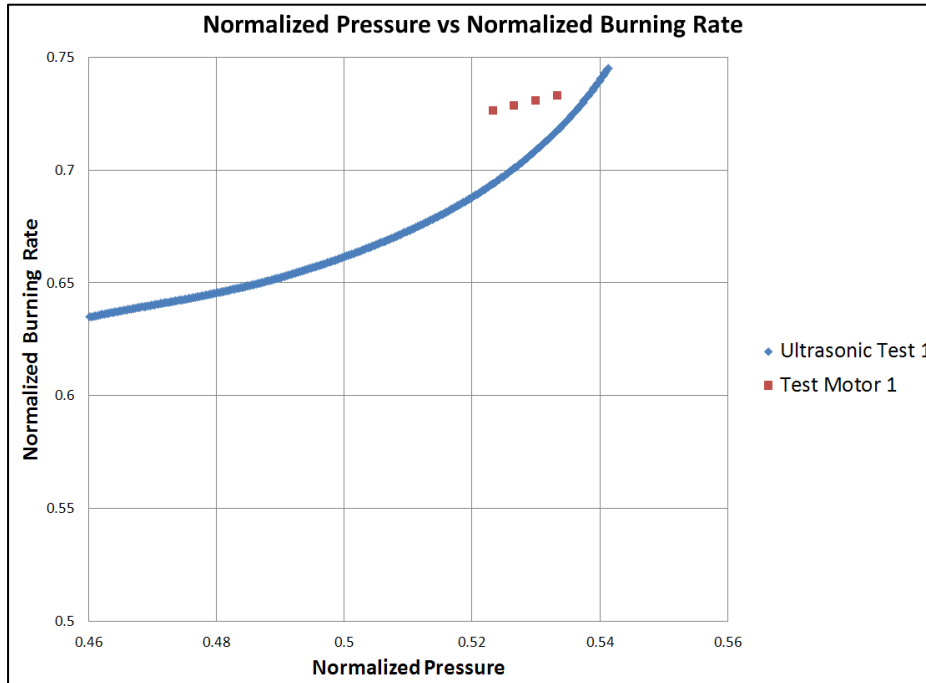


Figure 7.6 Normalized burning rate versus normalized combustion pressure for Test 1

Four test motor firing results are compared with ultrasonic burning rate results at the corresponding pressures. At the given pressures the burning rate differences between the ultrasonic test and static firing changes from about 3.37% to 4.45% and has 3.9% average. According to uncertainty analysis, these differences are acceptable and it can be said that the first test is successful.

7.6.2 The Second Test

The second, third and fourth tests are performed with same batch of composite propellants which do not include any aluminum particles. The propellant has 22.84 mm initial thickness and the coupling material has 35.01 mm initial thickness. The reflected signals obtained from the software at the initial time are as in Figure 7.7.

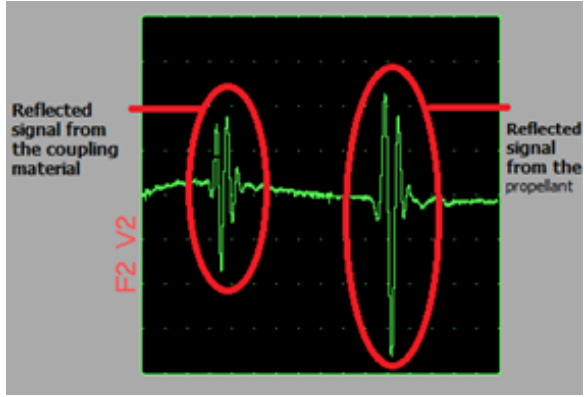
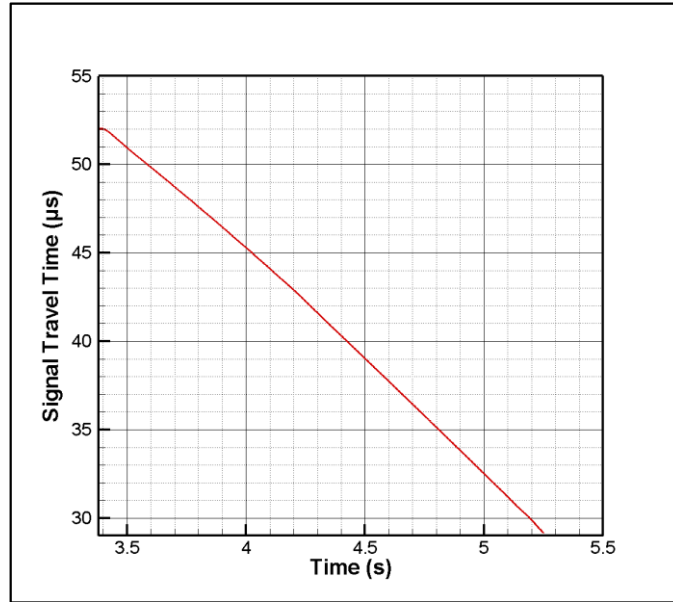
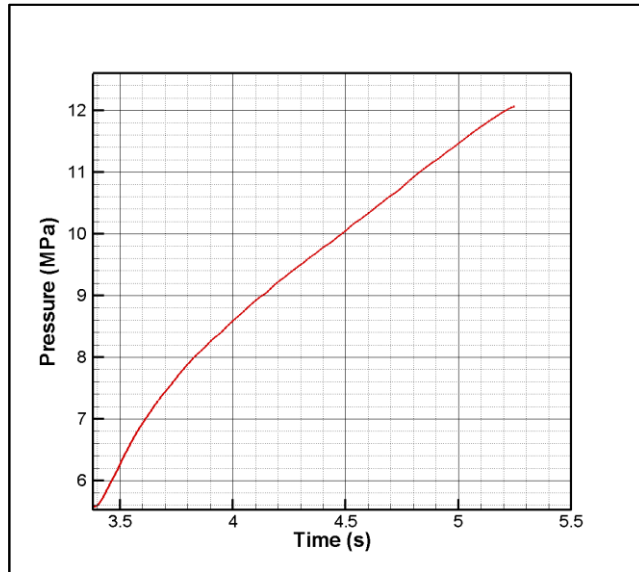


Figure 7.7 Reflected signals for Test 2 at the initial time

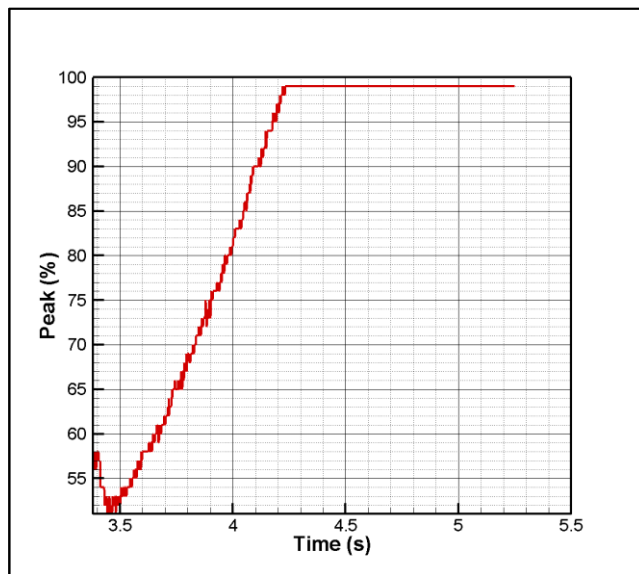
Signal travel time, pressure and signal peak information of this test are given in Figure 7.8:



a) Signal travel time



b) Pressure



c) Signal peak

Figure 7.8 Signal travel time (a), pressure (b) and signal peak (c) for Test 2

By looking signal travel time and pressure plots, it can be said that the test finishes at 5.25 second. However, the signal peak value reaches its maximum before the burning ends at 4.23 second. This is a sign of unsuccessful test. The effect of reaching maximum peak value of the signal can be seen in burning rate negatively.

By using the data obtained from the software of experimental setup, the burning rate is calculated by using Eq. (4.3). Besides, there are 4 test motor firings with this propellant. Burning rate is calculated from the test motor firings, too. The results are given in Figure 7.9.

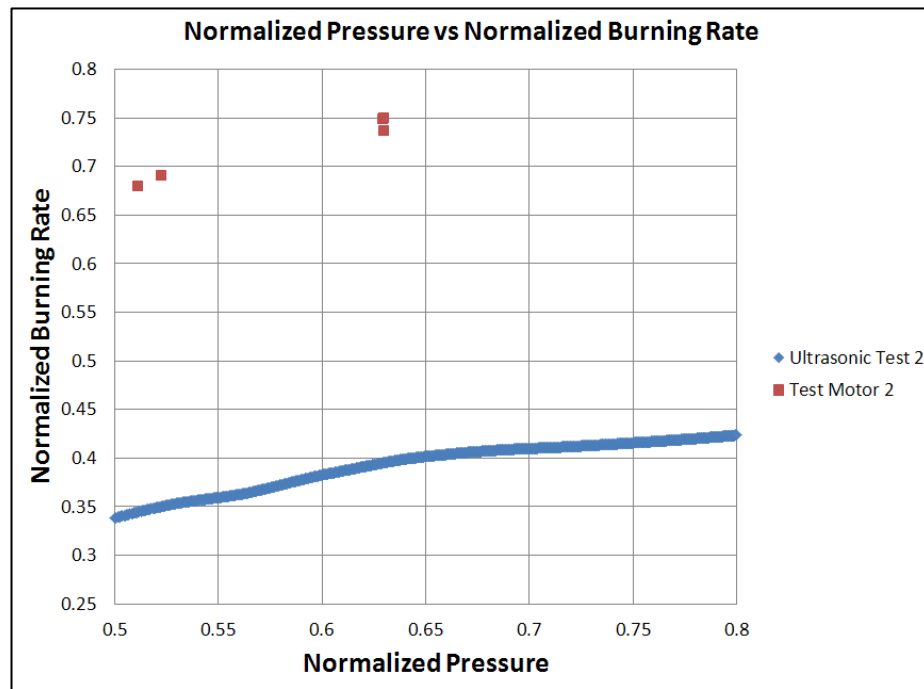


Figure 7.9 Normalized burning rate versus normalized combustion pressure for Test 2

Four test motor firing results are compared with ultrasonic burning rate results at the corresponding pressures. There are very large differences between the test motor firing results and the ultrasonic burning rate measurement method. These results are meaningless. And the test is unsuccessful. The reason of this situation is that the signal peak value reaches the maximum before the end of the test. As told before, adjusting the gain of the signal and the position of the gates are very important before the test. There can be a problem during the adjustment of the gain and the gates. Furthermore, it is thought fire can leak into the inhibitor and it can cause a problem during the burning. As a result, more careful initial adjustments are made in the next tests. The inhibitor's curing time is increased for the next tests, also.

7.6.3 The Third Test

The information about the coupling material and the propellant used in test are given in Table 7.1. The propellant has 25.51 mm initial thickness and the coupling material has 35.12 mm initial thickness. The reflected signals at the initial time are as in Figure 7.10:

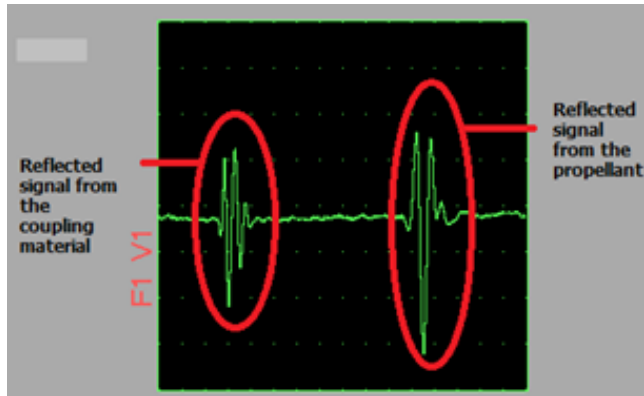
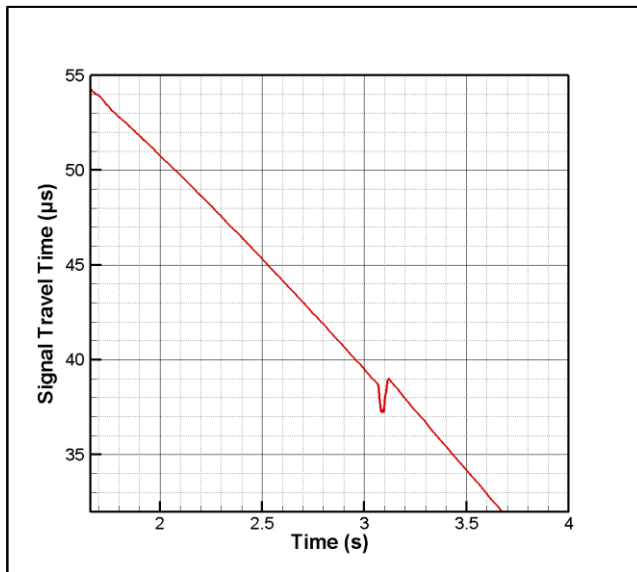
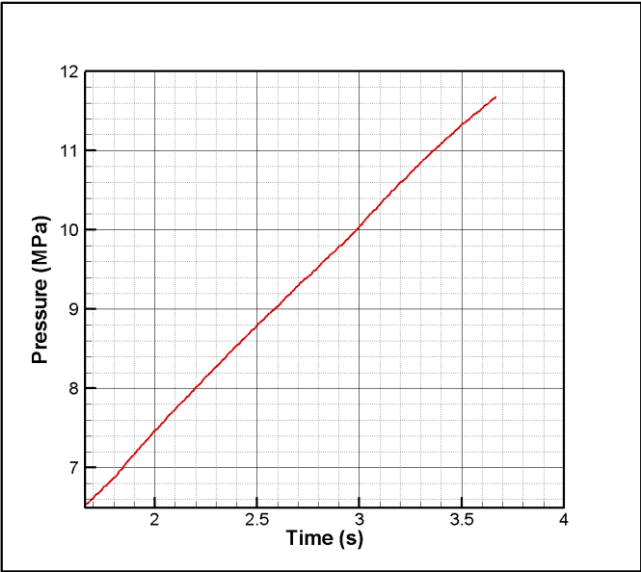


Figure 7.10 Reflected signals for Test 3 at the initial time

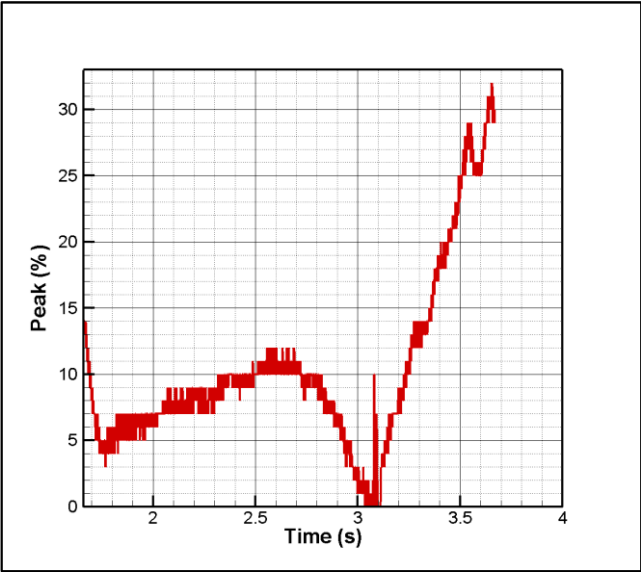
Signal travel time, pressure and peak of this test can be seen in Figure 7.11:



a) Signal travel time



b) Pressure



c) Signal peak

Figure 7.11 Signal travel time (a), pressure (b) and signal peak (c) for Test 3

At 3.67 second, the decrease of signal travel time and the increase of pressure finish. The signal peak reaches its maximum value. In other words, the test finishes at this moment.

The burning rate of the test is calculated by the help of the Eq. (4.3). There are 4 test motor firings with this propellant. The burning rates of test motor firings are found by applying Eq. (3.1). The results are given in Figure 7.12.

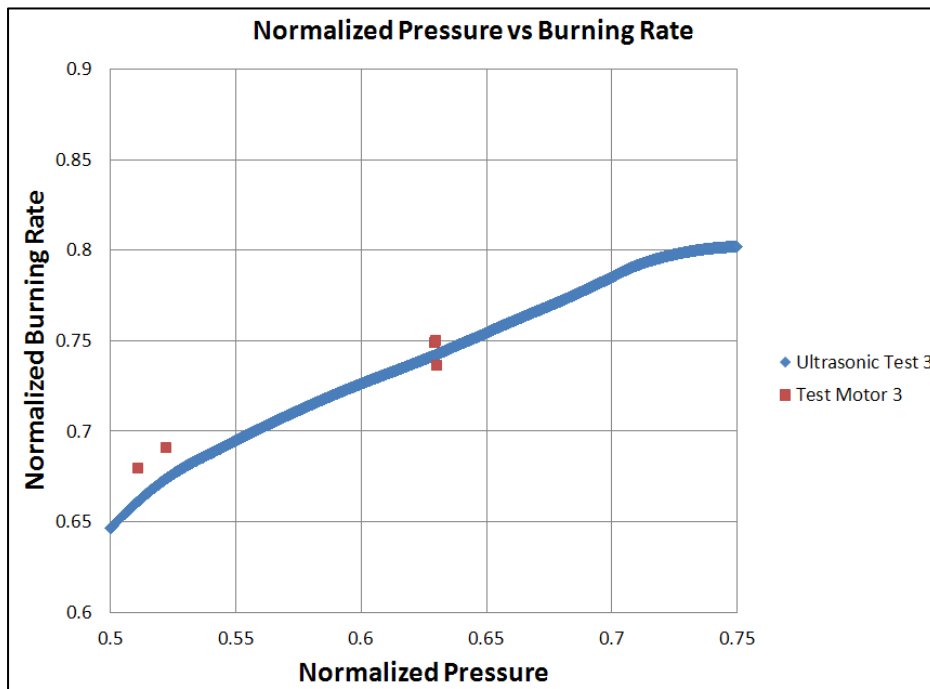


Figure 7.12 Normalized burning rate versus normalized combustion pressure for Test 3

If the burning rates of the test motor firings and the ultrasonic burning rate measurement method are compared at the corresponding pressures, the difference between them changes from 0.84% to 2.41% and the average is 1.3%. Taking into account the uncertainty analysis, it is obvious that these differences are in the limit and the test is successful.

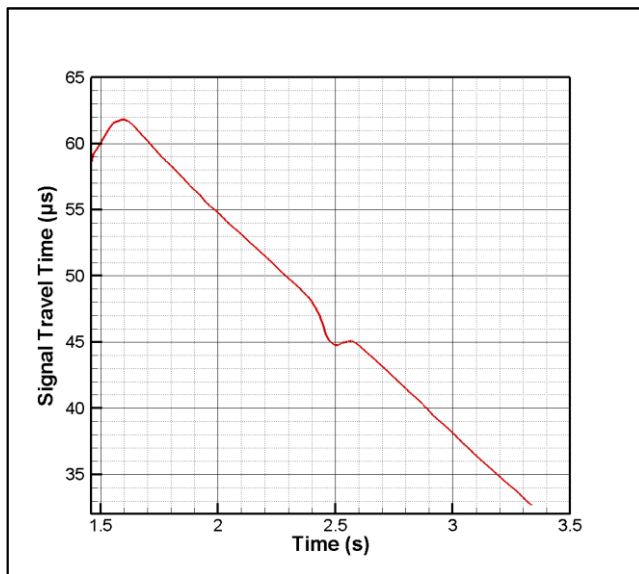
7.6.4 The Fourth Test

In Table 7.1 the propellant and coupling material is defined for this test. The propellant has 30.58 mm initial thickness and the coupling material has 35.08 mm initial thickness. The reflected signals at the initial time are as in Figure 7.13:

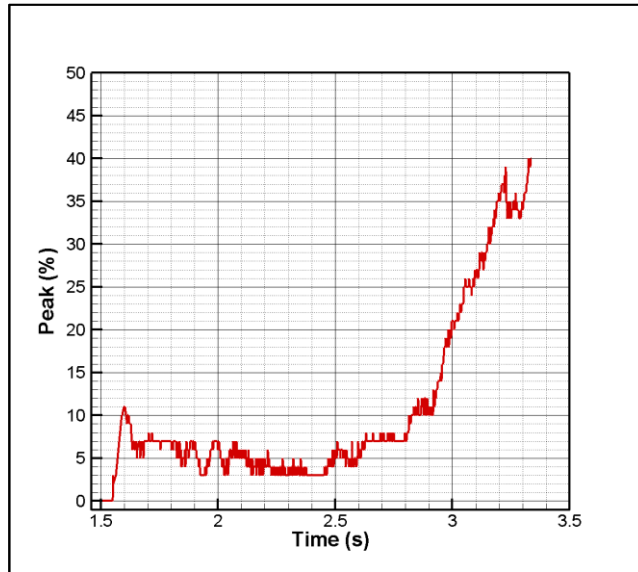


Figure 7.13 Reflected signals for Test 4 at the initial time

Signal travel time, and signal peak data obtained from the data acquisition system can be seen in Figure 7.14:



a) Signal travel time



b) Signal peak

Figure 7.14 Signal travel time (a) and signal peak (b) for Test 4

Pressure data can't be collected properly in this test because another system is tried for pressure collection but it was unsuccessful. The burning rate of ultrasonic measurement method can't be calculated since there is no pressure data. This test has been unsuccessful because the pressure data can't be collected. The lesson learned from this test is, another data collection system shouldn't be used except the main system.

7.6.5 The Fifth Test

The fifth, sixth, seventh and eighth tests are performed with same batch of composite propellants which do not include any aluminum particles. The propellant has 26 mm initial thickness and the coupling material has 34.7 mm initial thickness. The detailed information about the propellant and the coupling material used in test is given in Table 7.1. The reflected signals at the initial time are as in Figure 7.15.

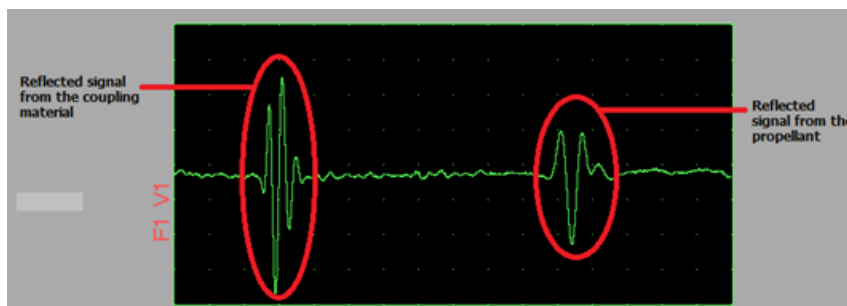
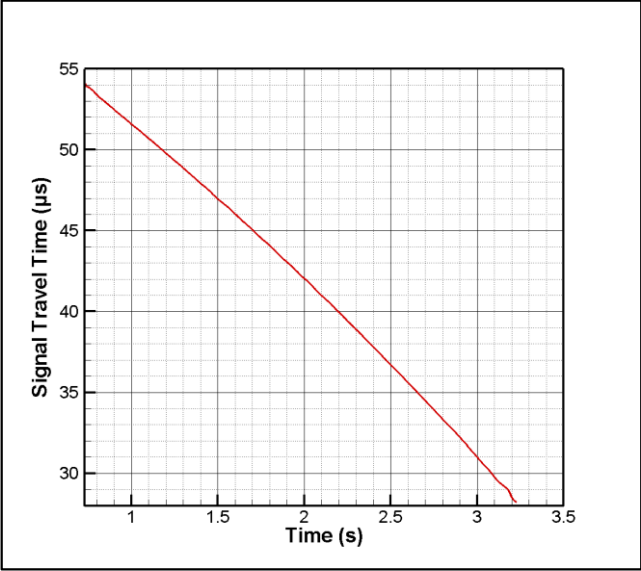
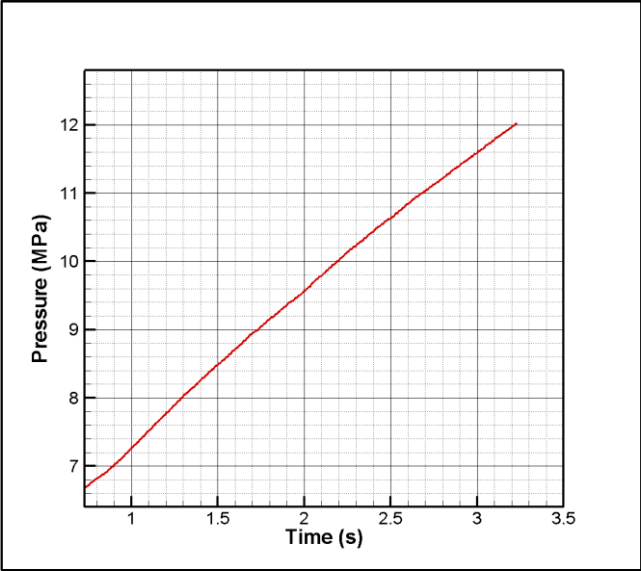


Figure 7.15 Reflected signals for Test 5 at the initial time

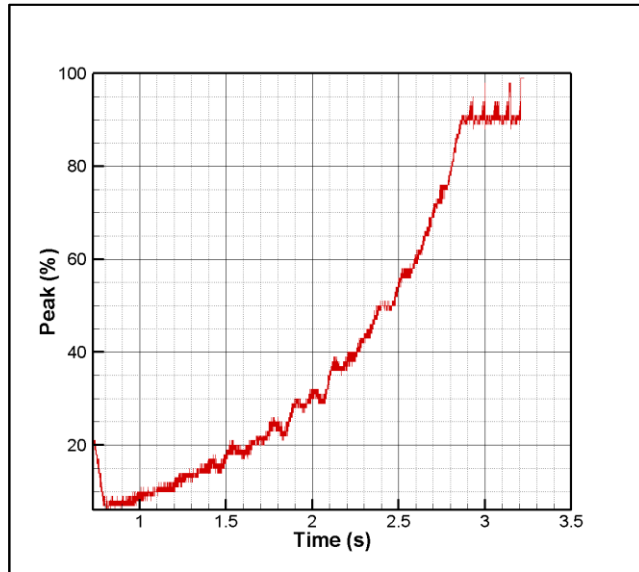
The related data obtained from the data acquisition system are plotted in Figure 7.16:



a) Signal travel time



b) Pressure



c) Signal peak

Figure 7.16 Signal travel time (a), pressure (b) and signal peak (c) for Test 5

By looking these three graphs, it can be understood that the burning ending time is consistent for three of them. Furthermore, signal travel time decreases, pressure increases and signal peak reaches its maximum at the end of the burning, as expected. These are signs of a successful test.

Also 4 test motor firings performed with the same propellant. Burning rates are obtained from two of the methods and the normalized results are given in Figure 7.17.

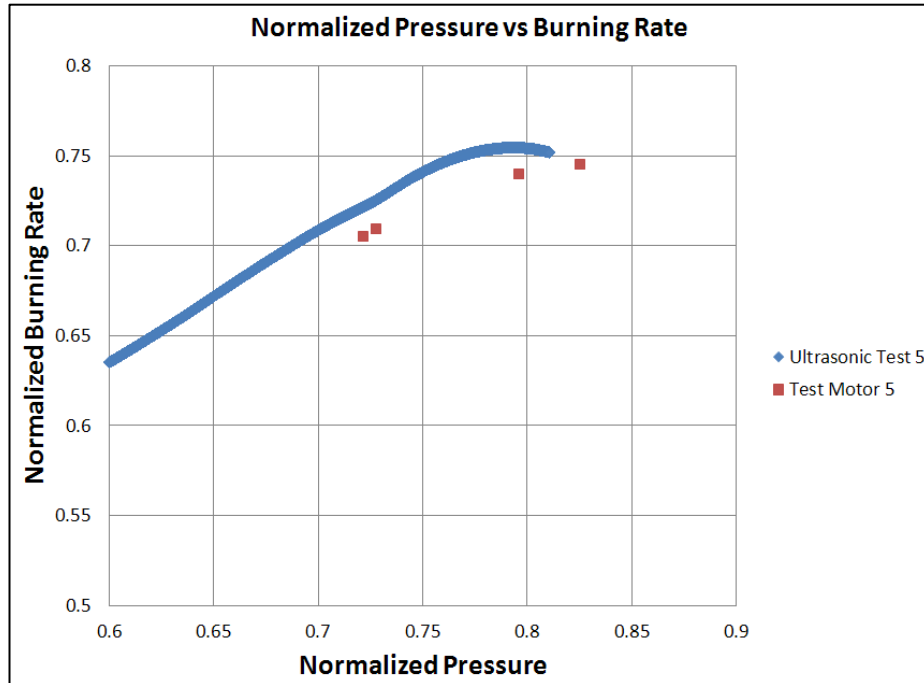


Figure 7.17 Normalized burning rate versus normalized combustion pressure for Test 5

Although there are four test motor firings, three of their burning results are compared with ultrasonic burning rate results at the corresponding pressures since closed bomb firing can't reach the last test motor's pressure. The burning rate difference between the ultrasonic test and static firing results changes between 2.28% to 2.35% and the average difference is 2.3%. These differences are consistent with the uncertainty analysis and they are acceptable; so, the test is successful.

7.6.6 The Sixth Test

In Table 7.1, propellant and coupling material information about this test is given. The propellant has 25 mm initial thickness and the coupling material has 34.70 mm initial thickness. The reflected signals obtained from the software at the initial time are as in Figure 7.18.

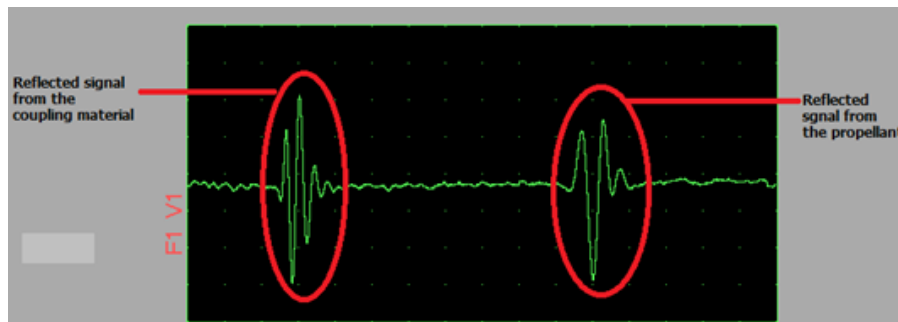
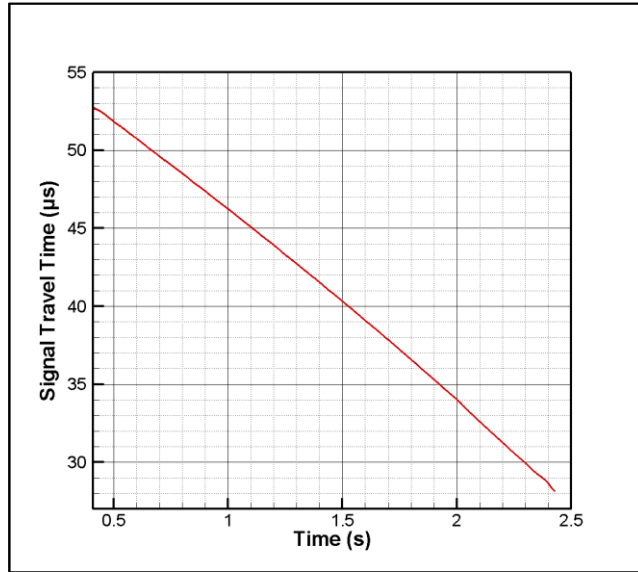
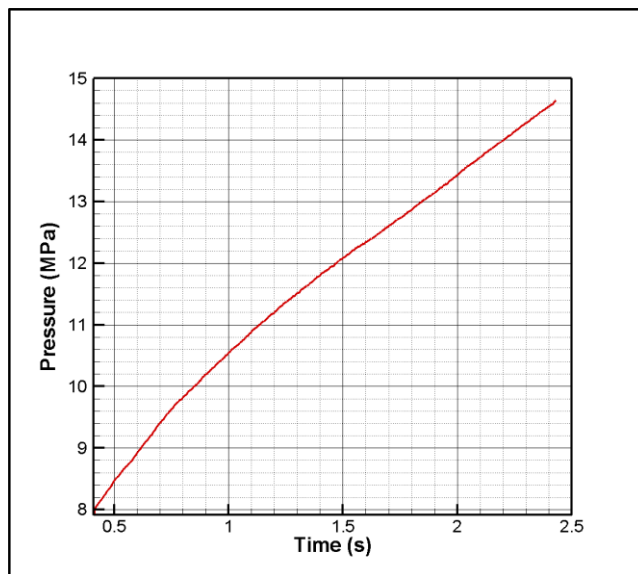


Figure 7.18 Reflected signals for Test 6 at the initial time

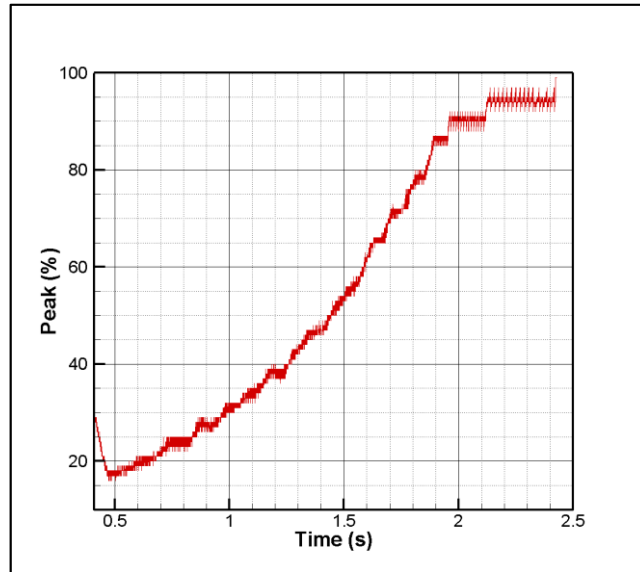
Signal travel time, and signal peak data obtained from the data acquisition system can be seen in Figure 7.19.



a) Signal travel time



b) Pressure



c) Signal peak

Figure 7.19 Signal travel time (a), pressure (b) and signal peak (c) for Test 6

It can be seen that the test ends at 2.43 second and there is no problem about reaching the peak of the signal at the end of the test. It can be said that it is a good test just by looking these plots.

After getting the raw data from the software of experimental setup, the burning rate is calculated by using Eq. (4.3). The burning rate values obtained from the test motor method is also calculated. The results are compared in Figure 7.20.

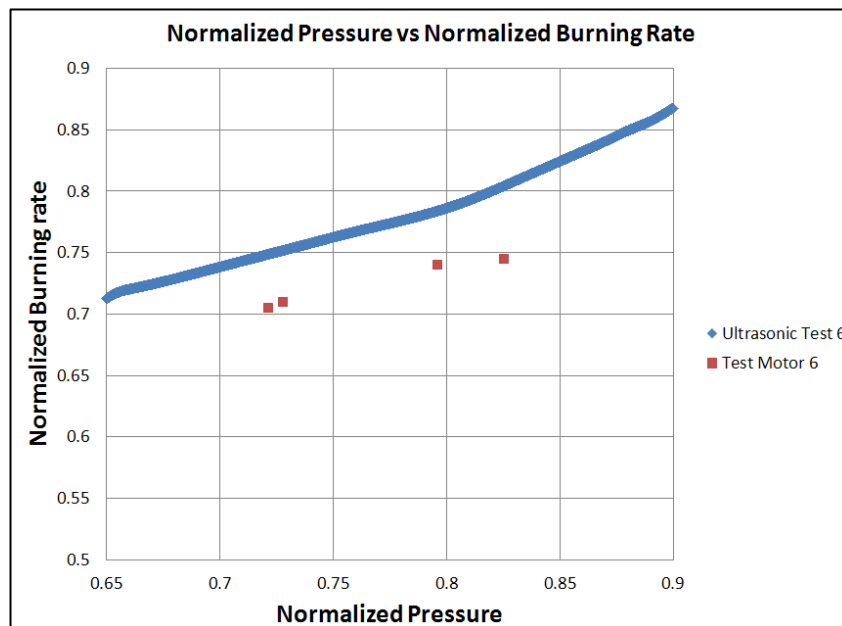


Figure 7.20 Normalized burning rate versus normalized combustion pressure for Test 6

At the corresponding pressures, the burning rate difference between the ultrasonic method and static firing is calculated which varies 5.99% to 7.99% and the average of the differences is about 6.5%. These differences are in the acceptable range due to uncertainty analysis.

7.6.7 The Seventh Test

Types and batches of the propellant and the coupling material used in this test are described in Table 7.1. The propellant has 23.15 mm initial thickness and the coupling material has 34.70 mm initial thickness. The reflected signals obtained from the software at the initial time are as in Figure 7.21.

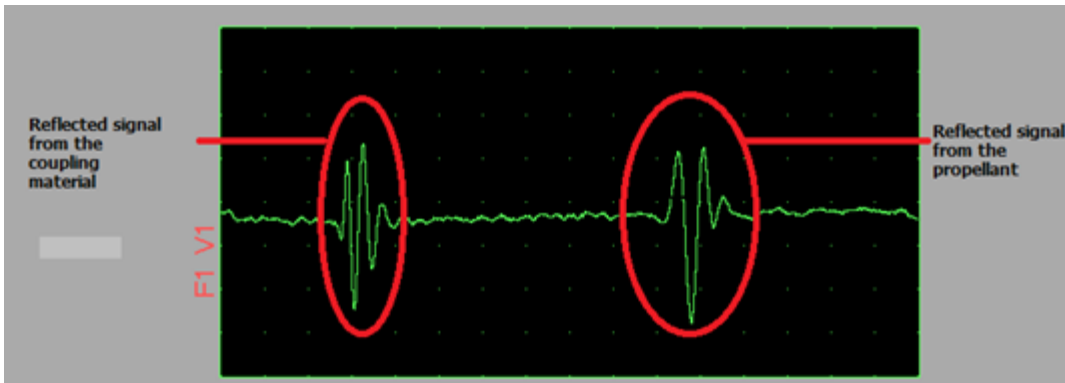
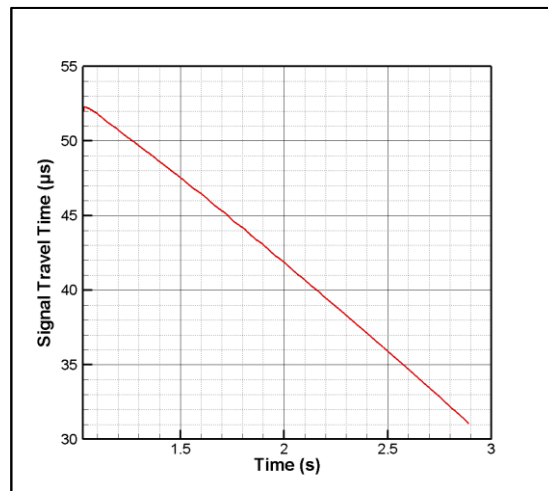
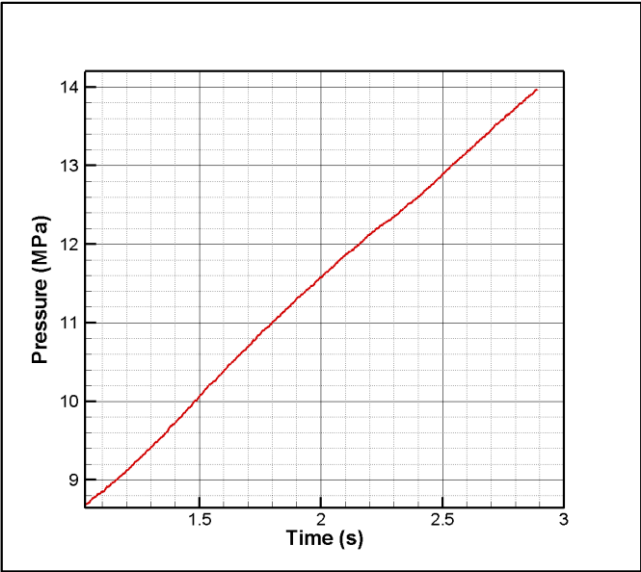


Figure 7.21 Reflected signals for Test 7 at the initial time

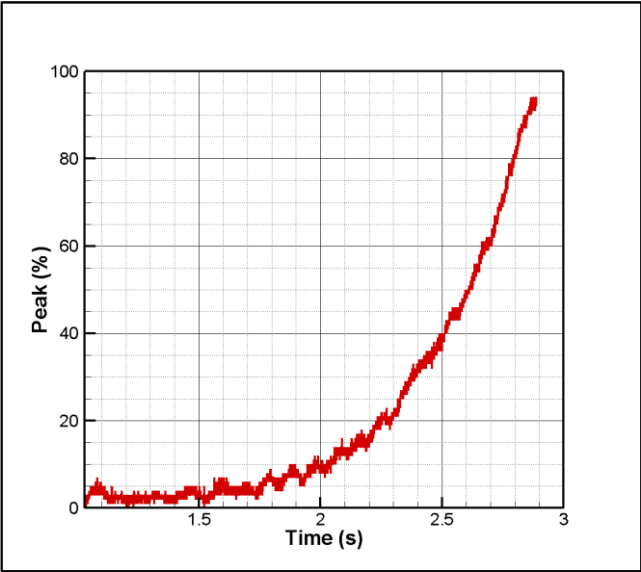
Signal travel time, and signal peak data obtained from the data acquisition system can be seen in Figure 7.22.



a) Signal travel time



b) Pressure



c) Signal peak

Figure 7.22 Signal travel time (a), pressure (b) and signal peak (c) for Test 7

The decrease of signal travel time and the increase of the pressure continue till 2.89 second which is the ending moment of burning. The signal peak reaches its maximum at the end of the test. These are good signs for a successful a test.

Burning rate results of ultrasonic method and test motor firing method for this test are shown in Figure 7.23.

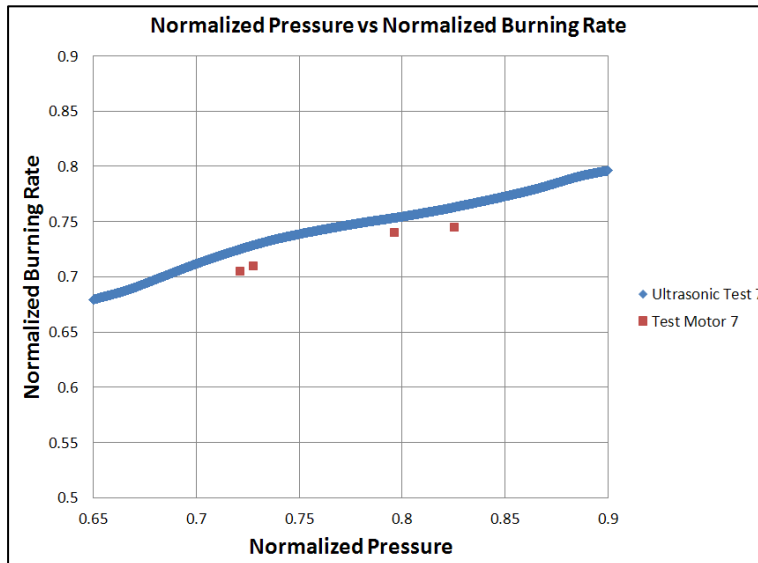


Figure 7.23 Normalized burning rate versus normalized combustion pressure for Test 7

Four test motor firing results are compared with ultrasonic burning rate results at the corresponding pressures. The burning rate difference between the ultrasonic test and static firing at given pressure is found between 1.84% and 2.86% while the average difference is 2.5%. By looking the uncertainty analysis, it can be said that this test is successful.

7.6.8 The Eighth Test

The eighth test is last performed ultrasonic test. The propellant has 22.20 mm initial thickness and the coupling material has 35.06 mm initial thickness. The reflected signals obtained from the software at the initial time are as in Figure 7.24.

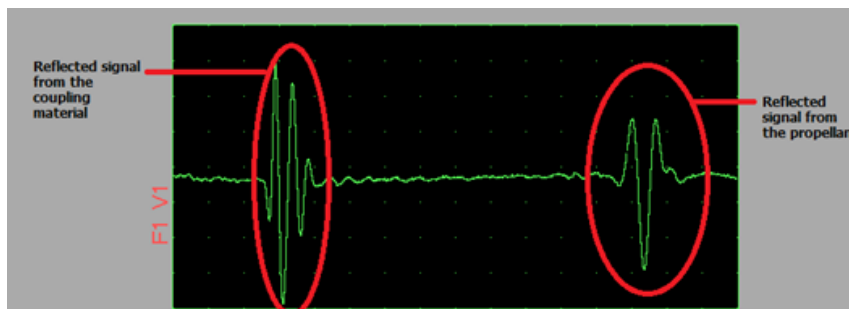
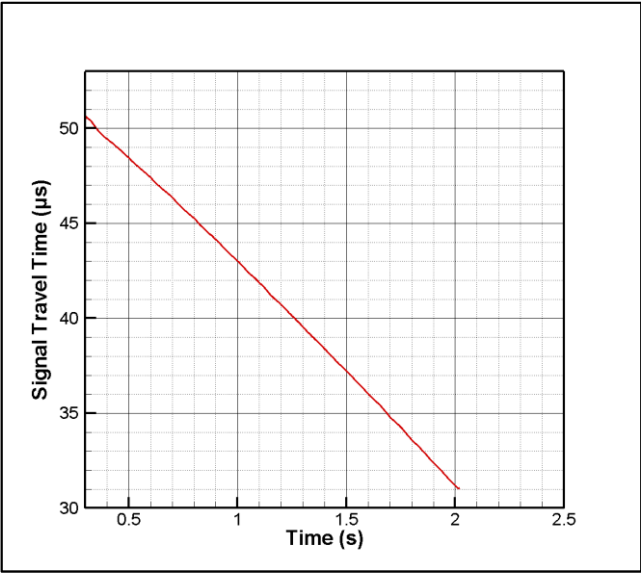
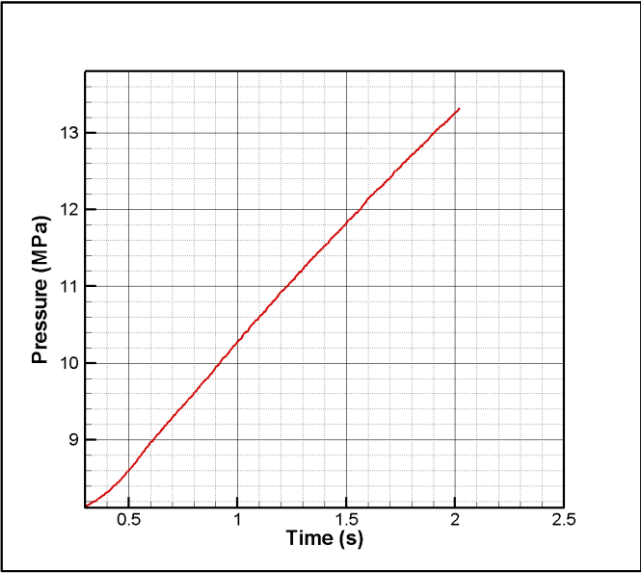


Figure 7.24 Reflected signals for Test 8 at the initial time

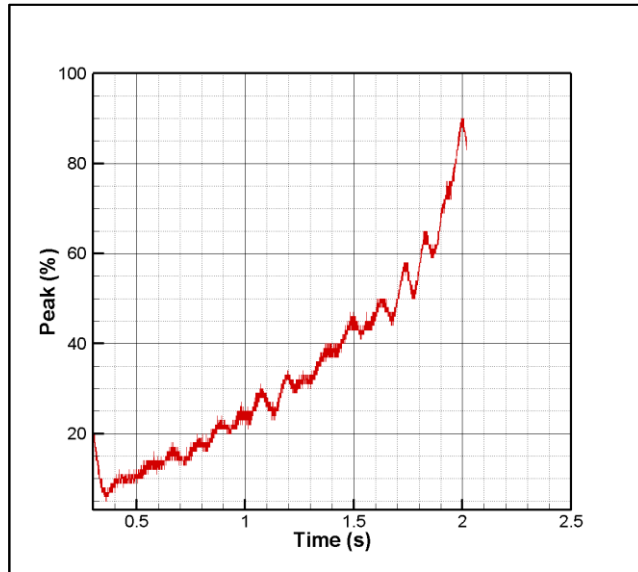
The related data obtained from the data acquisition system are plotted in Figure 7.25.



a) Signal travel time



b) Pressure



c) Signal peak

Figure 7.25 Signal travel time (a), pressure (b) and signal peak (c) for Test 8

By looking these three graphs, it can be understood that the burning ending time is consistent for three of them. Furthermore, signal travel time decreases, pressure increases and signal peak reaches its maximum at the end of the burning, as expected. These are signs of a successful test.

Also 4 test motor firings performed with the same propellant. Burning rates are obtained from two of the methods and the normalized results are given in Figure 7.26.

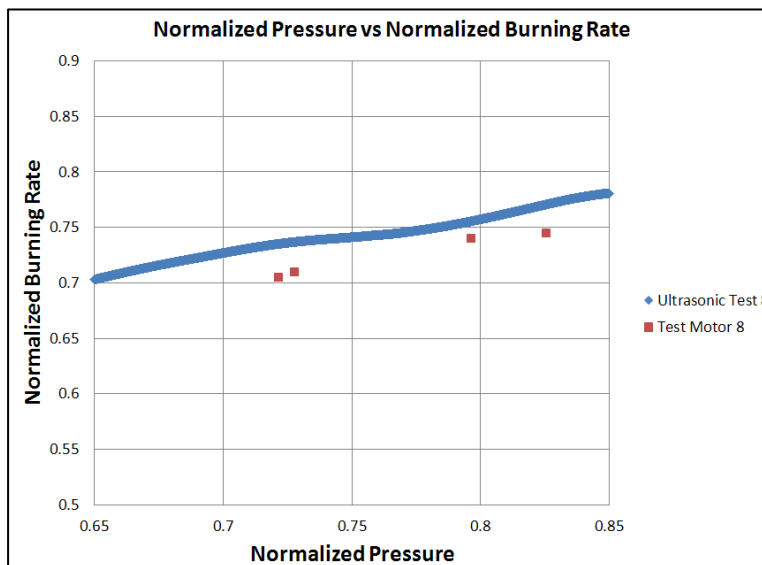


Figure 7.26 Normalized burning rate versus normalized combustion pressure for Test 8

Ultrasonic burning rate results are compared with four test motor firing results at the corresponding pressures. The burning rate difference between the ultrasonic test and static firing changes 2.13% to 4.27% and the average difference is 3.44%. These values stays in the limits determined in the uncertainty analysis and the test is successful.

7.6.9 Comparison of the Ultrasonic Tests for Propellant 2

Ultrasonic Test 5, Ultrasonic Test 6, Ultrasonic Test 7 and Ultrasonic Test 8 are performed with Propellant 2. They are also from the same batch. By looking Figure 7.27, it can be said that these tests are consistent with each other and show similarity.

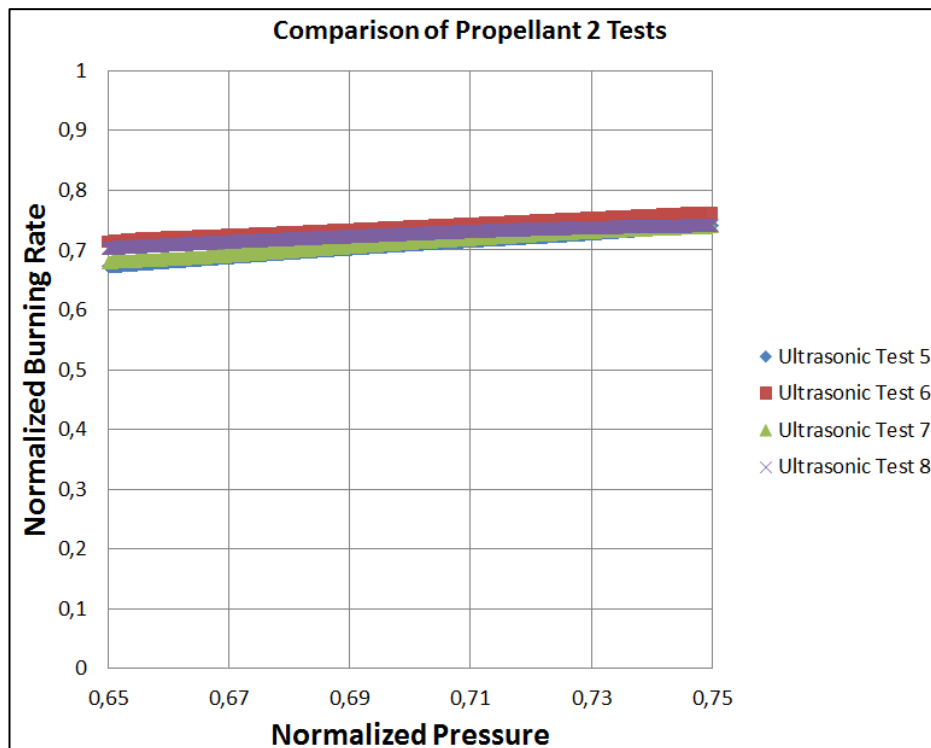


Figure 7.27 Comparison of propellant 2 tests

CHAPTER 8

CONCLUSION AND FUTURE WORK

8.1 Conclusion

In this thesis study, application of ultrasonic burning rate measurement method to closed bombs was performed. Two different types of propellants were produced for the burning tests. Both of the propellants are heterogeneous composite propellants which do not contain aluminum.

Before the main burning tests, some pre-tests were performed for affirmation of the ultrasonic transducer and data acquisition system with water column experimental setup. Furthermore, the reference mechanical wave velocities, acoustic impedances and pressure coefficients are determined.

Uncertainty analysis is performed to find burning rate uncertainties of both ultrasonic burning rate measurement method and test motor firing method. Uncertainty of the ultrasonic burning rate measurement method changes 2.68% to 2.76% while uncertainty of the test motor firing method changes 5.76% to 6.13%. It can be said that ultrasonic burning rate measurement method is more accurate than the test motor firing method.

Eight burning rate measurement tests were performed with ultrasonic burning rate measurement method for getting burning rates of propellants. Propellant and coupling material details are given in Table 7.1. For every ultrasonic test, test motor firings were performed with same propellants.

The average differences between ultrasonic burning rate measurement method and test motor firing method for every test are as in Table 8.1.

Table 8.1 Differences of the Tests

Test Number	Average Difference
1	3.9%
2	N/A
3	1.3%
4	N/A
5	2.3%
6	6.5%
7	3.5%
8	3.4%

The successful tests' difference range is between 1.3% and 6.5%. The sixth test's difference is greater than the other successful tests. This may occur due to some dimensional measurement error of the propellant and the coupling material of this test. The differences for the tests are found to be reasonable by taking into account the uncertainty analysis.

The tests made with Propellant 2 (Test 5-6-7-8) can be compared between them. Their burning rate results are consistent with each other.

The second test was unsuccessful because of wrong adjustment of the amplitude of the signal or wrong adjustment of the gate position. Furthermore, it is thought fire can leak into the inhibitor and it can cause a problem during the burning. So, more careful initial adjustments were made in the next tests and the inhibitor's curing time is increased for the next tests.

In the fourth test, another system for pressure data collection was tried, but the data couldn't be collected correctly, also. The lesson learned from this test was, another data collection system shouldn't be used except the main system.

As a result, applicability of ultrasonic burning rate measurement method to closed bombs was proved successfully with six successful tests. An economical and practical burning rate measurement method has been gained.

8.2 Future Work

For this study;

- Preparing coupling material for propellants which contain aluminum
- Performing tests with propellants which contain aluminum

- Obtaining burning rate with this method from a test motor
- Performing erosive burning studies with this method
- Burning instability studies

will be the future work for more research.

REFERENCES

- [1] Frederick, R.A., Traineau, J-C., “*Non-Intrusive Burning Rate Measurement Techniques*”, RTO Technical Report 43, February 2002.
- [2] Hale, H.J., “*The Demonstration of an Ultrasonic Technique to Measure Solid Propellant Burning Rates Under Actual Combustion Conditions*”, M.S. Thesis, Virginia Polytechnic Institute, Blacksburg, Virginia, June 1967.
- [3] Wright, W.A., “*Ultrasonic Thickness Monitoring Technique*”, Aerospace Related Technology for Industry, NASA SP-5075, May 1969, pp. 69-73.
- [4] Cauty, F., Demarais, J.C., “Ultrasonic Measurement of the Uncured Solid Propellant Burning Rate”, 21st International Congress of ICT, Karlsruhe, July 3-6 1990.
- [5] Cauty, F., Demarais, J.C., Erades, C., “Determination of Solid Propellant Burning Rate Sensitivity to Initial Temperature by the Ultrasonic Method”, 3rd International Symposium on Special Topics in Chemical Propulsion, Scheveningen, the Netherlands, May 10-13 1993
- [6] Louwers, J., Gadiot, G., Versluis, M., Landman, A.J., van der Meer, T., and Roekaerts, D., “Measurement of Steady and Non-Steady Regression Rates of Hydrazinium Nitroformate with Ultrasound”, International Workshop on Measurement of Thermophysical and Ballistic Properties of Energetic Materials, Milano, Italy, June 1998.
- [7] Di Salvo, R., Dauch, F., Frederick, R.A., Moser, M.D., “Direct Ultrasonic Measurement of Solid Propellant Ballistics”, *The Review of Scientific Instruments*, Vol. 70, No. 11, November 1999.
- [8] Rochford, E., “Temperature Sensitivity Measurements of Solid Rocket Propellants”, M.S. Thesis, February 18 1999, The University of Alabama in Huntsville.
- [9] Dauch, F., Moser, M.D., Frederick, R.A., and Coleman, H.W., “Uncertainty Assessment of Ultrasonic Measurement of Propellant Burning Rate”, CPIA Pub 680, Vol. I, pp. 293-304, Dec 1998.
- [10] Murphy, J.J., Chai, S., Brdar, R., and Krier, H., “Response Function Measurement using an Ultrasonic Technique in an Oscillating Burner”, AIAA 2000-3797, July 2000.
- [11] Sutton, G.P., Biblarz, O., “*Rocket Propulsion Elements*”, 7th ed., John Wiley and Sons, Inc., New York, 2001.
- [12] Ertuğrul, S., “The Effects of Geometric Design Parameters on the Flow Behavior of a Dual Pulse Solid Rocket Motor during Secondary Firing”, M.S. Thesis, Dept. of Aerospace Engineering, METU, 2012.
- [13] Davenas, A., “*Solid Rocket Propulsion Technology*”, Pergamon Press, 1993.

- [14] “Solid Rocket Motor Metal Cases”, NASA, SP-8025, April 1970.
- [15] Evans, P. R., “Composite Motor Case Design”, Agard Lecture Series No. 150, Design Methods in Solid Rocket Motors, Revised Version, 1988.
- [16] Truchot, A., “Design and Analysis of Solid Rocket Motor Nozzle Internal Insulation”, Agard Lecture Series No. 150, Design Methods in Solid Rocket Motors, Revised Version, 1988.
- [17] “Solid Rocket Motor Igniters”, NASA, SP-8051, March 1971.
- [18] Truchot, A., “Design and Analysis of Solid Rocket Motor Nozzle”, Agard Lecture Series No. 150, Design Methods in Solid Rocket Motors, Revised Version, 1988.
- [19] Thakre P., Yang V., “Solid Propellants”, Encyclopedia of Aerospace Engineering, 2010.
- [20] Price, E.W., "Combustion of Metalized Propellants", Fundamentals of Solid Propellant Combustion, Progress in Astronautics and Aeronautics, Vol. 90, AIAA, pp. 479-514, 1984.
- [21] Lengelle, G., Duterque, J., Trubert, J.F., “Combustion of Solid Propellants”, RTO-EN-023, May 2002.
- [22] Clark, G.M., Zimmerman, C.A., “Phase Stabilized Ammonium Nitrate Selection and Development”, JANNAF Publication 435, pp. 65-75, October 1985.
- [23] Rocco, J.A.F.F., Lima, J.E.S., Frutuoso, A.G., Iha, K., Ionashiro, M., Matos, J.R., and Suarez-Iha, M.E.V., “TG Studies of a Composite Solid Rocket Propellant Based on HTPB-Binder”, Journal of Thermal Analysis and Calorimetry, Vol. 77, pp. 803-813, 2004.
- [24] Gaur, B., Lochab, B., Choudhary, V., and Varma, I.K., “Azido Polymers-Energetic Binders for Solid Rocket Propellants”, Journal of Macromolecular Science, Vol. C43, No. 4, pp. 505-545, 2003.
- [25] Gao, J., Wang, L., Yu, H., Xiao, A., and Ding, W., “Recent Research Progress in Burning Rate Catalysts”, Propellants Explos. Pyrotech., Vol. 36, pp. 404-409, 2011.
- [26] Muthiah, R., Somasundaran, U.I., Verghese, T.L., and Thomas, V.A., “Energetics and Compatibility of Plasticizers in Composite Solid Propellants”, Def. Sci. J., Vol. 39, No. 2, pp. 147-155, April 1989.
- [27] Kubota, N., “Propellants and Explosives: Thermochemical Aspects of Combustion”, Wiley-VCH Verlag GmbH & Co, 2002.
- [28] Asay, B.W., “Shock Wave Science and Technology Reference Library”, 5th ed., Springer Science+Business Media, pp.364, 2009.
- [29] Clarke, E. H., “Continuous Measurement of the Burning Rate of a Composite Solid Propellant”, AIAA Paper 69-1967, 1969
- [30] Frederick, R.A., Jr., Moser, M.D., “Research in Solid Propellant Ballistic at UAH”, AIAA Paper 2005-3620, 2005.

- [31] Eisenreich, N., Kugler, H.P., and Sinn, F., "An Optical System for Measuring the Burning Rate of Solid Propellant Strands ", *Propellants Explosives Pyrotechnics*, Vol. 12, pp. 78-80, 1987.
- [32] Carro, V.C., "High Pressure Testing of Composite Solid Rocket Propellant Mixtures: Burner Facility Characterization", M.S. Thesis, Dept. of Mechanical Material and Aerospace Engineering, University of Central Florida, 2007.
- [33] De Luca, L.T., "Burning Rate Fundamentals", RTO Technical Report 43, February 2002.
- [34] Strand, L.D., "Personal Communication Concerning WG27", January 1997.
- [35] Leighton, T.G., "What is Ultrasound?", *Progress in Biophysics and Molecular Biology*, Vol. 93, pp. 3-83, 2007.
- [36] Cauty, F., Carmicino, C., and Sorge, A.R., "The Pressure Sensitivity of the Ultrasonic Waves Velocity: A Contribution to a Better Determination of the Energetic Material Regression Rate ", ONERA, France, Begell House, Inc., 2005.
- [37] Cauty, F., Erades, C., "Ultrasound Measurement Method: Errors, Noise and Sensitivity", *Combustion Explosion and Shock Waves*, Vol. 36, No. 1, 2000.
- [38] Song S., Kim, H., Ko, S., Oh, H., Kim, I., Yoo, J., and Jung, Y., "Measurement of Solid Propellant Burning Rates by Analysis of Ultrasonic Full Waveforms", *Journal of Mechanical Science and Technology*, Vol. 23, pp. 1112-1117, 2009.
- [39] McQuade, W.W., Dauch, F., Moser, M.D., and Frederick, R.A. "Determination of the Ultrasonic Burning Rate Technique Resolution", AIAA-98-3555, 1998.
- [40] Frederick, R.A., Traineau, J.C., and Popo, M., "Review of Ultrasonic Technique for Steady State Burning Rate Measurements", AIAA Paper 2000-3801, July 2000.
- [41] Mumcu, B., Kalkan, O.O., Atak, Ö., Arkun, Ö.U., and Kurtuluş, D.F. "Ultrasonik Yanma Hızı Ölçüm Yönteminin Kapalı Bomba Uygulamaları", IV. Ulusal Havacılık ve Uzay Konferansı, UHUK-2012-0070, September 2012.
- [42] Frederick, R.A., Traineau, J.C., "Ultrasonic Measurements of Solid Propellant Burning Rates in Nozzleless Rocket Motors", 20th AIAA/ASME/SAE Joint Propulsion Conference and Exhibit, 1984.
- [43] Mabrouk, W.M., "Acoustic Impedance Inversion approach from Petrophysical data", *Journal of Petroleum Science and Engineering*, Vol. 73, pp 181-184, 2010.
- [44] Dauch, F., Moser, M.D., Frederick, R.A., Coleman, H.W., "Uncertainty Assessment of the Pulse-Echo Ultrasonic Burning Rate Measurement Technique", 35th AIAA / ASME/ SAE / ASEE Joint Propulsion Conference and Exhibit, 1999
- [45] Di Salvo, R., Dauch, F., Moser, M.D., "Evaluation of Elemental Error Sources in the Measurement of Burning Rate Using the Ultrasonic Technique", 10th Annual Symposium, 1998

APPENDIX A

DERIVATION OF EQUATION 4.3

For the initial condition;

$$\tau_{initial} = \frac{2W_{pini}}{C_{pref}} + \frac{2W_c}{C_{cref}} \quad (1)$$

Change of mechanical wave velocity due to pressure and temperature inside the propellant is stated as:

$$\frac{C_{pref}}{C_p} = [1 - k_p(P - P_{ref})][1 + k_T(T - T_{ref})] \quad (2)$$

So mechanical wave velocity inside the propellant is:

$$C_p = \frac{C_{pref}}{[1 - k_p(P - P_{ref})][1 + k_T(T - T_{ref})]} \quad (3)$$

Change of mechanical wave velocity due to temperature can be neglected so change of mechanical wave velocity due to pressure is stated as:

$$\frac{C_{pref}}{C_c} = [1 - l_p(P - P_{ref})] \quad (4)$$

Mechanical wave velocity inside the coupling material happens:

$$C_c = \frac{C_{cref}}{[1 - l_p(P - P_{ref})]} \quad (5)$$

Delta signal travel time is:

$$\Delta\tau = \tau_{initial} - \tau(t) \quad (6)$$

where τ_t is:

$$\tau(t) = 2 \int_{x_s}^{x_{int}} \frac{dx}{C_p} + 2 \int_{x_{int}}^{x_{tr}} \frac{dx}{C_c} \quad (7)$$

Delta signal travel time can be expressed as by combining Eq. (1) and Eq. (7):

$$\Delta\tau = \frac{2W_{pini}}{C_{pref}} + \frac{2W_c}{C_{cref}} - 2 \int_{x_s}^{x_{int}} \frac{dx}{C_p} - 2 \int_{x_{int}}^{x_{tr}} \frac{dx}{C_c} \quad (8)$$

If C_p and C_c values are put into Eq. (8):

$$\Delta\tau = \frac{2W_{pini}}{C_{pref}} + \frac{2W_c}{C_{cref}} - 2 \int_{x_s}^{x_{int}} \frac{[1-k_p(P-P_{ref})][1+k_T(T-T_{ref})]dx}{C_{pref}} - 2 \int_{x_{int}}^{x_{tr}} \frac{[1-l_p(P-P_{ref})]dx}{C_{cref}} \quad (9)$$

P , P_{ref} , k_p , l_p , C_{pref} , C_{cref} can be taken out of integral since they are indepent of x :

$$\begin{aligned} \Delta\tau &= \frac{2W_{pini}}{C_{pref}} + \frac{2W_c}{C_{cref}} - \frac{2[1-k_p(P-P_{ref})]}{C_{pref}} \int_{x_s}^{x_{int}} [1+k_T(T-T_{ref})]dx \\ &\quad - \frac{2[1-l_p(P-P_{ref})]W_c}{C_{cref}} \\ \Delta\tau &= \frac{2W_{pini}}{C_{pref}} + \frac{2W_c}{C_{cref}} - \frac{2[1-k_p(P-P_{ref})]}{C_{pref}} \int_{x_s}^{x_{int}} [1+k_T(T-T_{ref})]dx - \frac{2W_c}{C_{cref}} \\ &\quad + \frac{2W_c l_p (P - P_{ref})}{C_{cref}} \end{aligned}$$

$$\boxed{\Delta\tau = \frac{2W_{pini}}{C_{pref}} + \frac{2W_c l_p (P - P_{ref})}{C_{cref}} - \frac{2[1-k_p(P-P_{ref})]}{C_{pref}} \int_{x_s}^{x_{int}} [1+k_T(T-T_{ref})]dx} \quad (10)$$

By taking the derivative of this term with respect to time:

$$\frac{d\Delta\tau}{dt} = \underbrace{\frac{d}{dt} \left(\frac{2W_{pini}}{C_{pref}} \right)}_{1st \ Term} + \underbrace{\frac{d}{dt} \left(\frac{2W_c l_p (P - P_{ref})}{C_{cref}} \right)}_{2nd \ Term} - \underbrace{\frac{d}{dt} \left(\frac{2[1-k_p(P-P_{ref})]}{C_{pref}} \int_{x_s}^{x_{int}} [1+k_T(T-T_{ref})]dx \right)}_{3rd \ Term} \quad (11)$$

Derivatives can be taken separately for 3 terms:

1st Term:

$$\frac{d}{dt} \left(\frac{2W_{pini}}{C_{pref}} \right) = 0$$

2nd Term:

$$\frac{d}{dt} \left(\frac{2W_c l_p (P - P_{ref})}{C_{cref}} \right) = \frac{d}{dt} \left(\frac{2W_c l_p P}{C_{cref}} \right) - \frac{d}{dt} \left(\frac{2W_c l_p P_{ref}}{C_{cref}} \right)$$

$$\frac{d}{dt} \left(\frac{2W_c l_p (P - P_{ref})}{C_{c_{ref}}} \right) = \frac{2W_c l_p}{C_{c_{ref}}} \frac{dP}{dt} - 0$$

$$\frac{d}{dt} \left(\frac{2W_c l_p (P - P_{ref})}{C_{c_{ref}}} \right) = \frac{2W_c l_p}{C_{c_{ref}}} \frac{dP}{dt}$$

3rd Term:

$$\frac{d}{dt} \left(\frac{2[1 - k_p(P - P_{ref})]}{C_{p_{ref}}} \int_{x_s}^{x_{int}} [1 + k_T(T - T_{ref})] dx \right)$$

For the 3rd term; pressure, temperature and x are dependent to time. So when taking the derivative of this term, multiplication terms should be taken term by term:

$$\frac{d}{dt} \left(\underbrace{\frac{2[1 - k_p(P - P_{ref})]}{C_{p_{ref}}}}_{3.1. \text{ Term}} \int_{x_s}^{x_{int}} \underbrace{[1 + k_T(T - T_{ref})]}_{3.2.1. \text{ Term}} \underbrace{dx}_{3.2.2. \text{ Term}} \right)$$

3rd term is expanded as follows:

$$\begin{aligned} & \frac{d}{dt} \left(\underbrace{\frac{2[1 - k_p(P - P_{ref})]}{C_{p_{ref}}}}_{3.1. \text{ Term}} \int_{x_s}^{x_{int}} \underbrace{[1 + k_T(T - T_{ref})]}_{3.2.1. \text{ Term}} \underbrace{dx}_{3.2.2. \text{ Term}} \right) \\ &= -\frac{2k_p}{C_{p_{ref}}} \frac{dP}{dt} \int_{x_s}^{x_{int}} [1 + k_T(T - T_{ref})] dx \\ &+ \frac{2[1 - k_p(P - P_{ref})]}{C_{p_{ref}}} \frac{d}{dt} \left(\int_{x_s}^{x_{int}} [1 + k_T(T - T_{ref})] dx \right) \end{aligned}$$

Blue colored term should be found separately.

For steady-state burning, thermal profile in the propellant is defined as:

$$T - T_i = (T_s - T_i) \exp \left[\frac{-r_b(x - x_s)}{\alpha} \right]$$

$$T = T_i + (T_s - T_i) \exp \left[\frac{-r_b(x - x_s)}{\alpha} \right]$$

In this case;

$$\begin{aligned}
\int_{x_s}^{x_{int}} [1 + k_T(T - T_{ref})] dx &= \int_{x_s}^{x_{int}} \left[1 + k_T \left(T_i + (T_s - T_i) \exp \left[\frac{-r_b(x - x_s)}{\alpha} \right] - T_{ref} \right) \right] dx \\
&= \int_{x_s}^{x_{int}} \left(1 + k_T T_i + k_T (T_s - T_i) \exp \left[\frac{-r_b(x - x_s)}{\alpha} \right] - k_T T_{ref} \right) dx \\
&= \int_{x_s}^{x_{int}} (1 + k_T T_i - k_T T_{ref}) dx + \int_{x_s}^{x_{int}} k_T (T_s - T_i) \exp \left[\frac{-r_b(x - x_s)}{\alpha} \right] dx \\
&= \int_{x_s}^{x_{int}} [1 + k_T (T_i - T_{ref})] dx + \int_{x_s}^{x_{int}} k_T (T_s - T_i) \exp \left[\frac{-r_b(x - x_s)}{\alpha} \right] dx \\
&= [1 + k_T (T_i - T_{ref})] (x_{int} - x_s) + k_T (T_s - T_i) \frac{-\alpha}{r_b} \exp \left[\frac{-r_b(x - x_s)}{\alpha} \right] \Bigg|_{x_s}^{x_{int}} \\
&= [1 + k_T (T_i - T_{ref})] (x_{int} - x_s) + k_T (T_s - T_i) \frac{-\alpha}{r_b} \exp \left[\frac{-r_b(x_{int} - x_s)}{\alpha} \right] \\
&\quad - k_T (T_s - T_i) \frac{-\alpha}{r_b} \exp \left[\frac{-r_b(x_s - x_s)}{\alpha} \right] \\
&= [1 + k_T (T_i - T_{ref})] (x_{int} - x_s) - k_T (T_s - T_i) \frac{\alpha}{r_b} \exp \left[\frac{-r_b(x_{int} - x_s)}{\alpha} \right] \\
&\quad + k_T (T_s - T_i) \frac{\alpha}{r_b} \exp \left[\frac{-r_b(x_s - x_s)}{\alpha} \right] = \\
&= [1 + k_T (T_i - T_{ref})] (x_{int} - x_s) - k_T (T_s - T_i) \frac{\alpha}{r_b} \exp \left[\frac{-r_b(x_{int} - x_s)}{\alpha} \right] \\
&\quad + k_T (T_s - T_i) \frac{\alpha}{r_b} \\
&= [1 + k_T (T_i - T_{ref})] (x_{int} - x_s) \\
&\quad + k_T (T_s - T_i) \frac{\alpha}{r_b} \left\{ 1 - \exp \left[\frac{-r_b(x_{int} - x_s)}{\alpha} \right] \right\}
\end{aligned}$$

if R_b , α and x values are taken into account the exponential term gets value at the range of 10^{-44} . This value is very small and negligible if compared with 1. In this case:

$$\int_{x_s}^{x_{int}} [1 + k_T(T - T_{ref})] dx = [1 + k_T(T_i - T_{ref})](x_{int} - x_s) + k_T(T_s - T_i) \frac{\alpha}{r_b}$$

At the second term; k_T has 10^{-3} , α has 10^{-8} , T has 10^3 ve r_b has 10^{-3} magnitudes so the magnitude of the second term is 10^{-5} . According to Traineau and Kuentzmann [42] neglecting this term causes only 0.2% error. This term can be neglected:

$$\int_{x_s}^{x_{int}} [1 + k_T(T - T_{ref})] dx = [1 + k_T(T_i - T_{ref})](x_{int} - x_s)$$

Derivative of this term:

$$\begin{aligned} \frac{d}{dt} \left(\int_{x_s}^{x_{int}} [1 + k_T(T - T_{ref})] dx \right) &= \frac{d}{dt} ([1 + k_T(T_i - T_{ref})](x_{int} - x_s)) \\ &= -[1 + k_T(T_i - T_{ref})] \frac{dx_s}{dt} \end{aligned}$$

At the last case, 3rd term happens:

$$\begin{aligned} \frac{d}{dt} \left(\underbrace{\frac{2[1 - k_p(P - P_{ref})]}{C_{p_{ref}}}}_{3.1. \text{ Term}} \int_{x_s}^{x_{int}} \underbrace{[1 + k_T(T - T_{ref})]}_{3.2.1. \text{ Term}} \underbrace{dx}_{3.2.2. \text{ Term}} \right) \\ = -\frac{2k_p}{C_{p_{ref}}} \frac{dP}{dt} \int_{x_s}^{x_{int}} [1 + k_T(T - T_{ref})] dx \\ + \frac{2[1 - k_p(P - P_{ref})]}{C_{p_{ref}}} \frac{d}{dt} \left(\int_{x_s}^{x_{int}} [1 + k_T(T - T_{ref})] dx \right) \\ = -\frac{2k_p}{C_{p_{ref}}} \frac{dP}{dt} \int_{x_s}^{x_{int}} [1 + k_T(T - T_{ref})] dx \\ - \frac{2[1 - k_p(P - P_{ref})]}{C_{p_{ref}}} [1 + k_T(T_i - T_{ref})] \frac{dx_s}{dt} \end{aligned}$$

By collecting all of three terms together:

$$\begin{aligned} \frac{d\Delta\tau}{dt} = 0 + \frac{2W_c l_p}{C_{cref}} \frac{dP}{dt} + \frac{2k_p}{C_{pref}} \frac{dP}{dt} \int_{x_s}^{x_{int}} [1 + k_T(T - T_{ref})] dx \\ + \frac{2[1 - k_p(P - P_{ref})]}{C_{pref}} [1 + k_T(T_i - T_{ref})] \frac{dx_s}{dt} \end{aligned}$$

$$\frac{d\Delta\tau}{dt} = \left[\frac{W_c l_p}{C_{cref}} + \frac{2k_p}{C_{pref}} \int_{x_s}^{x_{int}} [1 + k_T(T - T_{ref})] dx \right] \frac{dP}{dt} + \frac{2[1 - k_p(P - P_{ref})]}{C_{pref}} [1 + k_T(T_i - T_{ref})] \frac{dx_s}{dt} \quad (12)$$

$\frac{dx_s}{dt}$ is the burning rate of the propellant; so:

$$\begin{aligned} \frac{C_{pref}}{2[1 - k_p(P - P_{ref})][1 + k_T(T_i - T_{ref})]} \left\{ \frac{d\Delta\tau}{dt} \right. \\ \left. - \left[\frac{2W_c l_p}{C_{cref}} + \frac{2k_p}{C_{pref}} \int_{x_s}^{x_{int}} [1 + k_T(T - T_{ref})] dx \right] \frac{dP}{dt} \right\} = R_b \end{aligned}$$

When the initial temperature is equal to reference temperature, $[1 + k_T(T_i - T_{ref})] = 1$. In this case burning rate formula becomes:

$$\frac{C_{pref}}{2[1 - k_p(P - P_{ref})]} \left\{ \frac{d\Delta\tau}{dt} - \left[\frac{2W_c l_p}{C_{cref}} + \frac{2k_p}{C_{pref}} \int_{x_s}^{x_{int}} [1 + k_T(T - T_{ref})] dx \right] \frac{dP}{dt} \right\} = R_b \quad (13)$$

Eq. (10) can be written as:

$$\begin{aligned} \frac{2[1 - k_p(P - P_{ref})]}{C_{pref}} \int_{x_s}^{x_{int}} [1 + k_T(T - T_{ref})] dx = \frac{2W_{pini}}{C_{pref}} + \frac{2W_c l_p(P - P_{ref})}{C_{cref}} - \Delta\tau \\ \frac{2}{C_{pref}} \int_{x_s}^{x_{int}} [1 + k_T(T - T_{ref})] dx = \frac{\frac{2W_{pini}}{C_{pref}} + \frac{2W_c l_p(P - P_{ref})}{C_{cref}} - \Delta\tau}{[1 - k_p(P - P_{ref})]} \end{aligned}$$

$$\frac{2k_p}{C_{p_{ref}}} \int_{x_s}^{x_{int}} [1 + k_T(T - T_{ref})] dx = k_p \left(\frac{\left(\frac{2W_{p_{ini}}}{C_{p_{ref}}} + \frac{2W_{clp}(P - P_{ref})}{C_{c_{ref}}} - \Delta\tau \right)}{[1 - k_p(P - P_{ref})]} \right) \quad (14)$$

When Eq. (14) integrated in Eq. (13):

$$R_b = \frac{C_{p_{ref}}}{2[1 - k_p(PC - P_{ref})]} \left\{ \frac{d\Delta\tau}{dt} - \left[\frac{2W_{clp}}{C_{c_{ref}}} + k_p \left(\frac{\left(\frac{2E_{p_i}}{C_{p_{ref}}} + \frac{2E_{clp}(PC - P_{ref})}{C_{c_{ref}}} - \Delta\tau \right)}{[1 - k_p(PC - P_{ref})]} \right) \right] \frac{dP}{dt} \right\}$$